

The Other Side of the Coin: Unveiling the Downsides of Model Aggregation in Federated Learning from a Layer-peeled Perspective

Guogang Zhu¹ Xuefeng Liu¹ Jianwei Niu¹ Shaojie Tang² Xinghao Wu¹

Abstract

In federated learning (FL), model aggregation is a critical step by which multiple clients share their knowledge with one another. However, it is also widely recognized that the aggregated model, when sent back to each client, performs poorly on local data until after several rounds of local training. This temporary performance drop can potentially slow down the convergence of the FL model. Most research in FL regards this performance drop as an inherent cost of knowledge sharing among clients and does not give it special attention. While some studies directly focus on designing techniques to alleviate the issue, an in-depth investigation of the reasons behind this performance drop has yet to be conducted. To address this gap, we conduct a layer-peeled analysis of model aggregation across various datasets and model architectures. Our findings reveal that the performance drop can be attributed to two major consequences of the aggregation process: (1) it disrupts feature variability suppression in deep neural networks (DNNs), and (2) it weakens the coupling between features and subsequent parameters. Based on these findings, we propose several simple yet effective strategies to mitigate the negative impacts of model aggregation while still enjoying the benefit it brings. To the best of our knowledge, our work is the first to conduct a layer-peeled analysis of model aggregation, potentially paving the way for the development of more effective FL algorithms.

1. Introduction

In recent years, federated learning (FL) has gained increasing interests since it can enable multiple clients to collaboratively train models without sharing their private data. FL is particularly attractive in fields where data privacy and security are paramount, such as medical diagnosis (Guan et al., 2024), where patient records must remain confidential, and financial analysis (Imteaj & Amini, 2022), where transactional data is highly sensitive.

A standard FL process involves iterative cycles in which local models are trained on each client, followed by aggregation of these locally updated models on a central server (McMahan et al., 2017), as presented in Figure 1. During local training, each client performs multiple rounds of model updates using its private data. Once local training is complete, the updated model is uploaded to the server. The server then aggregates the uploaded models by performing parameter-wise averaging, with each model weighted based on factors such as the number of training samples on each client (Acar et al., 2021; Li et al., 2020; Karimireddy et al., 2020). The aggregated model is then sent back to each client for the next round of local training. By transmitting model parameters instead of raw data, FL ensures collaborative model training while preserving privacy.

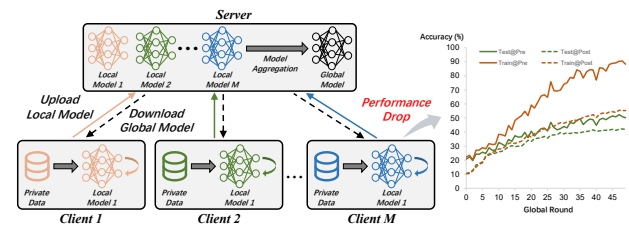


Figure 1. **Left:** Local model training and global model aggregation in a typical FL training process. **Right:** Performance comparison when evaluating models on local data, *@Pre refers to the evaluation results of the model before aggregation, while *@Post indicates the results after aggregation.

In the above process, model aggregation is a key step that facilitates knowledge sharing among clients in FL. However, it is well known that the model aggregation often leads to a significant performance drop compared to the model

¹School of Computer Science and Engineering, Beihang University, Beijing, China ²Department of Management Science and Systems, School of Management, Center for AI Business Innovation, University at Buffalo, Buffalo, NY, USA. Correspondence to: Xuefeng Liu <liu_xuefeng@buaa.edu.cn>.

before aggregation (Jin et al., 2022; Lee et al., 2022; Yao et al., 2024). This phenomenon is particularly pronounced when data distributions across clients are heterogeneous, a common scenario in practical applications due to factors such as variations in data acquisition conditions across different clients (Zhu et al., 2021; Li et al., 2021b). To further investigate this phenomenon, we conduct preliminary experiments in a typical data-heterogeneous FL setting. Figure 1 presents a performance comparison of the model before and after aggregation, evaluated on the local data from each client. As shown, the performance of the aggregated model significantly deteriorates compared to the model before aggregation.

Although this temporary performance drop can be mitigated after several rounds of local updates, its impact persists and continues to pose a challenge. The suboptimal initialization in each local update, caused by model aggregation, undermines the progress made in the previous round, potentially slowing the convergence rate of FL training. Most FL research treats this performance drop as an inherent cost of knowledge sharing among clients, giving it limited attention (McMahan et al., 2017; Wu et al., 2023; Li et al., 2021a). Recently, however, some studies have started to address this issue. For instance, some research attributes the problem to diverging model parameters caused by heterogeneous data distributions and propose various model regularization techniques to reduce parameter divergence (Li et al., 2020; Karimireddy et al., 2020). Other studies link this issue to ‘knowledge forgetting’, where task-specific patterns are averaged out or diluted during model aggregation, and suggest several knowledge distillation methods (Jin et al., 2022; Lee et al., 2022). However, these studies rely on assumed causes of the performance drop, often without deeply exploring the fundamental reasons behind it.

To address this gap, we provide a comprehensive analysis of the impact of model aggregation in FL from a layer-peeled feature extraction perspective. Our focus is twofold: first, on *feature structure*, which evaluates the intrinsic quality of the features, and second, on *feature-parameter alignment*, which assesses the degree of coupling between features and the parameters of subsequent layers.

We conduct this layer-peeled feature analysis across multiple datasets and model architectures. Our findings show that the performance degradation in model aggregation can be primarily attributed to two factors from a layer-wise feature extraction perspective: (1) disruption of feature variability suppression in deep neural networks (DNNs), and (2) a weakening of the coupling between features and the parameters of subsequent layers. Firstly, DNNs are known to progressively compress features layer by layer (Wang et al., 2023b; Rangamani et al., 2023; Masarczyk et al., 2024). However, during model aggregation, this feature

compression process is compromised, leading to scattered features. This effect accumulates across layers as the network deepens, significantly degrading the quality of the penultimate layer features. Secondly, the mismatch between the penultimate layer features and the classifier worsens after aggregation, further deteriorating model performance. Based on these findings, we propose several simple yet effective strategies to directly address these issues, thereby improving the FL model performance.

The contributions of this paper are as follows:

- To the best of our knowledge, we are the first to comprehensively understand the impact of model aggregation from a layer-peeled feature extraction perspective.
- We conduct an extensive layer-peeled feature evaluation across multiple datasets and model architectures, which uncovers the major causes of performance drop in model aggregation. This analysis examines both feature quality and feature-parameter alignment, while also highlighting the challenges introduced by the stacked architecture of DNNs.
- We propose strategies to improve the aggregated model, addressing key drawbacks and enabling the development of enhanced FL algorithms based on our insights.

2. Preliminaries

2.1. Problem Formulation of FL

In this paper, we consider a standard FL system consisting of a central server and M distributed clients. We assume that each client m contains N_m training samples, which are drawn from the data distribution \mathcal{D}_m . In practice, the underlying data distribution \mathcal{D}_m for each client is typically different from one another due to the variations in data collection conditions. Formally, the training samples on client m can be represented as $(\mathbf{x}_m^i, \mathbf{y}_m^i)_{i=1}^{N_m}$, where $\mathbf{x}_m^i \in \mathcal{X}_m \subseteq \mathbb{R}^n$ denotes the raw input data for the DNNs, and $\mathbf{y}_m^i \in \mathcal{Y}_m \subseteq \{0, 1\}^C$ represents the corresponding ground truth labels used to optimize the DNNs, with C denoting the number of classes.

We denote the DNN for client m as $\psi_m(\cdot)$, with parameters represented by Θ_m . The optimization objective for an FL system can then be formulated as:

$$\arg \min_{\Theta_1, \dots, \Theta_M} \mathcal{L}(\Theta_1, \dots, \Theta_M) \triangleq \arg \min_{\Theta_1, \dots, \Theta_M} \frac{1}{M} \sum_{m=1}^M \mathcal{L}_m(\Theta_m), \quad (1)$$

where $\mathcal{L}_m(\Theta_m)$ represents the empirical risk for client m , which is computed based on its private data samples, as shown in the following equation:

$$\mathcal{L}_m(\Theta_m) := \frac{1}{N_m} \sum_{i=1}^{N_m} \ell(\mathbf{y}_m^i, \hat{\mathbf{y}}_m^i), \quad (2)$$

where $\hat{\mathbf{y}}_m^i = \psi_m(\mathbf{x}_m^i; \Theta_m)$ represents the predicted output of \mathbf{x}_m^i given the model $\psi_m(\cdot)$ for \mathbf{x}_m^i , $\ell: \mathcal{Y} \times \mathcal{Y} \rightarrow \mathbb{R}$ is the loss function used to measure the prediction error.

To optimize Equation (1) in a privacy-preserving manner, FL is typically carried out in two iterative stages: local model training and global model aggregation. During the local model training phase, each client optimizes its model for E epochs by minimizing the loss function defined in Equation (2). Once local training is complete, each client uploads its updated model to the server. The server then performs model aggregation to generate the global model. A common aggregation strategy involves applying a weighted average for each parameter within the model based on the number of training samples per client, which is expressed as follows:

$$\tilde{\Theta} = \sum_{m=1}^M \frac{N_m}{\sum_{m=1}^M N_m} \Theta_m \quad (3)$$

Here, $\tilde{\Theta}$ represents the aggregated global model. By repeating the above procedures for several rounds, the model eventually converges, resulting in the final FL model. For simplicity, we will sometimes refer to the locally updated model Θ_m as the *pre-aggregated model*, and $\tilde{\Theta}$ as the *post-aggregated model*. Additionally, we may omit the client and sample indices for simplicity.

In this paper, we focus on uncovering how the feature extraction process varies across model depth due to model aggregation. We reformulate the parameters of the FL model as $\Theta = \{\mathbf{W}^\ell\}_{\ell=1}^L$, where L represents the total number of layers in the model, and the depth increases with ℓ . This stacked DNN progressively transforms the input data into prediction outputs, from the shallow layers to the deeper layers. However, there is still a lack of investigation into how model aggregation affects layer-wise feature extraction. In this paper, we aim to explore the variations in intermediate features during layer-wise feature extraction. The features of the ℓ -th layer for an input sample \mathbf{x} can be formulated as:

$$\mathbf{z}^\ell = \mathbf{W}^\ell \dots \mathbf{W}^1 \mathbf{x} = \mathbf{W}^{\ell:1} \mathbf{x}, \forall \ell = 1, \dots, L-1 \quad (4)$$

where \mathbf{z}^ℓ denotes the intermediated features of ℓ -th layer and we denote $\mathbf{z}^0 = \mathbf{x}$.

2.2. Feature Evaluation Metric

We apply the following metrics to evaluate the features generated by the models before aggregation and after aggregation, including the *feature variance*, *alignment between features and parameters*, *accuracy of linear probing*, *pairwise*

distance of features or models, *relative change of evaluated metrics*.

- **Feature Variance.** We calculate the normalized within-class variance, which quantifies feature compression within the same class, and the normalized between-class variance, which measures the discrimination between different classes. Together, these metrics assess the quality of features given the evaluated dataset.
- **Alignment between Features and Parameters.** We assess the alignment between features and parameters to evaluate the degree of coupling between them during the feature extraction process.
- **Accuracy of Linear Probing.** This metric evaluates the generalization of features across different distributions. We attach a randomly initialized linear layer to features extracted from various layers of DNNs, then train this linear classifier on a evaluated dataset and report the average testing accuracy.
- **Pairwise Distance of Features or Models.** This metric evaluates the differences between the parameters or features generated by the models before and after aggregation.
- **Relative Change of Evaluated Metrics.** This measures the change in the metrics after aggregation, offering insights into the degree of impact that aggregation introduces to feature extraction.

3. Evaluation Setup

3.1. Dataset Description and Partition

We focus on the cross-domain FL setting in our experiments, which is a common scenario for FL with heterogeneous data. This frequently appears in practical applications such as medical image analysis, traffic surveillance, and autonomous driving (Li et al., 2021b; Zhu et al., 2022).

Building upon previous studies (Li et al., 2021b; Zhu et al., 2022; Huang et al., 2023), we use three public datasets to establish the FL system: Digit-Five, PACS (Li et al., 2017), and DomainNet (Peng et al., 2019). Each of these datasets consists of data samples from different domains, with each domain containing images in various styles.

For these datasets, the samples (including both training and tests datasets) from each domain are assigned to a client to construct a cross-domain FL system. The number of training samples for each client is set to 500 for all datasets. For Digit-Five, the testing dataset contains 1,000 samples for each client. For DomainNet and PACS, the testing datasets contain 500 samples for each client.

The sample size for Digit-Five is set to 32×32 , while for DomainNet and PACS, it is set to 224×224 . For Digit-Five, each channel is normalized with a mean of 0.5 and a standard deviation of 0.5 for both training and testing datasets. For DomainNet and PACS, we apply random flipping and rotational augmentations to the training samples.

3.2. Implementation Details

We evaluate feature variations between the pre-aggregated and post-aggregated models across various architectures. For Digit-Five, we adopt a convolutional network followed by fully connected (FC) layers (ConvNet), ResNet18, and ResNet34. For DomainNet and PACS, the implemented models including VGG13_BN (Simonyan & Zisserman, 2014), three variants of ResNet (ResNet18, ResNet34, and ResNet50) (He et al., 2016), and ViT_B-16 (Dosovitskiy et al., 2021). Unless otherwise specified, the models are trained from randomly initialized parameters.

We apply the standard FedAvg (McMahan et al., 2017) algorithm for federated training. Stochastic gradient descent (SGD) is used to optimize the models on local clients, with a learning rate of 0.01 and a momentum of 0.5. The batch size for local training is set to 64. Local models are trained for 10 epochs within each global round, with a total of 50 global rounds. On the server, we perform model aggregation by weighted averaging the parameters, using the number of training samples as the weight for each client. To reduce the impact of randomness, each experiment is repeated three times with different random seeds.

We extract features from various layers, ranging from shallow to deep, for feature evaluation. Specifically, we evaluate the features passed to each convolutional layer, pooling layer, and FC layer in the convolutional neural network (CNN). For ViT_B/16, we evaluate the features passed to the multilayer perceptron (MLP), self-attention layers, layer normalization layers, and the final classifier.

4. Main Results

In this section, we present the key findings observed across multiple datasets and model architectures during our layer-peeled analysis of model aggregation in FL. Due to space limitations, we only present representative results here. More detailed results are available in the Appendix.

4.1. Understanding Model Aggregation in FL

4.1.1. MODEL AGGREGATION LEADS TO PERFORMANCE DROP ON LOCAL DATA

We first confirm the claim that aggregating multiple local models trained on each client results in a significant performance drop when the aggregated model is sent back

to the local clients for inference. Figure 2 shows the average training and testing accuracy of the models before and after aggregation during the FL training process. It can be observed that the aggregated model suffers from a substantial performance degradation across various model architectures, both on the training and testing datasets. This temporary performance drop erases the gains made during the previous local updates on clients, thereby slowing down the convergence rate of FL training. Therefore, we seek to understand what happens during model aggregation from the perspective of layer-peeled feature extraction.

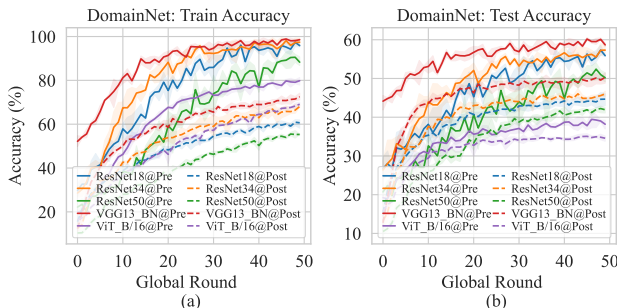


Figure 2. Averaged training and testing accuracy curves of the model before and after aggregation, evaluated on the local dataset during FL training. The experiments are conducted on DomainNet, using multiple model architectures as the backbone.

4.1.2. MODEL AGGREGATION DISRUPTS FEATURE VARIABILITY SUPPRESSION

Previous studies have shown that deep neural networks (DNNs) progressively suppress raw data, generating task-specific features. However, in our experiments, we observe that model aggregation disrupts this training objective of DNNs. Specifically, we make the following observations:

(1) Features become increasingly compressed within the same class as training progresses and layer depth increases. As shown in Figures 3 (a) and 5 (a), during training, the features within the same class become progressively more compressed. Moreover, as the layers deepen, the features become also more compressed. This observation suggests that, from the perspective of feature variation suppression, the overall training objective of FL aligns with what has been observed in centralized learning (CL).

(2) Features become increasingly discriminative across different class as training progresses and layer depth increases. In contrast to the normalized within-class feature variance, the normalized between-class feature variance increases as the training progresses and layer depth increases, as shown in Figure 4 (a) and 6 (a). This demonstrates that the features across different classes become increasingly discriminative.

(3) Model aggregation disrupts feature variation suppression during FL training. As shown in Figures 3 (a)

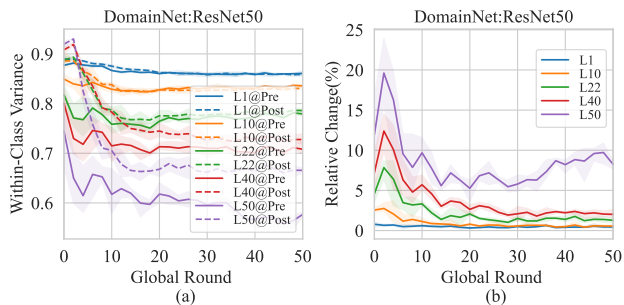


Figure 3. Normalized within-class variance of features at different layers during FL training. The model is trained on DomainNet using ResNet50: (a) normalized within-class variance, (b) relative change of the variance before and after model aggregation.

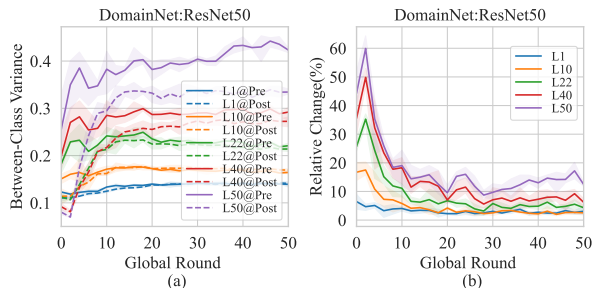


Figure 4. Normalized between-class variance of features at different layers during FL training. The model is trained on DomainNet using ResNet50: (a) normalized between-class variance, (b) relative change of the variance before and after model aggregation.

and 5 (a), the normalized within-class variance increases, while the normalized between-class variance decreases after model aggregation. This is in contrast to the training objective of DNNs. Additionally, the feature visualization in Figure 7 clearly shows the features generated by different layers of the models before and after aggregation, providing further evidence of this disruption.

(4) Deeper features begin to compress only after model aggregation. As shown in Figures 3 - 6, during the training of the FL model, the shadow features initially converge to a certain level of feature variation and then the deeper layer can start to converge. If this condition is not met, model aggregation may cause the features to scatter from the shadow and deeper layers. This characteristic makes the convergence of the model aggregation more challenging.

4.1.3. FEATURE VARIATION DISRUPTION ACCUMULATE AS MODEL DEPTH INCREASES

In experiments, we find that the stacked architecture of DNNs has specific impacts on model aggregation. Specifically, we observe that the disruption of feature variation suppression progressively accumulates as the depth of layer increases. As shown in Figures 3 (b) and 5 (b), we compute the relative changes in normalized within-class variance.

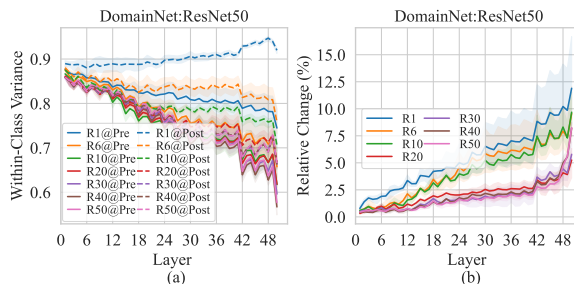


Figure 5. Changes in normalized within-class variance across layers for specific global rounds, with larger X-axis values indicating deeper layers. The model is trained on DomainNet using ResNet50: (a) normalized within-class variance, (b) relative change of the variance before and after model aggregation.

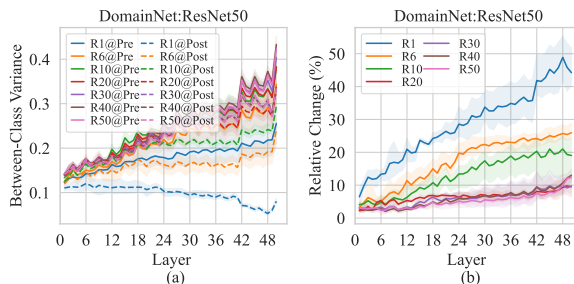


Figure 6. Changes in normalized between-class variance across layers for specific global rounds, with larger X-axis values indicating deeper layers. The model is trained on DomainNet using ResNet50: (a) normalized between-class variance, (b) relative change of the variance before and after model aggregation.

It can be observed that the relative changes in normalized within-class variance progressively increase as we move deeper into the DNNs. This issue suggests that DNNs may not be ideal for model aggregation in FL training.

Additionally, we examined the layer-wise parameter and feature distances between the model before and after aggregation. The results are shown in Figure 8. The magnitudes of the parameter distances are much smaller compared to the feature distances. The parameter distance shows a decreasing trend as the model deepens, except for the final classifier, while the feature distance shows an increasing trend with deeper layers. This phenomenon suggests that the performance drop may not only be due to parameter divergence but could be more closely related to the accumulation of feature disruption. This issue causes the features in the penultimate layer to degrade more significantly, which can substantially affect the model’s performance.

4.1.4. FEATURE MISMATCH WITH PARAMETERS IN FINAL DECISION STAGE

In the previous sections, we observed that the features from the model experience significant quality degradation due to the accumulation of feature disruption across the depth of

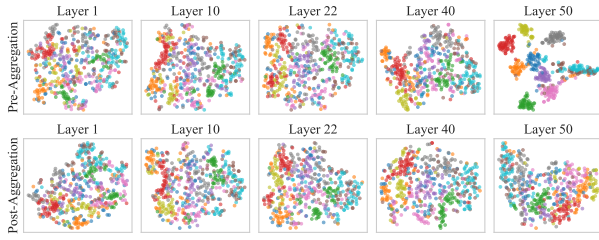


Figure 7. T-SNE visualization of features at different layers on the ‘Quickdraw’ domain of DomainNet before and after aggregation. The features are extracted from ResNet50 in the final global round.

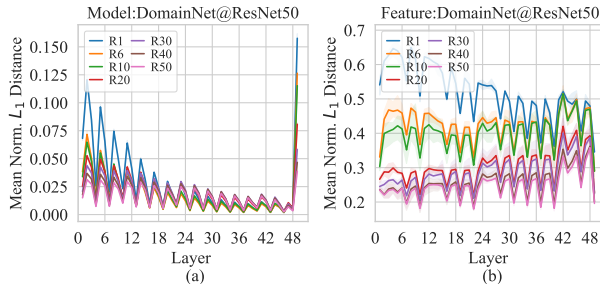


Figure 8. Changes in normalized L_1 distance of the features and parameters obtained from models before and after aggregation across model layers for specific global rounds, with larger X-axis values indicating deeper layers. The model is trained on DomainNet using ResNet50: (a) distance of model parameters (b) distance of features.

DNNs. However, the final decision of DNNs is not only influenced by the feature quality, but also by the model parameters that progressively process the generated features. Figures 9 and 10 show the alignment between features and the subsequent parameters. It is evident that there is a disruption in this alignment after model aggregation. This disruption exhibits an accumulation phenomenon similar to feature variations, which causes the penultimate layer’s features to significantly mismatch with the subsequent classifier. This mismatch further degrade the performance.

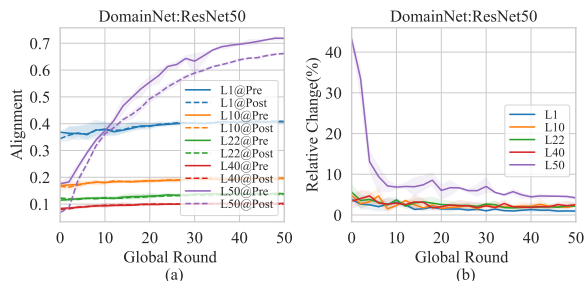


Figure 9. Alignment between features and parameters at different layers during FL training. The model is trained on DomainNet using ResNet50: (a) original alignment value between features and parameters, (b) relative change of the alignment values before and after model aggregation.

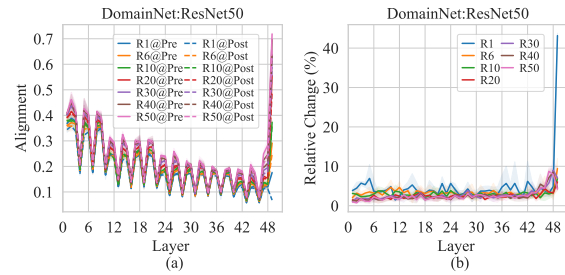


Figure 10. Changes in alignment of features and parameters across model layers for specific global rounds, with larger X-axis values indicating deeper layers. The model is trained on DomainNet using ResNet50: (a) original alignment value between features and parameters, (b) relative change of the alignment values before and after model aggregation.

4.1.5. MODEL AGGREGATION IMPROVES MODEL GENERALIZATION

In this section, we demonstrate that model aggregation improves the model’s generalization across various datasets. We perform linear probing on both the pre-aggregated and post-aggregated models using different datasets from local clients. As shown in Figure 11, after local training on clients, the linear probing accuracy on its local data generally improves, indicating that the model gradually adapts. However, when tested on datasets from other clients, the model performs worse. This demonstrates that the model before aggregation struggles to extract universal features applicable across different clients. In contrast, the post-aggregated model exhibits much better performance, suggesting that it generalizes more effectively, as the knowledge learned from different clients is fused through the aggregation process.

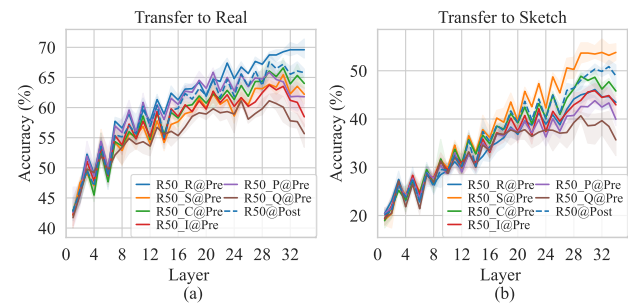


Figure 11. Accuracy of linear probing at different layers on ‘Clipart’ and ‘Infograph’ domains in DomainNet. The experiments are performed using the ResNet34 model in global round 50. In the figures, E50@Post represents the results using the post-aggregated model, while E50_*@Pre represents the results using the model pre-aggregated model for domain *.

4.2. More Factors Related to Feature Extraction

4.2.1. PARAMETER PERSONALIZATION

Parameter personalization is a key method in personalized federated learning (PFL). In this section, we conduct experiments to investigate how parameter personalization impacts the feature extraction process. We first examine two typical PFL methods: FedPer (Arivazhagan et al., 2019), which personalizes the classifier, and FedBN (Li et al., 2021b), which personalizes the batch normalization (BN) layers. Additionally, inspired by (Sun et al., 2021), we explore a successive personalization approach that targets multiple layers, starting from the first layer. The experimental results are presented in Figure 12. As shown, personalizing more parameters within the feature extractor generally results in more compressed within-class features and less relative change after model aggregation. This effect can be attributed to the fact that personalizing shallow layers helps mitigate the accumulation of feature degradation, where the feature extraction capacity learned from local data in these personalized layers remain unaffected by model aggregation.

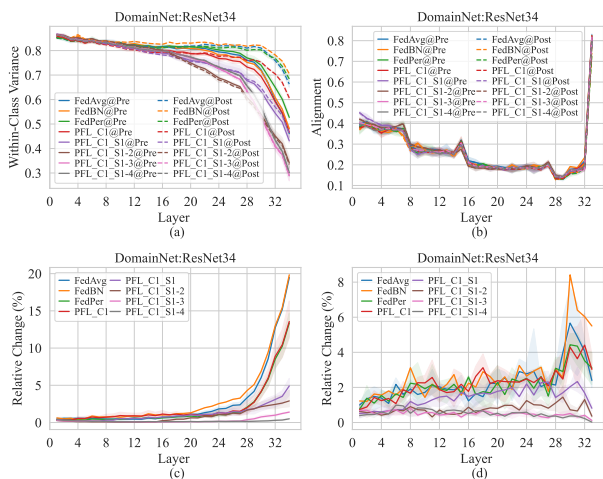


Figure 12. Changes in the normalized within-class feature variance and the alignment between features and parameters when personalizing different parts of the model. The results are obtained by the model in global round 30, using ResNet34 as the backbone and is trained on DomainNet. PFL_* denotes the PFL methods that personalize different parts, with C1 referring to the first convolutional layer and S* referring to the stage block.

4.2.2. LOCAL UPDATING EPOCHS

In this section, we conduct experiments to investigate its impact on model aggregation. The experimental results are presented in Figure 13. To ensure a fair comparison, we maintain a consistent total number of updating epochs across comparisons. The results show that increasing the number of local epochs will compress the within-class features more effectively. However, when the models are aggregated, the

relative change for larger local update epochs is noticeably greater than for smaller ones. This highlights the sensitivity of the model aggregation process to the number of local updating epochs.

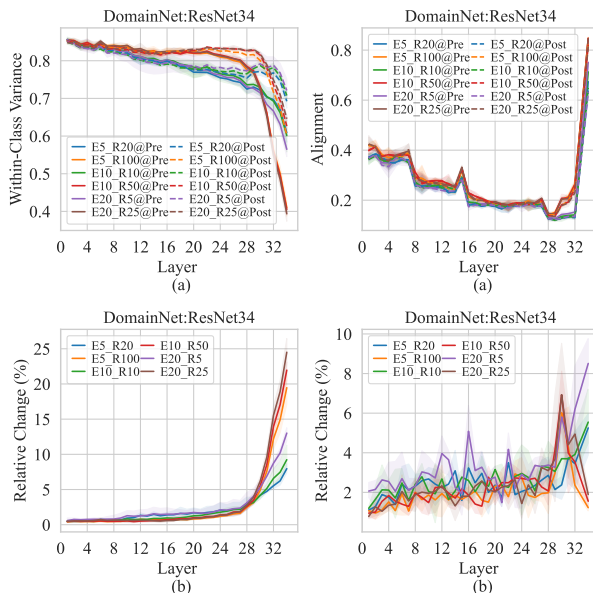


Figure 13. Changes in the normalized within-class feature variance and the alignment between features and parameters when training the FL model with different local update epochs. The model is trained on DomainNet using ResNet34 as backbone. We present two groups of experiments, keeping the total number of updating epochs ($E \times R$) fixed at 100 and 500.

4.2.3. RESIDUAL CONNECTION

Since residual connections have become a standard component in modern DNNs, we explore their impact on model aggregation. Figure 14 compares the results with and without residual connections. The experiments are conducted using ResNet34 on the DomainNet dataset. We removed the residual connections from ResNet34 while keeping the rest of the architecture unchanged, resulting in the Plain_ResNet34 model. As shown in Figure 14, the relative change in the normalized within-class feature variance, as well as the alignment between features and parameters, is greater in the Plain_ResNet34 compared to the original ResNet34. This may be because that residual connections help reduce feature degradation by allowing less disrupted features from earlier layers to be passed to deeper layers. This suggests that residual connections potentially help mitigate the accumulation of feature degradation during model aggregation.

4.3. Mitigating Negative Impacts of Model Aggregation

In this section, we provide several simple yet effective strategies that can help us to mitigate the downsides introduced by model aggregation, including initialization with pre-trained

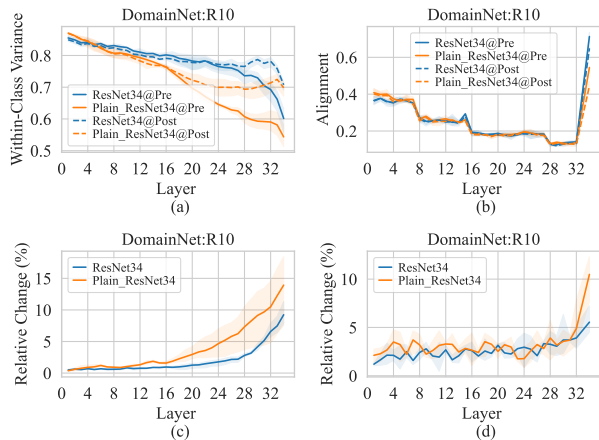


Figure 14. Comparison of feature metrics across layers with and without the use of residual connections (Plain_ResNet34) in ResNet34. This evaluation is performed on DomainNet dataset using the model at global round 10.

parameters, and fine-tuning classifiers.

4.3.1. INITIALIZATION WITH PRE-TRAINED PARAMETERS ON LARGE-SCALED DATASET

As shown in Figures 15 and 16, both the normalized within-class variance and the alignment between features and parameters exhibit less changes compared with those trained from randomly initialized parameters. This is likely because, after pre-training, the shallow layers are capable of extracting meaningful features, allowing the model to focus on training the deeper layers. This helps alleviate the accumulation of feature degradation during model training, making the pre-trained model more suitable for FL.

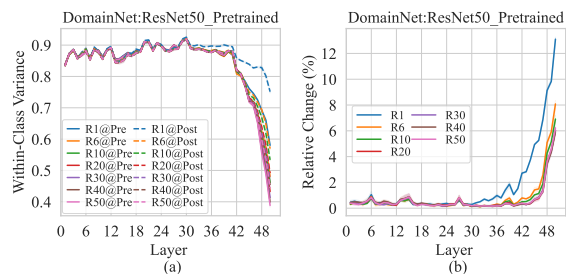


Figure 15. Changes in normalized within-class variance of features across model layers for specific global rounds, with larger X-axis values indicating deeper layers. The model is trained on DomainNet using ResNet50 pre-trained on ImageNet: (a) normalized within-class variance, (b) relative change of the variance before and after model aggregation.

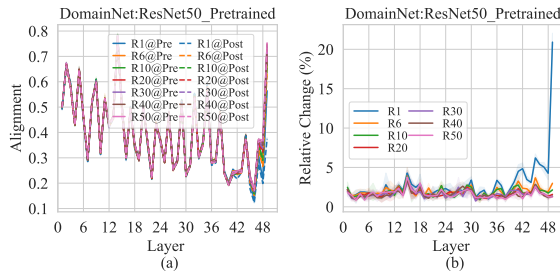


Figure 16. Changes in alignment of features and parameters across model layers for specific global rounds, with larger X-axis values indicating deeper layers. The model is trained on DomainNet using ResNet50 pre-trained on ImageNet: (a) original alignment value between features and parameters, (b) relative change of the alignment values before and after model aggregation.

4.3.2. FINE-TUNING CLASSIFIER WHEN RELOADING GLOBAL FEATURE EXTRACTOR

As mentioned earlier, when the global model is sent back to local clients, the features from the penultimate layer exhibit an increased mismatch with the subsequent classifier. In this subsection, we show that simply fine-tuning the classifier can significantly enhance the models performance. Figure 17 illustrates the accuracy and feature-parameter alignment when fine-tuning the classifier at various global rounds during training. It can be observed that after fine-tuning the classifier, the alignment between the features and the classifier consistently improves as the FL training progresses. As a result, the testing accuracy also improves.

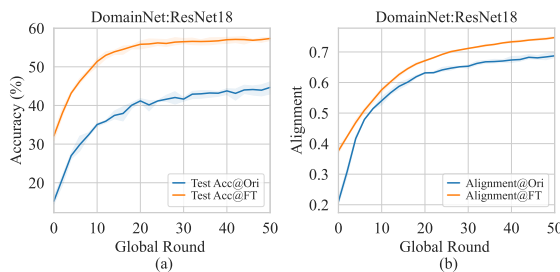


Figure 17. Accuracy and alignment between features and parameters during classifier fine-tuning across global rounds.

5. Conclusion

To the best of our knowledge, this paper presents the first attempt to explain model aggregation in FL from the perspective of layer-peeled feature analysis. We focus on the performance drop in model aggregation. Through our layer-peeled feature analysis, we identify several factors that contribute to this performance drop. In particular, from the perspective of feature variations suppression, we observe that the features after aggregation tend to be less compressed than before. More importantly, due to the stacked architecture of

modern DNNs, this phenomenon accumulates throughout the feature extraction process, significantly degrading the quality of the final features used for decision-making. As a result, training DNNs using FL becomes increasingly challenging. Additionally, we find that the penultimate layer features exhibit significant mismatches with the classifier after aggregation. This further degrades the performance of the aggregated model. Building on these insights, we explore techniques to mitigate these issues and, in turn, enhance the model performance. This work deepens the understanding of model aggregation in FL and provides a new perspective for developing more effective FL algorithms.

Impact Statement

This paper presents work whose goal is to advance the field of Machine Learning. There are many potential societal consequences of our work, none which we feel must be specifically highlighted here.

References

- Acar, D. A. E., Zhao, Y., Matas, R., Mattina, M., Whatmough, P., and Saligrama, V. Federated learning based on dynamic regularization. In *International Conference on Learning Representations*, 2021. URL <https://openreview.net/forum?id=B7v4QMR6Z9w>.
- Alain, G. and Bengio, Y. Understanding intermediate layers using linear classifier probes, 2017. URL <https://openreview.net/forum?id=ryF7rTqgl>.
- Allen-Zhu, Z. and Li, Y. Backward feature correction: How deep learning performs deep (hierarchical) learning. In *The Thirty Sixth Annual Conference on Learning Theory*, pp. 4598–4598. PMLR, 2023.
- Ansuini, A., Laio, A., Macke, J. H., and Zoccolan, D. Intrinsic dimension of data representations in deep neural networks. *Advances in Neural Information Processing Systems*, 32, 2019.
- Arivazhagan, M. G., Aggarwal, V., Singh, A. K., and Choudhary, S. Federated learning with personalization layers. *arXiv preprint arXiv:1912.00818*, 2019.
- Björck, . and Golub, G. H. Numerical methods for computing angles between linear subspaces. *Mathematics of computation*, 27(123):579–594, 1973.
- Chen, T., Kornblith, S., Norouzi, M., and Hinton, G. A simple framework for contrastive learning of visual representations. In *International conference on machine learning*, pp. 1597–1607. PMLR, 2020.
- Collins, L., Hassani, H., Mokhtari, A., and Shakkottai, S. Exploiting shared representations for personalized federated learning. In *International Conference on Machine Learning*, pp. 2089–2099. PMLR, 2021.
- Dong, X., Zhang, S. Q., Li, A., and Kung, H. Spheredef: Hyperspherical federated learning. In *European Conference on Computer Vision*, pp. 165–184. Springer, 2022.
- Dosovitskiy, A., Beyer, L., Kolesnikov, A., Weissenborn, D., Zhai, X., Unterthiner, T., Dehghani, M., Minderer, M., Heigold, G., Gelly, S., Uszkoreit, J., and Houlsby, N. An image is worth 16x16 words: Transformers for image recognition at scale. In *International Conference on Learning Representations*, 2021. URL <https://openreview.net/forum?id=YicbFdNTTy>.
- Evcı, U., Dumoulin, V., Larochelle, H., and Mozer, M. C. Head2toe: Utilizing intermediate representations for better transfer learning. In *International Conference on Machine Learning*, pp. 6009–6033. PMLR, 2022.
- Ganin, Y. and Lempitsky, V. S. Unsupervised domain adaptation by backpropagation. In *Int. Conf. Machin. Learn.*, pp. 1180–1189, 2015.
- Guan, H., Yap, P.-T., Bozoki, A., and Liu, M. Federated learning for medical image analysis: A survey. *Pattern Recognition*, pp. 110424, 2024.
- Harun, M. Y., Lee, K., Gallardo, J., Prashanth, G., and Kanan, C. What variables affect out-of-distribution generalization in pretrained models? In *The Thirty-eighth Annual Conference on Neural Information Processing Systems*, 2024. URL <https://openreview.net/forum?id=pOXgdFEB7q>.
- He, K., Zhang, X., Ren, S., and Sun, J. Deep residual learning for image recognition. In *Proceedings of the IEEE conference on computer vision and pattern recognition*, pp. 770–778, 2016.
- He, K., Chen, X., Xie, S., Li, Y., Dollár, P., and Girshick, R. Masked autoencoders are scalable vision learners. In *Proceedings of the IEEE/CVF Conference on Computer Vision and Pattern Recognition*, pp. 16000–16009, 2022.
- Huang, W., Ye, M., Shi, Z., Li, H., and Du, B. Rethinking federated learning with domain shift: A prototype view. In *2023 IEEE/CVF Conference on Computer Vision and Pattern Recognition (CVPR)*, pp. 16312–16322. IEEE, 2023.
- Hull, J. J. A database for handwritten text recognition research. *IEEE Trans. Pattern Anal. Mach. Intell.*, 16(5): 550–554, 1994.
- Imteaj, A. and Amini, M. H. Leveraging asynchronous federated learning to predict customers financial distress. *Intelligent Systems with Applications*, 14:200064, 2022.

- Jin, H., Bai, D., Yao, D., Dai, Y., Gu, L., Yu, C., and Sun, L. Personalized edge intelligence via federated self-knowledge distillation. *IEEE Transactions on Parallel and Distributed Systems*, 34(2):567–580, 2022.
- Jordan, C. Essai sur la géométrie à n dimensions. *Bulletin de la Société mathématique de France*, 3:103–174, 1875.
- Karimireddy, S. P., Kale, S., Mohri, M., Reddi, S., Stich, S., and Suresh, A. T. Scaffold: Stochastic controlled averaging for federated learning. In *International conference on machine learning*, pp. 5132–5143. PMLR, 2020.
- Krizhevsky, A., Sutskever, I., and Hinton, G. E. Imagenet classification with deep convolutional neural networks. *Advances in neural information processing systems*, 25, 2012.
- Kumar, A., Raghunathan, A., Jones, R. M., Ma, T., and Liang, P. Fine-tuning can distort pretrained features and underperform out-of-distribution. In *International Conference on Learning Representations*, 2022. URL <https://openreview.net/forum?id=UYneFzXSJWh>.
- LeCun, Y., Bottou, L., Bengio, Y., and Haffner, P. Gradient-based learning applied to document recognition. *Proc. IEEE (USA)*, pp. 2278–2324, 1998.
- Lee, G., Jeong, M., Shin, Y., Bae, S., and Yun, S.-Y. Preservation of the global knowledge by not-true distillation in federated learning. *Advances in Neural Information Processing Systems*, 35:38461–38474, 2022.
- Li, D., Yang, Y., Song, Y.-Z., and Hospedales, T. M. Deeper, broader and artier domain generalization. In *Proceedings of the IEEE international conference on computer vision*, pp. 5542–5550, 2017.
- Li, Q., He, B., and Song, D. Model-contrastive federated learning. In *Proceedings of the IEEE/CVF conference on computer vision and pattern recognition*, pp. 10713–10722, 2021a.
- Li, T., Sahu, A. K., Zaheer, M., Sanjabi, M., Talwalkar, A., and Smith, V. Federated optimization in heterogeneous networks. *Proceedings of Machine learning and systems*, 2:429–450, 2020.
- Li, X., JIANG, M., Zhang, X., Kamp, M., and Dou, Q. Fedbn: Federated learning on non-iid features via local batch normalization. In *International Conference on Learning Representations*, 2021b.
- Li, X., Liu, S., Zhou, J., Lu, X., Fernandez-Granda, C., Zhu, Z., and Qu, Q. Understanding and improving transfer learning of deep models via neural collapse. *Transactions on Machine Learning Research*, 2024. ISSN 2835-8856. URL <https://openreview.net/forum?id=o8r84MzTQB>.
- Li, Z., Shang, X., He, R., Lin, T., and Wu, C. No fear of classifier biases: Neural collapse inspired federated learning with synthetic and fixed classifier. In *Proceedings of the IEEE/CVF International Conference on Computer Vision (ICCV)*, pp. 5319–5329, October 2023.
- Liang, P. P., Liu, T., Ziyin, L., Allen, N. B., Auerbach, R. P., Brent, D., Salakhutdinov, R., and Morency, L.-P. Think locally, act globally: Federated learning with local and global representations. *arXiv preprint arXiv:2001.01523*, 2020.
- Luo, M., Chen, F., Hu, D., Zhang, Y., Liang, J., and Feng, J. No fear of heterogeneity: Classifier calibration for federated learning with non-iid data. *Advances in Neural Information Processing Systems*, 34:5972–5984, 2021.
- Masarczyk, W., Ostaszewski, M., Imani, E., Pascanu, R., Miłoś, P., and Trzcinski, T. The tunnel effect: Building data representations in deep neural networks. *Advances in Neural Information Processing Systems*, 36, 2024.
- McMahan, B., Moore, E., Ramage, D., Hampson, S., and y Arcas, B. A. Communication-efficient learning of deep networks from decentralized data. In *Artificial intelligence and statistics*, pp. 1273–1282. PMLR, 2017.
- Netzer, Y., Wang, T., Coates, A., Bissacco, A., Wu, B., and Ng, A. Y. Reading digits in natural images with unsupervised feature learning. 2011.
- Oh, J., Kim, S., and Yun, S.-Y. Fedbabu: Toward enhanced representation for federated image classification. In *International Conference on Learning Representations*, 2022.
- Papayan, V., Han, X., and Donoho, D. L. Prevalence of neural collapse during the terminal phase of deep learning training. *Proceedings of the National Academy of Sciences*, 117(40):24652–24663, 2020.
- Paszke, A., Gross, S., Massa, F., Lerer, A., Bradbury, J., Chanan, G., Killeen, T., Lin, Z., Gimelshein, N., Antiga, L., et al. Pytorch: An imperative style, high-performance deep learning library. *Advances in neural information processing systems*, 32, 2019.
- Peng, X., Bai, Q., Xia, X., Huang, Z., Saenko, K., and Wang, B. Moment matching for multi-source domain adaptation. In *Proceedings of the IEEE/CVF international conference on computer vision*, pp. 1406–1415, 2019.

- Raghu, M., Unterthiner, T., Kornblith, S., Zhang, C., and Dosovitskiy, A. Do vision transformers see like convolutional neural networks? *Advances in neural information processing systems*, 34:12116–12128, 2021.
- Rangamani, A., Lindegaard, M., Galanti, T., and Poggio, T. A. Feature learning in deep classifiers through intermediate neural collapse. In *International Conference on Machine Learning*, pp. 28729–28745. PMLR, 2023.
- Sarfi, A. M., Karimpour, Z., Chaudhary, M., Khalid, N. M., Ravanelli, M., Mudur, S., and Belilovsky, E. Simulated annealing in early layers leads to better generalization. In *Proceedings of the IEEE/CVF Conference on Computer Vision and Pattern Recognition*, pp. 20205–20214, 2023.
- Shi, Y., Liang, J., Zhang, W., Tan, V., and Bai, S. Towards understanding and mitigating dimensional collapse in heterogeneous federated learning. In *The Eleventh International Conference on Learning Representations*, 2023a. URL <https://openreview.net/forum?id=EXnIyMVTl8s>.
- Shi, Y., Liang, J., Zhang, W., Xue, C., Tan, V. Y., and Bai, S. Understanding and mitigating dimensional collapse in federated learning. *IEEE Transactions on Pattern Analysis and Machine Intelligence*, 2023b.
- Simonyan, K. and Zisserman, A. Very deep convolutional networks for large-scale image recognition. *arXiv preprint arXiv:1409.1556*, 2014.
- Stich, S. U. Local sgd converges fast and communicates little. In *International Conference on Learning Representations*, 2018.
- Sun, B., Huo, H., Yang, Y., and Bai, B. Partialfed: Cross-domain personalized federated learning via partial initialization. *Advances in Neural Information Processing Systems*, 34:23309–23320, 2021.
- Tan, Y., Long, G., Liu, L., Zhou, T., Lu, Q., Jiang, J., and Zhang, C. Fedproto: Federated prototype learning across heterogeneous clients. In *Proceedings of the AAAI Conference on Artificial Intelligence*, volume 36, pp. 8432–8440, 2022.
- Wang, L., Zhang, K., Li, Y., Tian, Y., and Tedrake, R. Does learning from decentralized non-iid unlabeled data benefit from self supervision? In *The Eleventh International Conference on Learning Representations*, 2023a.
- Wang, L., Bian, J., Zhang, L., Chen, C., and Xu, J. Taming cross-domain representation variance in federated prototype learning with heterogeneous data domains. In *The Thirty-eighth Annual Conference on Neural Information Processing Systems*, 2024. URL <https://openreview.net/forum?id=6SRPizFuaE>.
- Wang, P., Li, X., Yaras, C., Zhu, Z., Balzano, L., Hu, W., and Qu, Q. Understanding deep representation learning via layerwise feature compression and discrimination. *arXiv preprint arXiv:2311.02960*, 2023b.
- Woodworth, B., Patel, K. K., Stich, S., Dai, Z., Bullins, B., McMahan, B., Shamir, O., and Srebro, N. Is local sgd better than minibatch sgd? In *International Conference on Machine Learning*, pp. 10334–10343. PMLR, 2020.
- Wu, X., Niu, J., Liu, X., Ren, T., Huang, Z., and Li, Z. pfdedf: Enabling personalized federated learning via gradient fusion. In *2022 IEEE International Parallel and Distributed Processing Symposium (IPDPS)*, pp. 639–649. IEEE, 2022.
- Wu, X., Liu, X., Niu, J., Zhu, G., and Tang, S. Bold but cautious: Unlocking the potential of personalized federated learning through cautiously aggressive collaboration. In *Proceedings of the IEEE/CVF International Conference on Computer Vision*, pp. 19375–19384, 2023.
- Wu, X., Liu, X., Niu, J., Wang, H., Tang, S., Zhu, G., and Su, H. Decoupling general and personalized knowledge in federated learning via additive and low-rank decomposition. *arXiv preprint arXiv:2406.19931*, 2024.
- Yao, D., Zhu, Z., Liu, T., Xu, Z., and Jin, H. Rethinking personalized federated learning from knowledge perspective. In *Proceedings of the 53rd International Conference on Parallel Processing*, pp. 991–1000, 2024.
- Yosinski, J., Clune, J., Bengio, Y., and Lipson, H. How transferable are features in deep neural networks? *Advances in neural information processing systems*, 27, 2014.
- Zeiler, M. D. and Fergus, R. Visualizing and understanding convolutional networks. In *Computer Vision—ECCV 2014: 13th European Conference, Zurich, Switzerland, September 6–12, 2014, Proceedings, Part I 13*, pp. 818–833. Springer, 2014.
- Zhao, Y., Li, M., Lai, L., Suda, N., Civin, D., and Chandra, V. Federated learning with non-iid data. *arXiv preprint arXiv:1806.00582*, 2018.
- Zheng, K., Liu, X., Zhu, G., Wu, X., and Niu, J. Channelfed: Enabling personalized federated learning via localized channel attention. In *GLOBECOM 2022-2022 IEEE Global Communications Conference*, pp. 2987–2992. IEEE, 2022.
- Zhou, T., Zhang, J., and Tsang, D. H. Fedfa: Federated learning with feature anchors to align features and classifiers for heterogeneous data. *IEEE Transactions on Mobile Computing*, 2023.

Zhu, G., Liu, X., Tang, S., and Niu, J. Aligning before aggregating: Enabling cross-domain federated learning via consistent feature extraction. In *2022 IEEE 42nd International Conference on Distributed Computing Systems (ICDCS)*, pp. 809–819. IEEE, 2022.

Zhu, G., Liu, X., Tang, S., and Niu, J. Aligning before aggregating: Enabling communication efficient cross-domain federated learning via consistent feature extraction. *IEEE Transactions on Mobile Computing*, 2023.

Zhu, H., Xu, J., Liu, S., and Jin, Y. Federated learning on non-iid data: A survey. *Neurocomputing*, 465:371–390, 2021.

A. Related Work

Federated Learning. FedAvg (McMahan et al., 2017) is widely recognized as the pioneering work in FL. It facilitates collaborative model training by iteratively performing independent training on each client and aggregating the models on the server. While FedAvg demonstrates satisfactory performance in IID settings (Stich, 2018; Woodworth et al., 2020), a performance drop is commonly observed when data distributions are non-IID. This phenomenon has led to multiple explanations for the degradation, such as ‘client drift’ (Zhao et al., 2018; Karimireddy et al., 2020) and ‘knowledge forgetting’ (Jin et al., 2022). To address the challenges posed by non-IID data, various solutions have been proposed, including local model regularization (Li et al., 2020), correction techniques (Karimireddy et al., 2020; Wu et al., 2022), knowledge distillation (Jin et al., 2022; Lee et al., 2022), and partial parameter personalization (Li et al., 2021b; Collins et al., 2021; Arivazhagan et al., 2019; Liang et al., 2020; Sun et al., 2021; Zheng et al., 2022; Wu et al., 2023; 2024). However, these methods generally adhere to the standard framework of local training and global aggregation introduced by FedAvg. There remains a lack of in-depth exploration into how model aggregation intuitively impacts model training from a feature extraction perspective.

Federated Learning within Feature Space. Numerous studies have recently observed that heterogeneous data can lead to suboptimal feature extraction in FL models and are working on improving FL models by directly calibrating the resulting suboptimal feature spaces. A common line of research attributes performance degradation to inconsistent feature spaces across clients. To tackle this problem, CCVR (Luo et al., 2021) introduces a post-calibration strategy that fine-tunes the classifier after FL training using virtual features generated by an approximate Gaussian Mixture Model (GMM). Several methods (Tan et al., 2022; Zhu et al., 2022; 2023; Zhou et al., 2023; Huang et al., 2023) propose using prototypes to align feature distributions across different clients, ensuring a consistent feature space. Studies such as FedBABU (Oh et al., 2022), SphereFed (Dong et al., 2022), and FedETF (Li et al., 2023) utilize various fixed classifiers (e.g., random or orthogonal initialization) as targets to align features across clients. In addition to inconsistent feature spaces, FedDecorr (Shi et al., 2023a;b) observed that heterogeneous data leads to severe dimensional collapse in the global model. To combat this, it applies a regularization term based on the Frobenius norm of the correlation matrix during local training, encouraging the different dimensions of features to remain uncorrelated. FedPLVM (Wang et al., 2024) discovers differences in domain-specific feature variance in cross-domain FL. Consequently, they propose dual-level prototype clustering that adeptly captures variance information and addresses the aforementioned problem. However, these studies primarily focus on calibrating features in the penultimate layer while overlooking intermediate features during feature extraction. In this paper, we present a layer-peeled analysis of how model aggregation affects the feature extraction process and identify several issues related to the hierarchical topology of DNNs.

Feature Learning in DNNs. Advanced DNNs are typically structured with hierarchical layers, enabling them to efficiently and automatically extract informative features from raw data (Krizhevsky et al., 2012; Allen-Zhu & Li, 2023; Wang et al., 2023b). Numerous efforts have been made to understand how DNNs transform raw data from shallow to deep layers. A commonly accepted view is that DNNs initially extract transferable universal features and then progressively filter out irrelevant information to form task-specific features (Yosinski et al., 2014; Zeiler & Fergus, 2014; Evci et al., 2022; Kumar et al., 2022). Another line of studies demonstrates that DNNs progressively learn features that are compressed within classes and discriminative between classes. Specifically, (Alain & Bengio, 2017) observes that the linear separability of features increases as the layers become deeper, using a linear probe. (Masarczyk et al., 2024) proposes the tunnel effect hypothesis, which states that the initial layers create linearly separable features, while the subsequent layers (referred to as the tunnel) compress these features. Meanwhile, certain research has extended the feature analysis of neural collapse (NC) originally observed in the penultimate layers (Papayan et al., 2020) to intermediate layers (Ansuini et al., 2019; Rangamani et al., 2023; Li et al., 2024), showing that the features of each layer exhibit gradual collapse as layer depth increases. (Wang et al., 2023b) provides a theoretical analysis of feature evolution across depth based on deep linear networks (DLNs). Although these studies focus on centralized training where there is no model aggregation during training, They provide solid support for us to effectively analyze feature evolution in FL, especially the influence of model aggregation on feature extraction.

B. Dataset Description and Partition

In the experiments, we primarily focus on the data-heterogeneous FL setting, where the distribution of raw input data differs across clients. This data heterogeneity, often referred to as cross-domain FL, is commonly observed in practical FL applications due to variations in data collection conditions across clients. Building on previous studies (Li et al., 2021b; Zhu et al., 2022; 2023; Wang et al., 2024), we use three widely used public cross-domain datasets: Digit-Five, PACS (Li et al.,

2017), and DomainNet (Peng et al., 2019). These datasets contain multiple domains, with each domain consisting of images with different backgrounds and styles, which effectively simulate the data heterogeneity caused by variations in raw input.

The Digit-Five dataset includes images across 10 classes and 5 domains, namely: MNIST-M (Ganin & Lempitsky, 2015), MNIST (LeCun et al., 1998), USPS (Hull, 1994), SynthDigits (Ganin & Lempitsky, 2015), and SVHN (Netzer et al., 2011). The PACS dataset includes 4 distinct domains with a total of 7 classes: Photo (P), Art (A), Cartoon (C), and Sketch (S). The DomainNet dataset comprises six domains: Clipart (C), Infograph (I), Painting (P), Quickdraw (Q), Real (R), and Sketch (S). Initially, the DomainNet dataset includes 345 classes per domain. Based on prior research (Li et al., 2021b; Zhu et al., 2022), we reduce the number of classes to 10 commonly used ones for our layer-peeled feature analysis. Figure 18 shows some example images from these three datasets. The representative images demonstrate significant variations across different domains, as observed in Figure 18.

To create the data-heterogeneous setting across different clients, we assign the images from a single domain to each client. As a result, there are 5 clients for the Digit-Five dataset, 4 clients for PACS, and 6 clients for DomainNet in our analysis. For the Digit-Five dataset, the number of training and testing samples are set to 500 and 1000, respectively. For both the PACS and DomainNet datasets, the number of training and testing samples is set to 500. The images in the Digit-Five dataset are scaled to 32×32 for both the training and testing datasets. For PACS and DomainNet, the images are scaled to 224×224 and we apply data augmentations such as random flipping and rotation for the training samples. No data augmentations are applied to the Digit-Five or test datasets across all experiments.

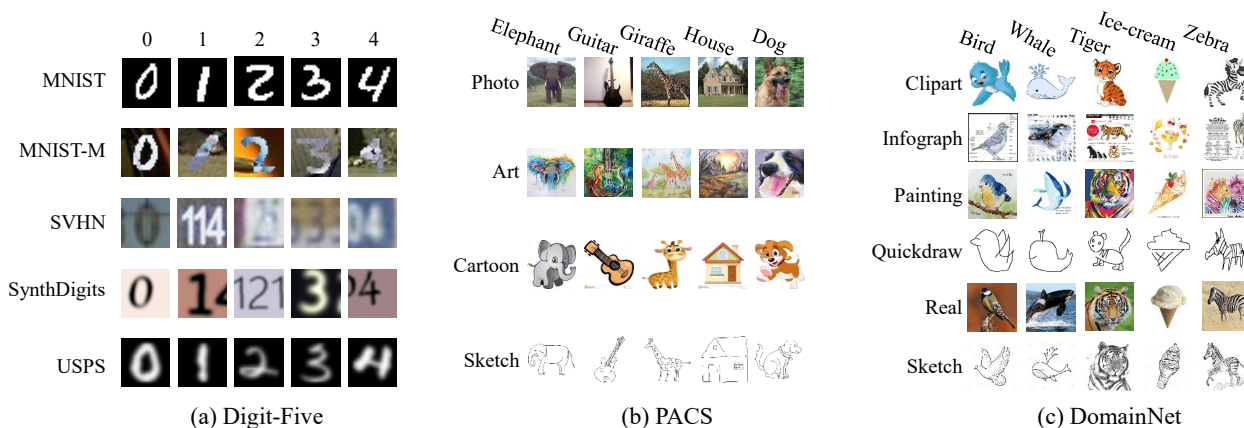


Figure 18. Visualization of example samples within the datasets used for layer-wise feature evaluation: (a) Digit-Five, (b) PACS, (c) DomainNet. For each domain within these adopted datasets, we show the representative samples from 5 classes.

C. Model Architectures

We utilize multiple models for the selected datasets to perform layer-wise feature extraction analysis, including both Convolutional Neural Networks (CNN) and Vision Transformers (ViT). Specifically, the CNN models we employ are ConvNet, VGG13_BN (Simonyan & Zisserman, 2014), and three variants of ResNet (He et al., 2016) (ResNet18, ResNet34, and ResNet50). For the ViT architecture, we apply ViT_B/16 (Dosovitskiy et al., 2021).

The ConvNet model consists of several convolutional layers followed by fully connected (FC) layers. The detailed architecture of ConvNet is presented in Table 1, with the output size calculated using the input scale of the Digit-Five dataset as an example. For the other models, we modify only the classifiers by adjusting the number of output classes to match the requirements of our dataset, while leaving the backbone architecture unchanged.

For the Digit-Five dataset, we use ConvNet, ResNet18, and ResNet34 for FL training. For both PACS and DomainNet datasets, we utilize ConvNet, VGG1_BN, ResNet18, ResNet34, ResNet50, and ViT_B/16 to accomplish the FL training.

Table 1: Detailed Architecture of ConvNet

Layer	Output Size	Description
Input	32x32x3	Input image
Conv1_1	32x32x64	5x5 Convolution, 64 filters, stride 1, padding 2
BN1_1	32x32x64	Batch Normalization
ReLU1_1	32x32x64	ReLU activation
MaxPool1_1	16x16x64	2x2 Max Pooling, stride 2
Conv1_2	16x16x64	5x5 Convolution, 64 filters, stride 1, padding 2
BN1_2	16x16x64	Batch Normalization
ReLU1_2	16x16x64	ReLU activation
MaxPool1_2	8x8x64	2x2 Max Pooling, stride 2
Conv1_3	8x8x128	5x5 Convolution, 128 filters, stride 1, padding 2
BN1_3	8x8x128	Batch Normalization
ReLU1_3	8x8x128	ReLU activation
Flatten	8192	Flatten layer for fully connected input
Linear2_1	2048	Fully connected layer, 2048 units
BN2_1	2048	Batch Normalization
ReLU2_1	2048	ReLU activation
Linear2_2	512	Fully connected layer, 512 units
BN2_2	512	Batch Normalization
ReLU2_2	512	ReLU activation
Output (C)	C	Output layer (number of classes)

D. Implementation Details of Experiments

In our experiments, we train the model using the standard FL training process introduced by FedAvg (McMahan et al., 2017). This process involves iterative local model updating and global model aggregation. During the local updating phase, the model is optimized using each client’s private data for E epochs, after which the local models are uploaded to the server for aggregation. In the model aggregation stage, we apply parameter-wise averaging, using the number of samples as weights for each client’s local model. The above procedures are repeated for R global rounds until the global model converges.

For local model updating, we use stochastic gradient descent (SGD) with momentum for model optimization, where the learning rate is set to 0.01 and the momentum is set to 0.5. The batch size for local updates is set to 64. Unless otherwise specified, the number of local update epochs E is set to 10, and the number of global rounds R is set to 50.

All of our experiments are conducted using the PyTorch framework (Paszke et al., 2019) and implemented on a four-card Nvidia V100 cluster. During the layer-peeled feature analysis, we use the *forward hook* in PyTorch to extract input features from each evaluated layer as we move from shallow to deeper layers.

For ConvNet, the features preceding each convolutional and linear layer are used for evaluation. For ResNet, the features before each convolutional layer (excluding the first convolutional layer), the global average pooling layer, and the classifier are used for evaluation. For VGG13_BN, the features before each convolutional layer, the linear layers, and the classifier are used for evaluation. For ViT_B/16, we evaluate the features passed to the multilayer perceptron (MLP), self-attention layers, layer normalization layers, and the final classifier.

To reduce computational cost during feature evaluation, we apply average pooling to the intermediate features, thereby lowering their dimensionality. For CNNs, let the intermediate features at the ℓ -th layer be represented as $B \times H^\ell \times W^\ell \times C^\ell$, where B denotes the batch size, and H^ℓ , W^ℓ , and C^ℓ are the height, width, and channel dimensions, respectively. Following previous studies (Sarfı et al., 2023; Harun et al., 2024), we apply 2×2 adaptive average pooling to the height and width dimensions ($H^\ell \times W^\ell$). After this adaptive average pooling operation, the intermediate features within the convolutional layers are reduced to $B \times 2 \times 2 \times C^\ell$. We then flatten this tensor into a one-dimensional vector and compute the feature metrics, where the features of one sample within the batch has a dimension of $4C^\ell$, and the total dimension of the samples within the batch is $B \times 4C^\ell$. For ViTs, following previous studies Raghu et al. (2021); Harun et al. (2024), we apply global average pooling to aggregate the image tokens, excluding the class token. For features input to the linear layer with a

two-dimensional shape of $B \times D^\ell$, we directly use these features to perform evaluation.

During feature evaluation, we process the features in a batch-wise manner, concatenating them across all batches in the evaluated dataset. The corresponding feature metrics are then computed based on these concatenated features. For all experiments, we evaluate the features every 20 local updating epochs, which corresponds to 2 global rounds when the local update epoch is set to 10. To minimize the impact of randomness, each experiment is repeated three times with different random seeds.

E. Feature Evaluation Metrics

We apply the following metrics to evaluate the features generated by the pre-aggregated model and post-aggregated model, including the *feature variance*, *alignment between features and parameters*, *accuracy of linear probing*, *pairwise distance of features and models*, *relative change of evaluated metrics*. For simplicity, we omit the client and sample indices and focus solely on the computation process of these metrics. As previously stated, the features in our experiments are first stacked into a two-dimensional tensor, and then used to compute the feature metrics. We assume that the stacked features at ℓ -th layer is denoted as $\mathbf{Z}^\ell \in \mathbb{R}^{N \times D^\ell}$, where N is the total number of samples used for feature evaluation, and D^ℓ denote the feature dimension for one sample at ℓ -th layer. The metrics used to evaluate features in this paper are computed as follows.

E.1. Feature Variance

Building on previous studies (Rangamani et al., 2023; Wang et al., 2023b), we use within-class feature variance and between-class feature variance to evaluate the feature structure. Specifically, the within-class variance quantifies the degree of feature compression within the same class, while the between-class variance measures the degree of feature discrimination between different classes.

Before calculating the within-class and between-class variances, we first compute the within-class, between-class, and total covariance matrices of the features at ℓ -th layer as follows:

$$\begin{aligned}\Sigma_W^\ell &= \frac{1}{N} \sum_{c=1}^C \sum_{i=1}^{N_c} (\mathbf{z}_{c,i}^\ell - \boldsymbol{\mu}_c^\ell) (\mathbf{z}_{c,i}^\ell - \boldsymbol{\mu}_c^\ell)^\top \\ \Sigma_B^\ell &= \frac{1}{C} \sum_{c=1}^C (\boldsymbol{\mu}_c^\ell - \boldsymbol{\mu}_G^\ell) (\boldsymbol{\mu}_c^\ell - \boldsymbol{\mu}_G^\ell)^\top \\ \Sigma_T^\ell &= \frac{1}{N} \sum_{c=1}^C \sum_{i=1}^{N_c} (\mathbf{z}_{c,i}^\ell - \boldsymbol{\mu}_G^\ell) (\mathbf{z}_{c,i}^\ell - \boldsymbol{\mu}_G^\ell)^\top,\end{aligned}\tag{5}$$

where

$$\boldsymbol{\mu}_c^\ell := \frac{1}{N_c} \sum_{i=1}^{N_c} \mathbf{z}_{c,i}^\ell \quad \boldsymbol{\mu}_G^\ell := \frac{1}{N} \sum_{c=1}^C \sum_{i=1}^{N_c} \mathbf{z}_{c,i}^\ell.\tag{6}$$

In the above equation, $\boldsymbol{\mu}_c^\ell$ is the mean class feature computed from the samples within the c -th class, and $\boldsymbol{\mu}_G^\ell$ as the global mean feature computed from all samples. N_c represents the number of samples within the c -th class. It should be noted that the total covariance matrix can be decomposed as the sum of the within-class and between-class covariances, i.e.,

$$\Sigma_T^\ell = \Sigma_W^\ell + \Sigma_B^\ell.\tag{7}$$

Based on the computed covariance matrices, we then use the total variance $\text{Tr}(\Sigma_T^\ell)$ as the normalization factor and compute the normalized within-class variance and between-class variance as follows:

$$\bar{\sigma}_W^\ell = \frac{\text{Tr}(\Sigma_W^\ell)}{\text{Tr}(\Sigma_T^\ell)},\tag{8}$$

$$\bar{\sigma}_B^\ell = \frac{\text{Tr}(\Sigma_B^\ell)}{\text{Tr}(\Sigma_T^\ell)}, \quad (9)$$

where $\text{Tr}(\cdot)$ denotes the trace of the covariance matrices. These two normalized variances are used to measure the within-class feature compression and between-class feature discrimination, respectively, in this paper.

E.2. alignment between features and parameters

Following previous studies, we use the principal angles between subspaces (PABS) (Rangamani et al., 2023; Jordan, 1875; Björck & Golub, 1973) denoted as $\theta_1, \dots, \theta_C$ to measure the alignment between the range space of class-wise feature means $\bar{\mathbf{Z}}^\ell$ and the top C -rank subspace of the subsequent input layer parameters $\mathbf{W}^{\ell+1}$.

Specifically, for a linear layer, we first apply singular value decomposition (SVD) to $\mathbf{W}^{\ell+1}$ and $\bar{\mathbf{Z}}^\ell$, i.e., $\mathbf{W}^{\ell+1} = \mathbf{U}_W^{\ell+1} \mathbf{S}_W^{\ell+1} (\mathbf{V}_W^{\ell+1})^T$ and $\bar{\mathbf{Z}}^\ell = \mathbf{U}_Z^\ell \mathbf{S}_Z^\ell (\mathbf{V}_Z^\ell)^T$. We then compute the PABS between $\mathbf{V}_W^{\ell+1}$ and \mathbf{U}_Z^ℓ , which represent the basis for the input subspace $\mathbf{W}^{\ell+1}$ and the range space of $\bar{\mathbf{Z}}^\ell$, respectively. The alignment is finally computed by the mean of the singular values of $(\mathbf{V}_W^{\ell+1})^T \mathbf{U}_Z^\ell$.

For the convolutional layer, assume the filter kernel has shape $\mathbf{W}^{\ell+1} \in \mathbb{R}^{C_{\text{out}}^{\ell+1} \times C_{\text{in}}^\ell \times k_H^{\ell+1} \times k_W^{\ell+1}}$, and the class-wise feature means have shape $\bar{\mathbf{Z}}^\ell \in \mathbb{R}^{C \times C_{\text{in}}^\ell \times H^\ell \times W^\ell}$. As previously stated, $\bar{\mathbf{Z}}^\ell$ can be reshaped into $C \times (C_{\text{in}}^\ell \times 4)$. We begin by flattening the features and parameters along the C_{in}^ℓ dimension, resulting in shapes $C_{\text{in}}^\ell \times (C \times 4)$ for the features and $C_{\text{in}}^\ell \times (C_{\text{out}}^{\ell+1} \times k_H^{\ell+1} \times k_W^{\ell+1})$ for the parameters. We then compute the alignment along the C_{in}^ℓ dimension as described above.

For the self-attention layer in a ViT, we compute the alignments of the features and the QKV matrices separately, and then take the average of these alignments as the final metric.

E.3. Stable Rank

The stable rank of a feature matrix identifies redundant or highly correlated features within a dataset, which is a measure that combines both the matrix’s rank and its singular values. It is defined as the ratio of the squared Frobenius norm of the matrix to the squared largest singular value. In our experiments, we compute the stable rank of centered features for each class and then average them. Mathematically, for a centered feature matrix of c -th class $\bar{\mathbf{Z}}_c^\ell$, the stable rank is given by:

$$\text{SRank}(\bar{\mathbf{Z}}_c^\ell) = \frac{\|\bar{\mathbf{Z}}_c^\ell\|_F^2}{\sigma_{\max}(\bar{\mathbf{Z}}_c^\ell)^2}, \quad (10)$$

where $\|\bar{\mathbf{Z}}_c^\ell\|_F$ is the Frobenius norm of $\bar{\mathbf{Z}}_c^\ell$, which is the square root of the sum of the squares of all entries in the feature matrix, and $\sigma_{\max}(\bar{\mathbf{Z}}_c^\ell)$ is the largest singular value of $\bar{\mathbf{Z}}_c^\ell$. It provides a more stable approximation of the rank by accounting for the distribution of the singular values, rather than just the rank itself. Unlike the true rank, which can be sensitive to small changes in the matrix, the stable rank remains more robust to perturbations in data. In our experiments, we average the stable rank of each class to obtain the stable rank of the given evaluated dataset, that is:

$$\text{SRank}(\bar{\mathbf{Z}}^\ell) = \frac{1}{C} \sum_{c=1}^C \bar{\mathbf{Z}}_c^\ell, \quad (11)$$

where C denotes the total number of classes.

E.4. Accuracy of Linear Probing

Linear probing is a technique used in transfer learning to evaluate the quality of learned features by training a simple linear classifier on top of the features extracted from a pre-trained model (Chen et al., 2020; He et al., 2022; Wang et al., 2023a). In this paper, we employ the linear probing technique to assess feature generalization across diverse data distributions. Specifically, after extracting features from different layers, we apply a randomly initialized linear classifier on top of these features. This classifier is then trained using the training subset of the evaluated datasets, and we compute accuracy by testing on the corresponding samples from the test datasets. The testing accuracy serves as the metric for evaluating feature generalization on each dataset.

E.5. Pairwise Distance of Features and Models

We use four metrics to evaluate the distance between two models or the features extracted by them: *mean normalized L_1 distance*, *mean squared distance*, *mean L_1 distance*, and *cosine similarity*. In this section, we focus on the computation of the distance between features, since the model parameters are reshaped into a single vector, which can be treated as a feature with a sample size of 1. Thus, the distance computation is applied to these features can be directly transferred to models. Let the features of the pre-aggregated and post-aggregated models be denoted as \mathbf{Z}_{pre}^ℓ and \mathbf{Z}_{post}^ℓ , respectively. The corresponding distance can then be computed as follows.

- **Mean Normalized L_1 Distance.** This measure computes the mean normalized L_1 distance between the pre-aggregated and post-aggregated feature matrices, and then averages the distances across all elements, as shown below.

$$D_{L_1}^\ell = \frac{1}{ND} \sum_{i=1}^N \sum_{j=1}^D \frac{|\mathbf{Z}_{pre}^\ell(i, j) - \mathbf{Z}_{post}^\ell(i, j)|}{|\mathbf{Z}_{pre}^\ell(i, j)| + |\mathbf{Z}_{post}^\ell(i, j)|} \quad (12)$$

- **Mean Squared Error.** This distance measure computes the average squared differences between corresponding elements of the feature vectors, as shown below.

$$D_s^\ell = \frac{1}{ND} \sum_{i=1}^N \sum_{j=1}^D (\mathbf{Z}_{pre}^\ell(i, j) - \mathbf{Z}_{post}^\ell(i, j))^2 \quad (13)$$

- **Mean L_1 Distance.** This distance computes the average L_1 distances between corresponding elements of the pre-aggregated and post-aggregated feature matrices, as shown below.

$$D_{L_1}^\ell = \frac{1}{ND} \sum_{i=1}^N \sum_{j=1}^D |\mathbf{Z}_{pre}^\ell(i, j) - \mathbf{Z}_{post}^\ell(i, j)| \quad (14)$$

- **Mean Cosine Similarity.** This measure computes the cosine of the angle between the pre-aggregated and post-aggregated features of the same samples, and then averages these values across all clients. It quantifies the cosine of the angle between the pre-aggregated and post-aggregated features, where a value of 1 indicates identical directions and a value of -1 indicates opposite directions. The formulation of the mean cosine similarity is shown below.

$$D_{cos}^\ell = \frac{1}{N} \sum_{i=1}^N \frac{\mathbf{Z}_{pre}^\ell(i, :) \cdot \mathbf{Z}_{post}^\ell(i, :)}{\|\mathbf{Z}_{pre}^\ell(i, :)\| \|\mathbf{Z}_{post}^\ell(i, :)\|} \quad (15)$$

where $\mathbf{Z}_{pre}^\ell(i, :) \cdot \mathbf{Z}_{post}^\ell(i, :)$ denotes the dot product of the pre-aggregated and post-aggregated features of sample i at ℓ -th layer, respectively, and $\|\mathbf{Z}_{pre}^\ell(i, :)\|$ and $\|\mathbf{Z}_{post}^\ell(i, :)\|$ denote the Euclidean norms of the pre-aggregated and post-aggregated features at ℓ -th layer, respectively.

E.6. Relative Change of Evaluated Metrics

Since the original metrics of features at different layers can vary in magnitude, we use the relative change in the evaluated metrics to measure the ratio of change before and after aggregation. Let V_{pre}^ℓ and V_{post}^ℓ represent the metrics of features generated by the models before and after aggregation at ℓ -th layer, respectively. The relative change in the evaluated metrics is then defined as:

$$\Delta^\ell(V) = \frac{|V_{post}^\ell - V_{pre}^\ell|}{|V_{pre}^\ell| + |V_{post}^\ell|} * 100\%. \quad (16)$$

F. Detailed Results of Performance Drop

In this section, we provide more detailed results that demonstrate the performance drop during model aggregation. In these experiments, we perform inference on both the training and testing datasets using the pre-aggregated and post-aggregated

models. The experimental results are shown in Figure 19. These experiments are conducted on different datasets, including Digit-Five, PACS, and DomainNet, and on various model architectures. From Figure 19, we can observe that the performance drop introduced by model aggregation is consistent across all adopted datasets and model architectures, on both training and testing dataset. The performance drop consistently occurs throughout the entire training procedure of FL. These results indicate that the performance drop during model aggregation is a common phenomenon in FL.

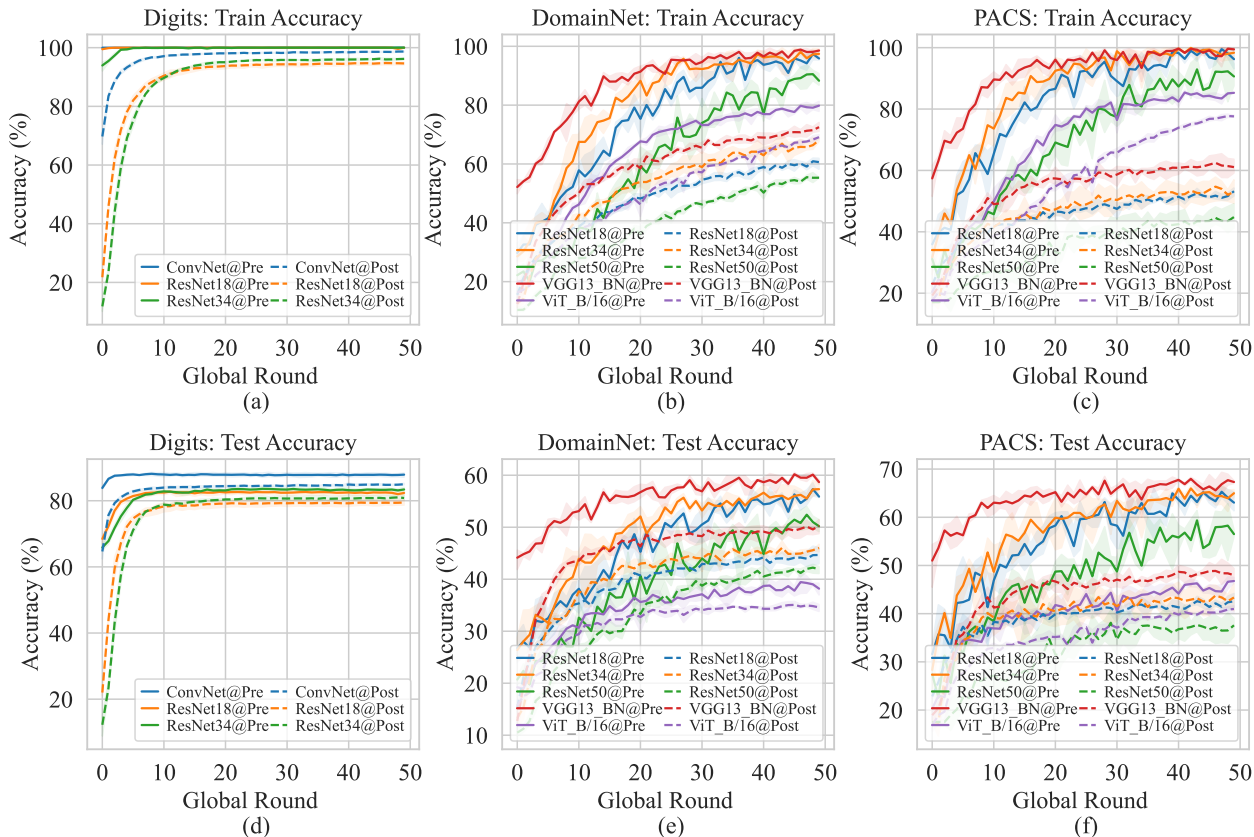


Figure 19. Training and testing accuracy curves of the model before and after aggregation, evaluated on the local dataset during FL training. The experiments are conducted on Digit-Five, DomainNet, and PACS, using multiple model architectures as the backbone.

G. Detailed Results of Feature Variance

In this section, we provide a detailed analysis of the layer-wise feature variance during FL training. Our experiments are conducted on three datasets: Digit-Five, PACS, and DomainNet, using various model architectures, as previously described. For each dataset, we present four types of feature variances: normalized within-class feature variance, normalized between-class feature variance, original unnormalized within-class feature variance, and original unnormalized between-class feature variance.

To better visualize feature evolution over time (across different epochs of FL training) and space (across different layers), we employ two types of visualizations. The first visualizes feature changes across different layers while keeping the training global round fixed. The second focuses on visualizing feature evolution across training rounds while fixing specific layers.

The experimental results are presented in the following sections. From these results, we observe that both the original within-class and between-class feature variances increase as the layer depth increases. In contrast, the normalized within-class feature variance decreases with both layer depth and training rounds, which is in contrast to the normalized between-class feature variance. This suggests that features within the same class become more compressed, while features across different classes become more discriminative.

However, after model aggregation, the normalized within-class variance increases while the normalized between-class

variance decreases. This indicates that model aggregation disrupts the feature compression objective during DNN training. More importantly, this disruption progressively accumulates across model layers, causing the features in the penultimate layer (which are used for final decision-making) to degrade more significantly.

G.1. Changes of Feature Variance Across Layers

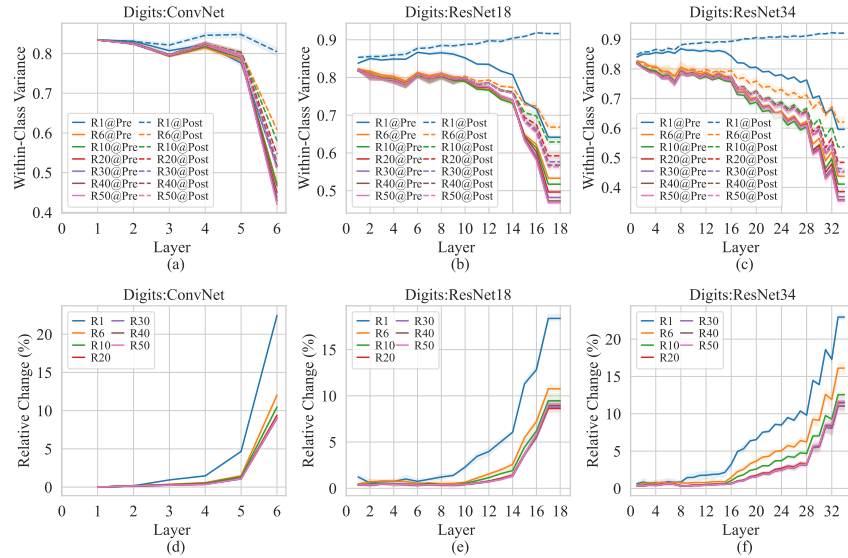


Figure 20. Changes in the normalized within-class variance of features across model layers for specific global rounds, with larger X-axis values indicating deeper layers. The model is trained on Digit-Five with multiple models that are randomly initialized. The top half of the figure shows the normalized within-class variance, while the bottom half displays the relative change in variance before and after model aggregation.

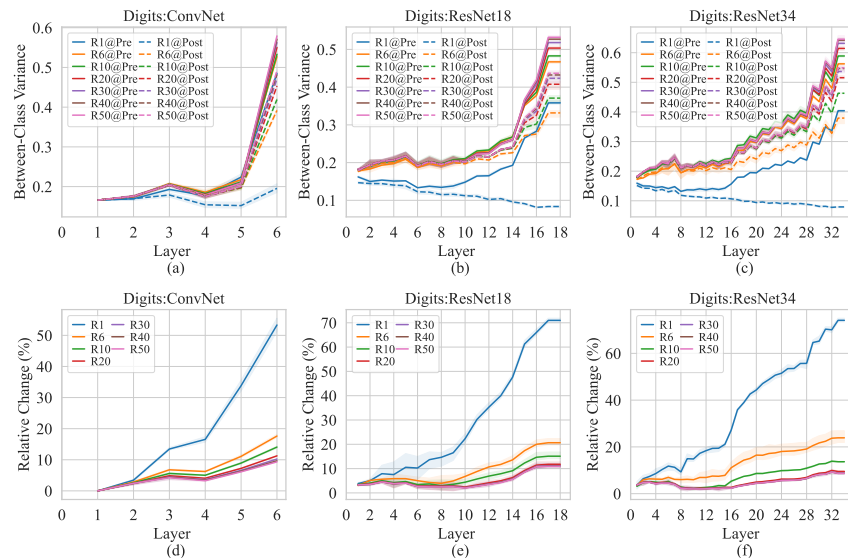


Figure 21. Changes in the normalized between-class variance of features across model layers for specific global rounds, with larger X-axis values indicating deeper layers. The model is trained on Digit-Five with multiple models that are randomly initialized. The top half of the figure shows the normalized between-class variance, while the bottom half displays the relative change in variance before and after model aggregation.

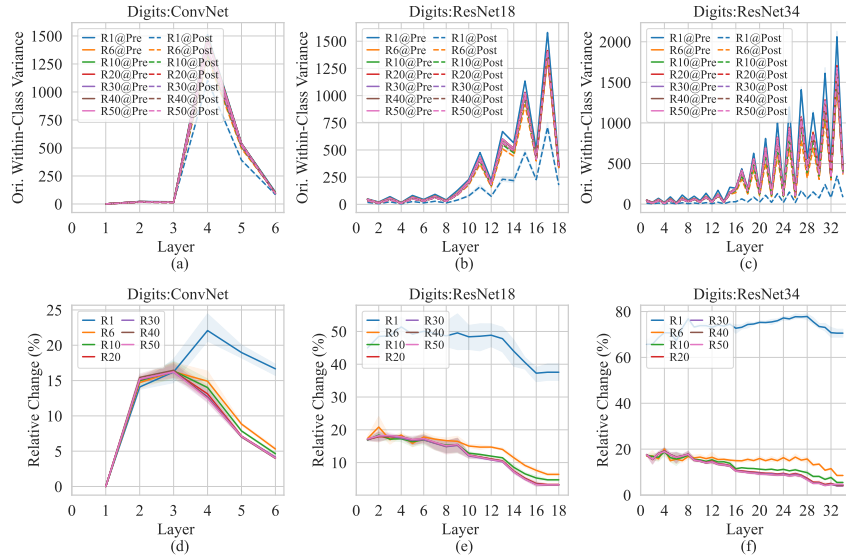


Figure 22. Changes in the original unnormalized within-class variance of features across model layers for specific global rounds, with larger X-axis values indicating deeper layers. The model is trained on Digit-Five with multiple models that are randomly initialized. The top half of the figure shows the original unnormalized within-class variance, while the bottom half displays the relative change in variance before and after model aggregation.

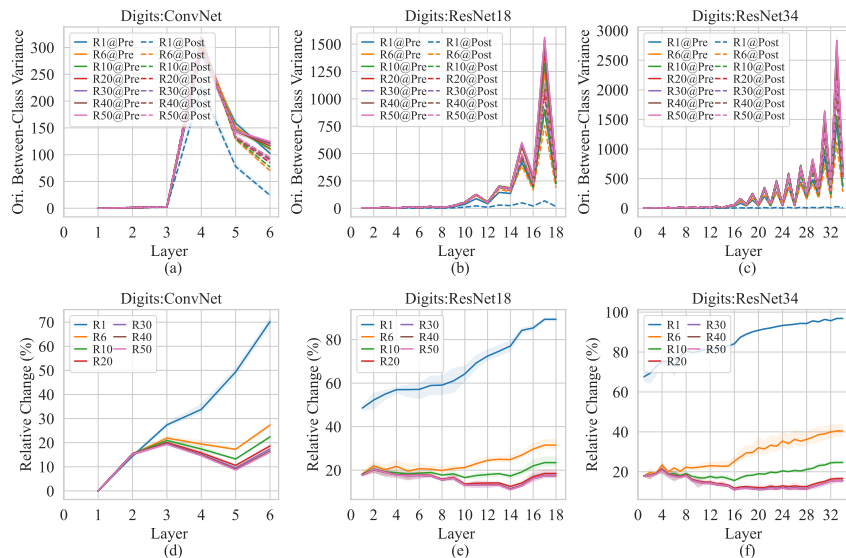


Figure 23. Changes in the original unnormalized between-class variance of features across model layers for specific global rounds, with larger X-axis values indicating deeper layers. The model is trained on Digit-Five with multiple models that are randomly initialized. The top half of the figure shows the original unnormalized between-class variance, while the bottom half displays the relative change in variance before and after model aggregation.

Unveiling the Downsides of Model Aggregation in Federated Learning from a Layer-peeled Perspective

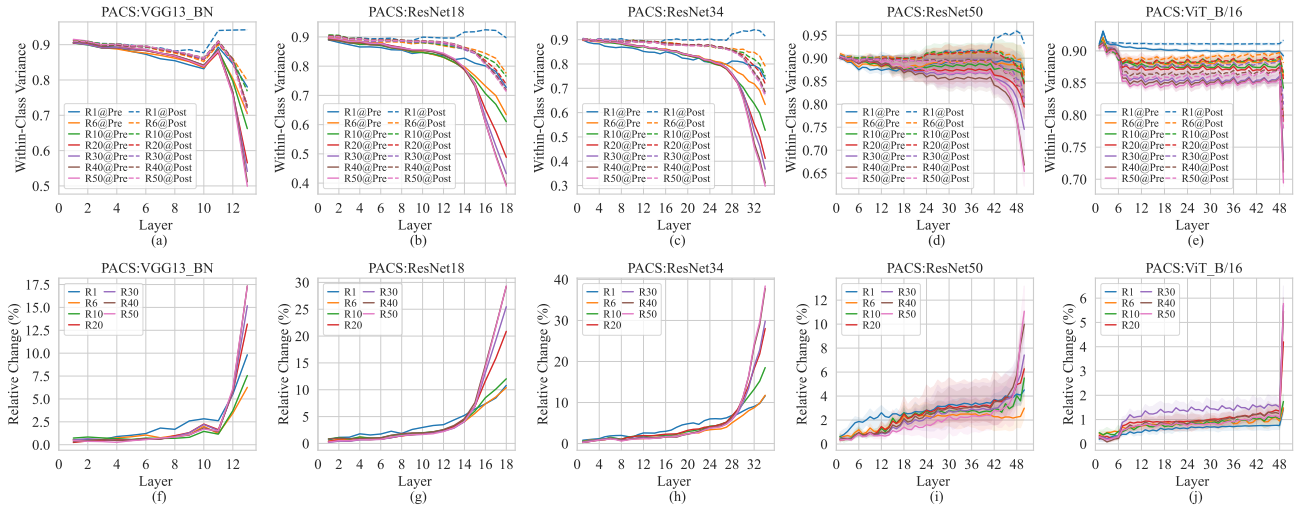


Figure 24. Changes in the normalized within-class variance of features across model layers for specific global rounds, with larger X-axis values indicating deeper layers. The model is trained on PACS with multiple models that are randomly initialized. The top half of the figure shows the normalized within-class variance, while the bottom half displays the relative change in variance before and after model aggregation.

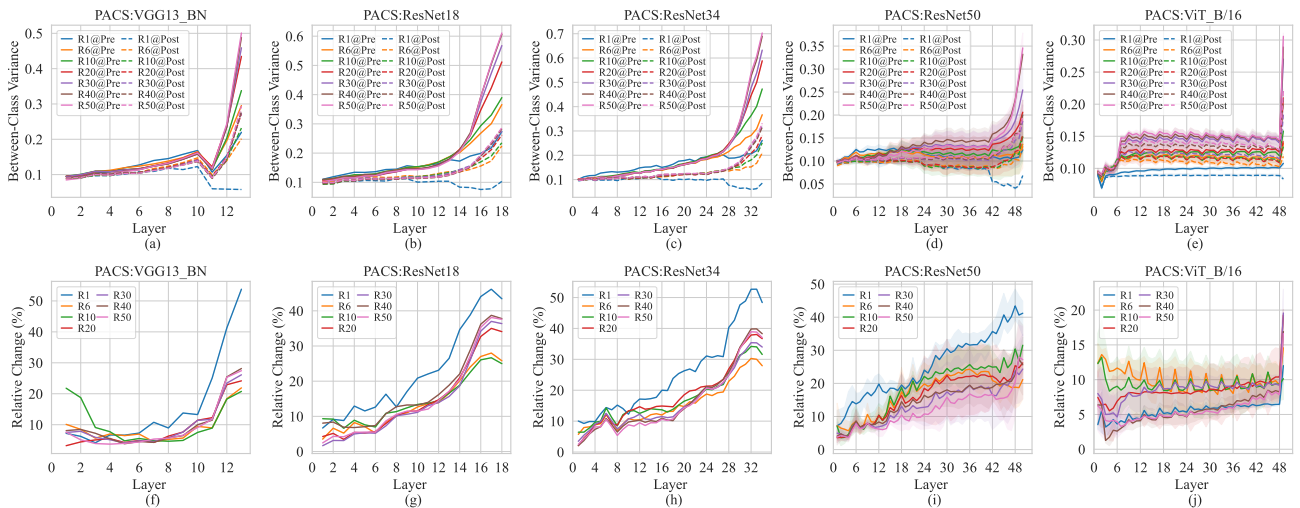


Figure 25. Changes in the normalized between-class variance of features across model layers for specific global rounds, with larger X-axis values indicating deeper layers. The model is trained on PACS with multiple models that are randomly initialized. The top half of the figure shows the normalized between-class variance, while the bottom half displays the relative change in variance before and after model aggregation.

Unveiling the Downsides of Model Aggregation in Federated Learning from a Layer-peeled Perspective

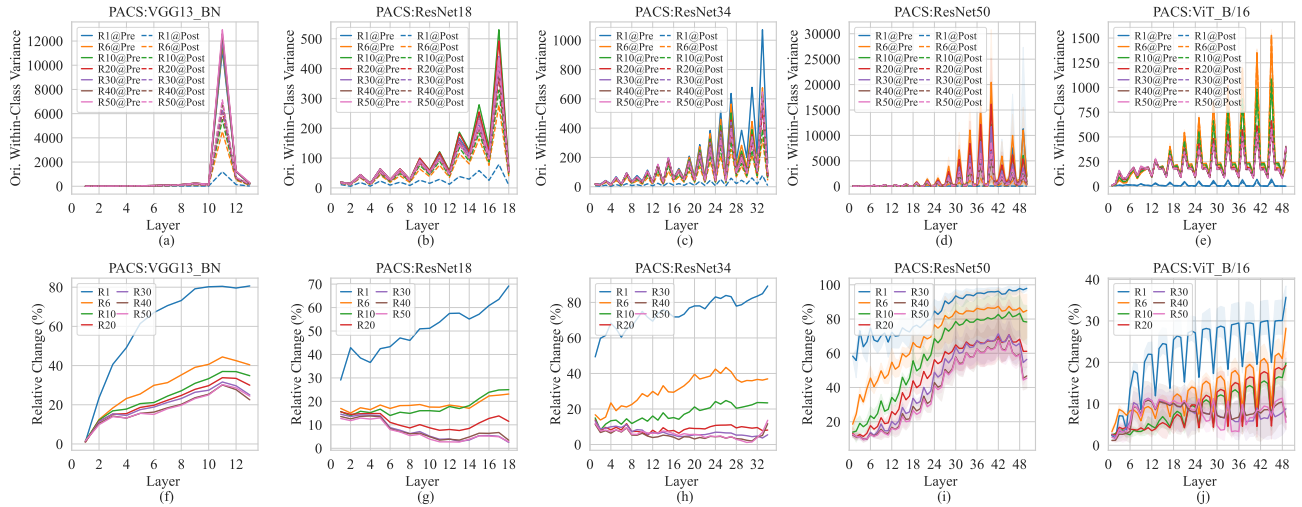


Figure 26. Changes in the original unnormalized within-class variance of features across model layers for specific global rounds, with larger X-axis values indicating deeper layers. The model is trained on PACS with multiple models that are randomly initialized. The top half of the figure shows the original unnormalized within-class variance, while the bottom half displays the relative change in variance before and after model aggregation.

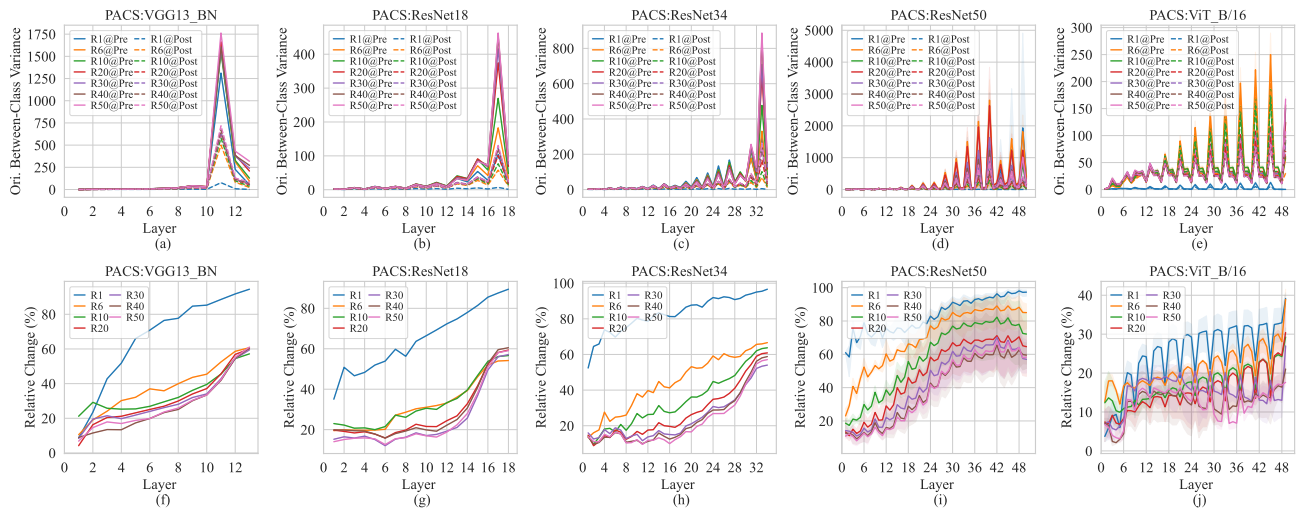


Figure 27. Changes in the original unnormalized between-class variance of features across model layers for specific global rounds, with larger X-axis values indicating deeper layers. The model is trained on PACS with multiple models that are randomly initialized. The top half of the figure shows the original unnormalized between-class variance, while the bottom half displays the relative change in variance before and after model aggregation.

Unveiling the Downsides of Model Aggregation in Federated Learning from a Layer-peeled Perspective

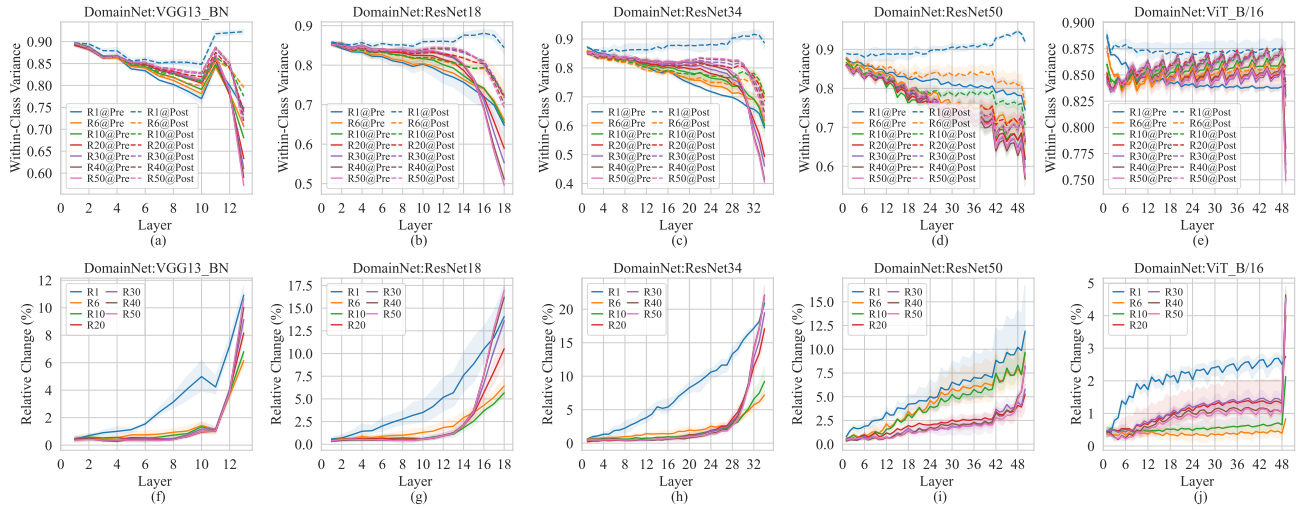


Figure 28. Changes in the normalized within-class variance of features across model layers for specific global rounds, with larger X-axis values indicating deeper layers. The model is trained on DomainNet with multiple models that are randomly initialized. The top half of the figure shows the normalized within-class variance, while the bottom half displays the relative change in variance before and after model aggregation.

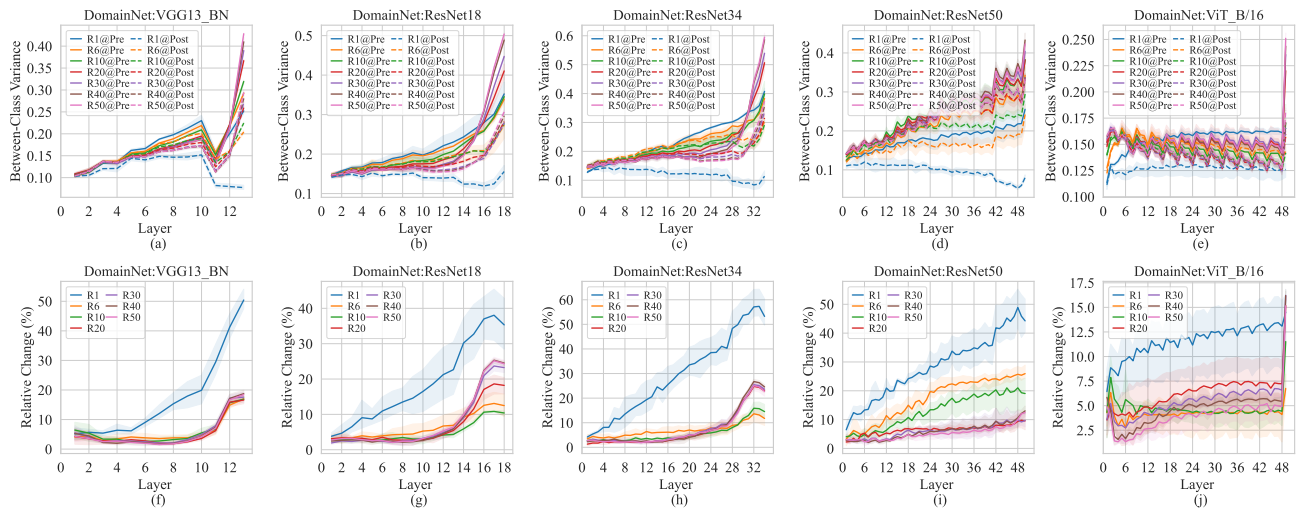


Figure 29. Changes in the normalized between-class variance of features across model layers for specific global rounds, with larger X-axis values indicating deeper layers. The model is trained on DomainNet with multiple models that are randomly initialized. The top half of the figure shows the normalized between-class variance, while the bottom half displays the relative change in variance before and after model aggregation.

Unveiling the Downsides of Model Aggregation in Federated Learning from a Layer-peeled Perspective

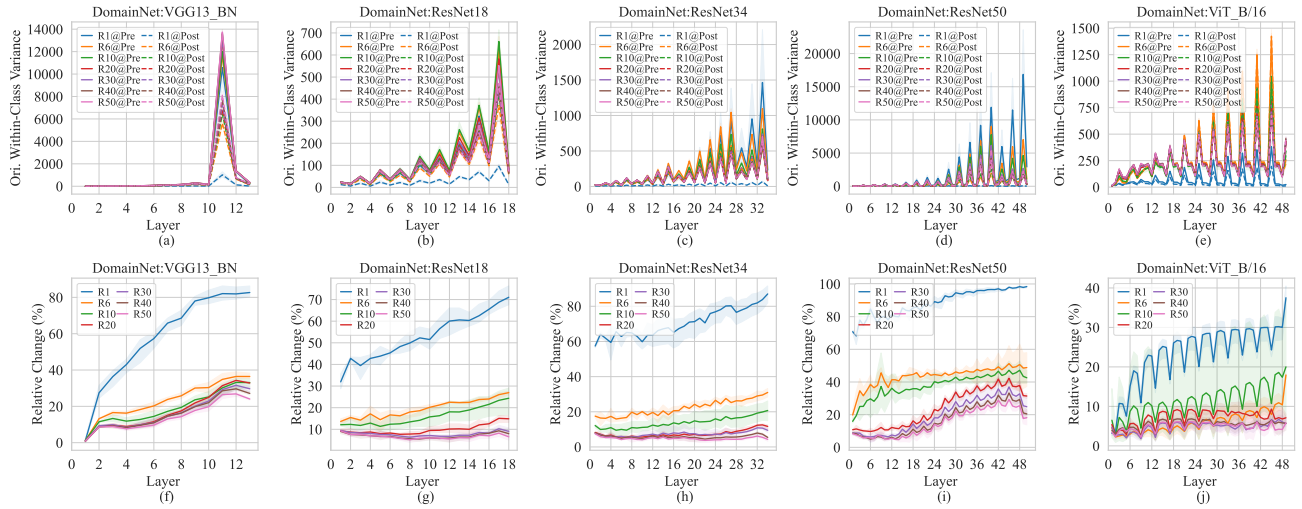


Figure 30. Changes in the unnormalized within-class variance of features across model layers for specific global rounds, with larger X-axis values indicating deeper layers. The model is trained on DomainNet with multiple models that are randomly initialized. The top half of the figure shows the original unnormalized within-class variance, while the bottom half displays the relative change in variance before and after model aggregation.

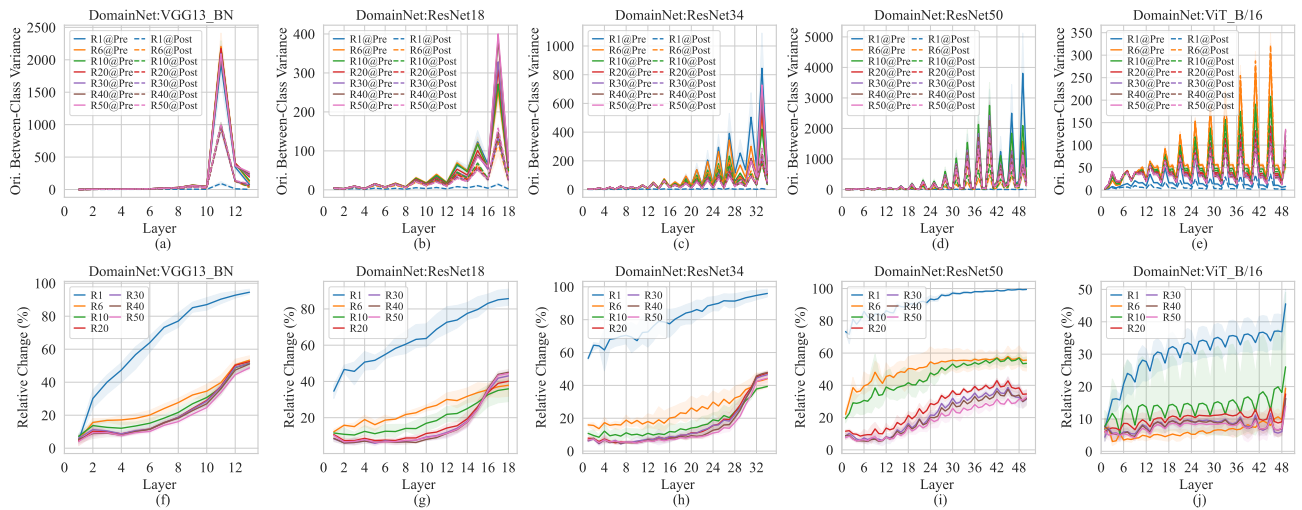


Figure 31. Changes in the unnormalized between-class variance of features across model layers for specific global rounds, with larger X-axis values indicating deeper layers. The model is trained on DomainNet with multiple models that are randomly initialized. The top half of the figure shows the original unnormalized between-class variance, while the bottom half displays the relative change in variance before and after model aggregation.

G.2. Changes of Feature Variance Across Training Rounds

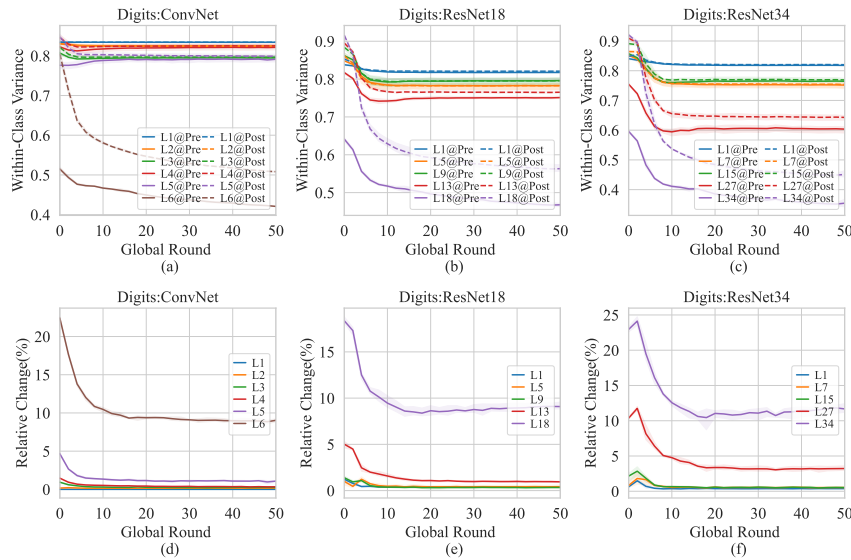


Figure 32. Changes in the normalized within-class variance of features across FL training at specific model layers. The model is trained on Digit-Five with multiple models that are randomly initialized. The top half of the figure shows the normalized within-class variance, while the bottom half displays the relative change in variance before and after model aggregation.

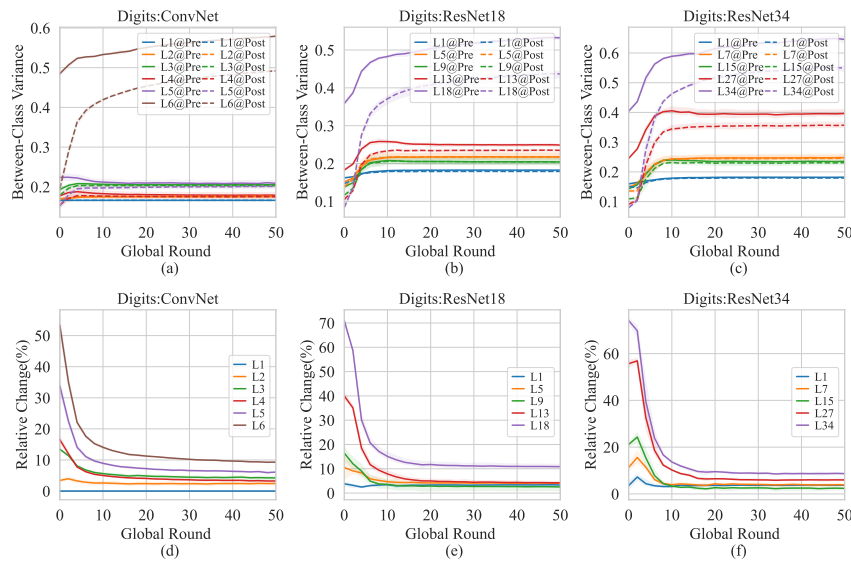


Figure 33. Changes in the normalized between-class variance of features across FL training at specific model layers. The model is trained on Digit-Five with multiple models that are randomly initialized. The top half of the figure shows the normalized between-class variance, while the bottom half displays the relative change in variance before and after model aggregation.

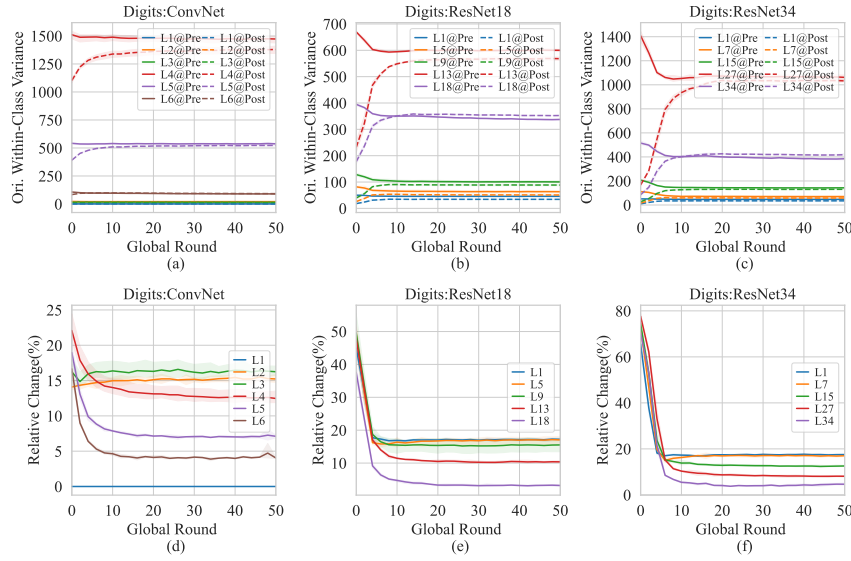


Figure 34. Changes in the original unnormalized within-class variance of features across FL training at specific model layers. The model is trained on Digit-Five with multiple models that are randomly initialized. The top half of the figure shows the original unnormalized within-class variance, while the bottom half displays the relative change in variance before and after model aggregation.

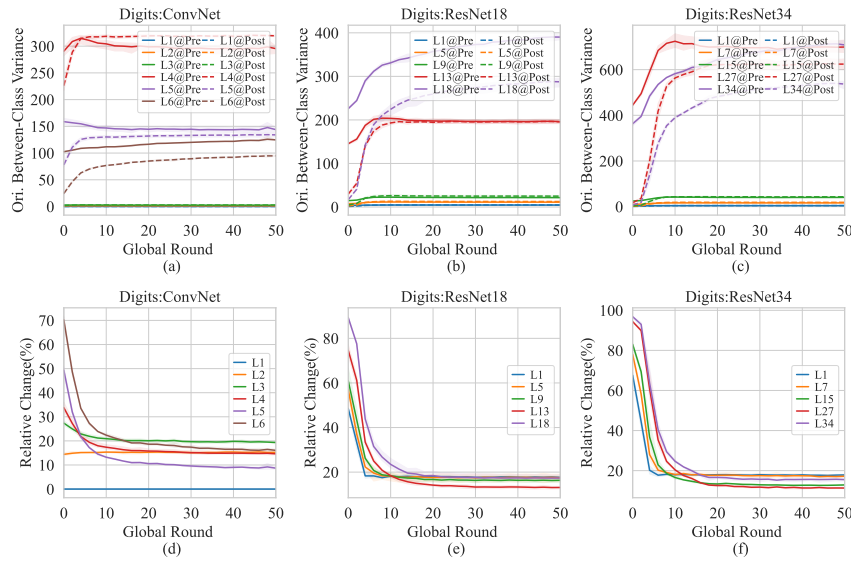


Figure 35. Changes in the original unnormalized between-class variance of features across FL training at specific model layers. The model is trained on Digit-Five with multiple models that are randomly initialized. The top half of the figure shows the original unnormalized between-class variance, while the bottom half displays the relative change in variance before and after model aggregation.

Unveiling the Downsides of Model Aggregation in Federated Learning from a Layer-peeled Perspective

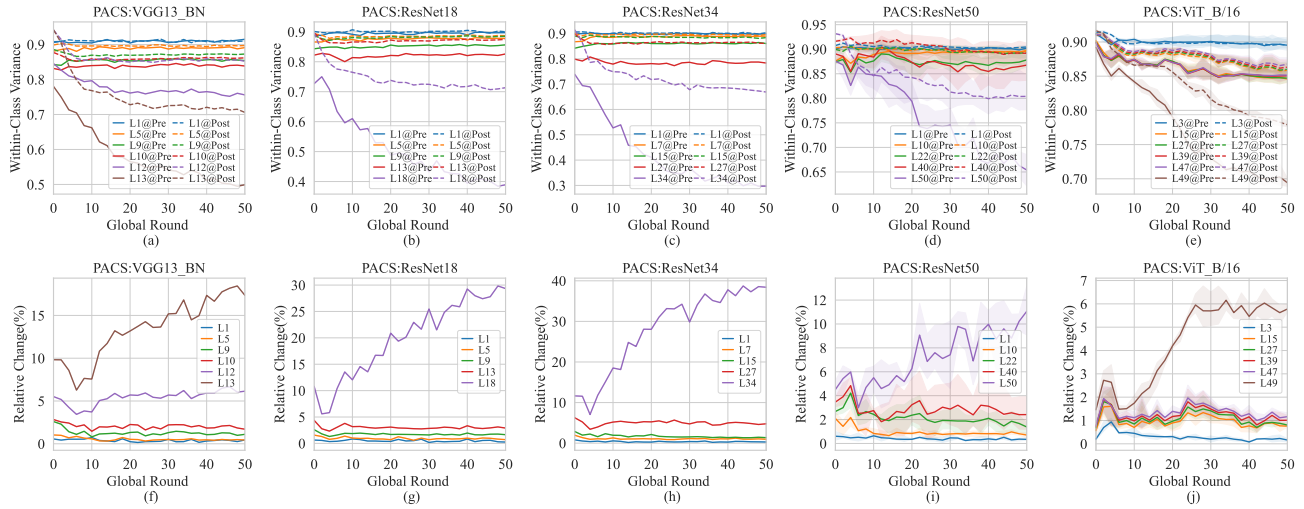


Figure 36. Changes in the normalized within-class variance of features across FL training at specific model layers. The model is trained on PACS with multiple models that are randomly initialized. The top half of the figure shows the normalized within-class variance, while the bottom half displays the relative change in variance before and after model aggregation.

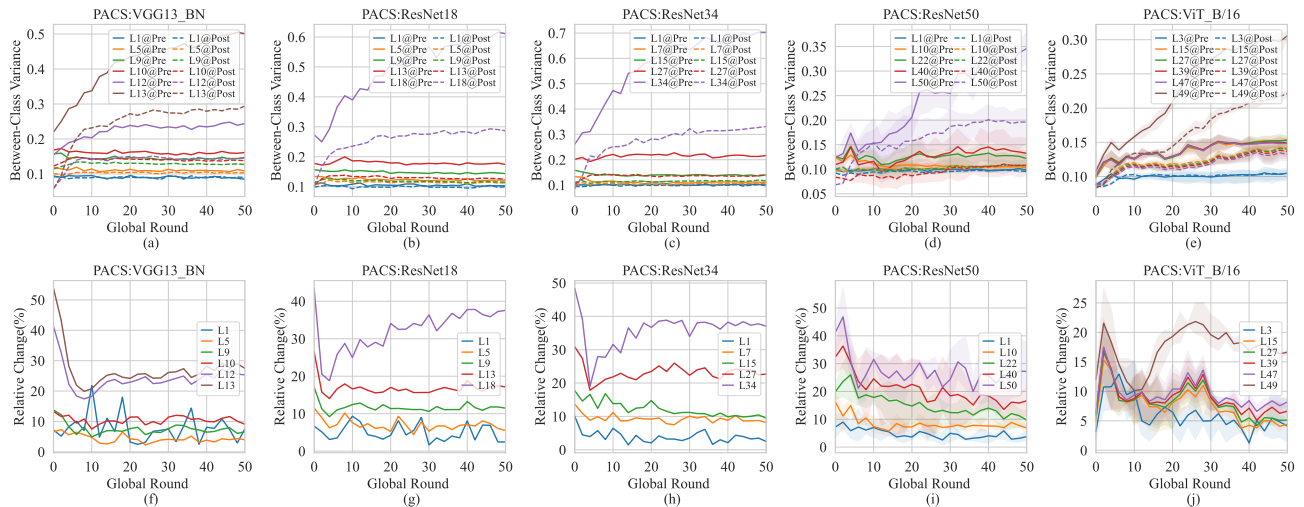


Figure 37. Changes in the normalized between-class variance of features across FL training at specific model layers. The model is trained on PACS with multiple models that are randomly initialized. The top half of the figure shows the normalized between-class variance, while the bottom half displays the relative change in variance before and after model aggregation.

Unveiling the Downsides of Model Aggregation in Federated Learning from a Layer-peeled Perspective

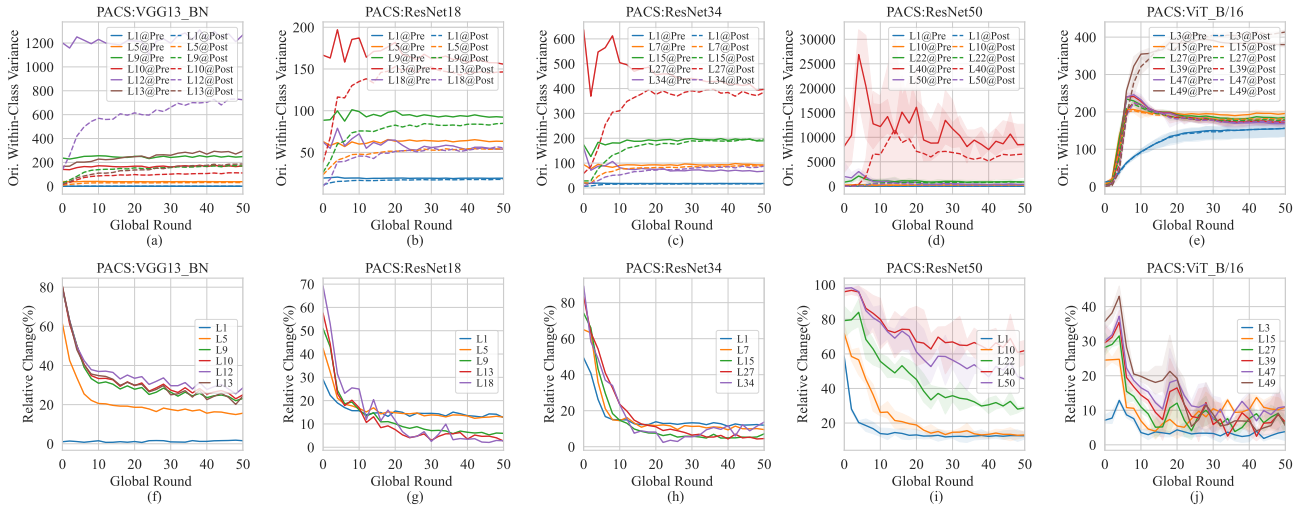


Figure 38. Changes in the original unnormalized within-class variance of features across FL training at specific model layers. The model is trained on PACS with multiple models that are randomly initialized. The top half of the figure shows the original unnormalized within-class variance, while the bottom half displays the relative change in variance before and after model aggregation.

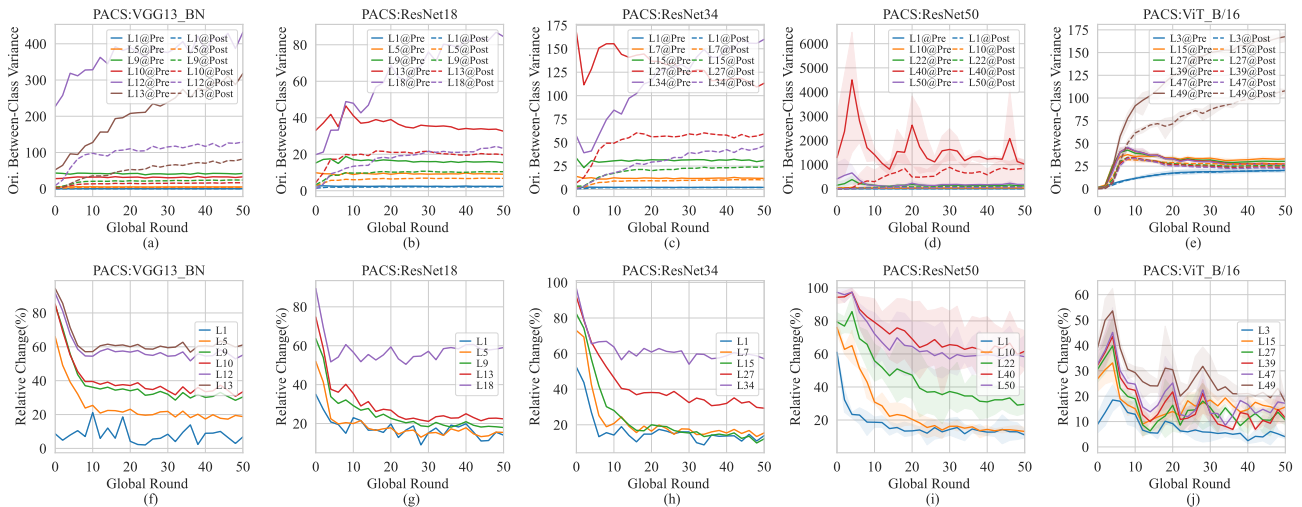


Figure 39. Changes in the original unnormalized between-class variance of features across FL training at specific model layers. The model is trained on PACS with multiple models that are randomly initialized. The top half of the figure shows the original unnormalized between-class variance, while the bottom half displays the relative change in variance before and after model aggregation.

Unveiling the Downsides of Model Aggregation in Federated Learning from a Layer-peeled Perspective

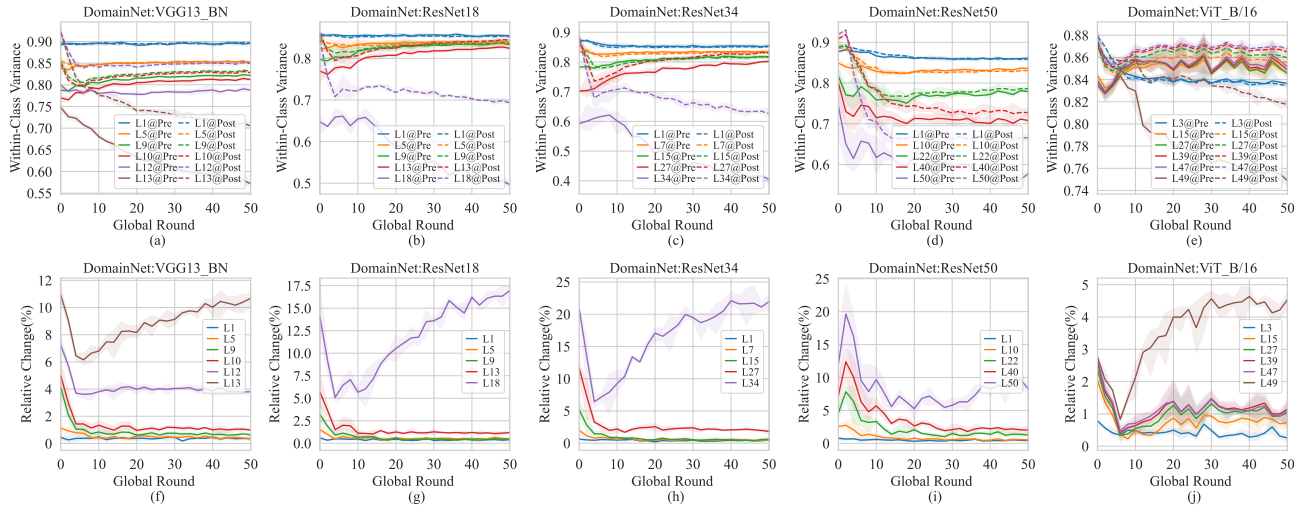


Figure 40. Changes in the normalized within-class variance of features across FL training at specific model layers. The model is trained on DomainNet with multiple models that are randomly initialized. The top half of the figure shows the normalized within-class variance, while the bottom half displays the relative change in variance before and after model aggregation.

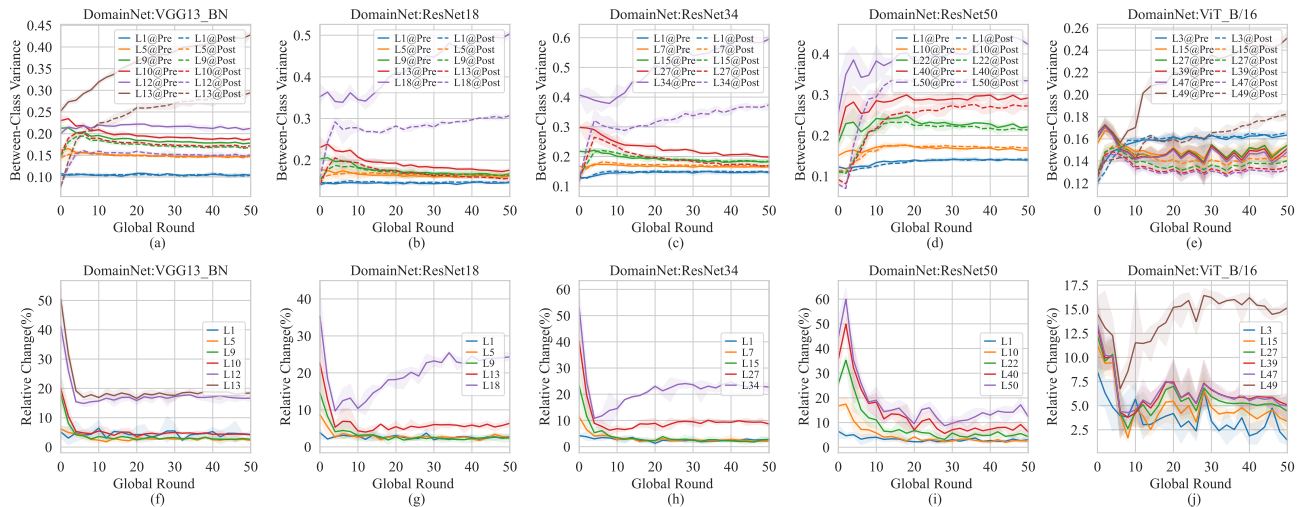


Figure 41. Changes in the normalized between-class variance of features across FL training at specific model layers. The model is trained on DomainNet with multiple models that are randomly initialized. The top half of the figure shows the normalized between-class variance, while the bottom half displays the relative change in variance before and after model aggregation.

Unveiling the Downsides of Model Aggregation in Federated Learning from a Layer-peeled Perspective

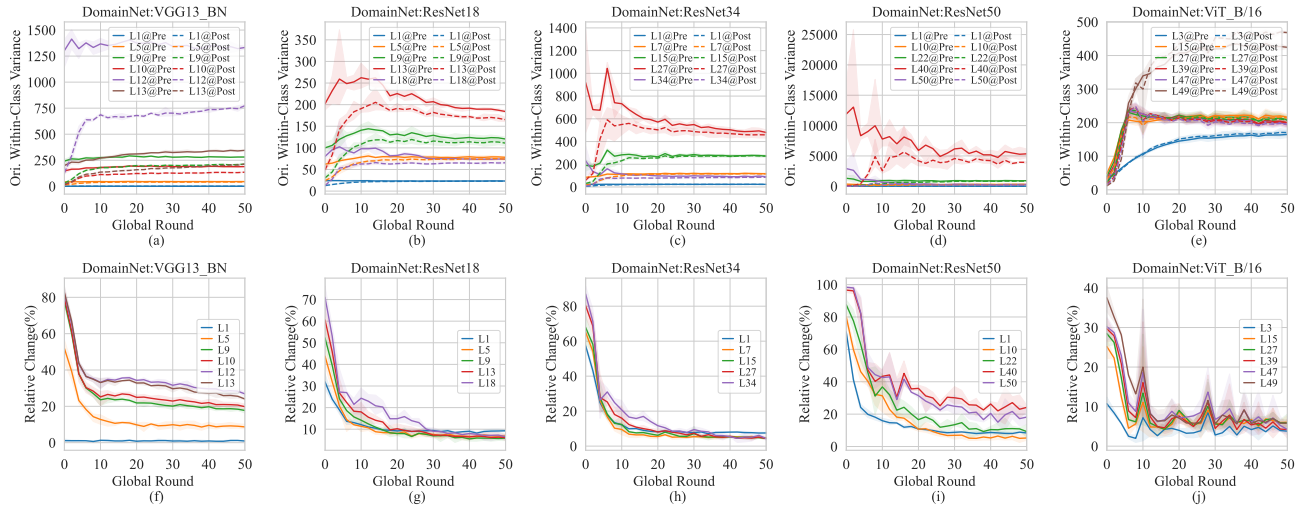


Figure 42. Changes in the original unnormalized within-class variance of features across FL training at specific model layers. The model is trained on DomainNet with multiple models that are randomly initialized. The top half of the figure shows the original unnormalized within-class variance, while the bottom half displays the relative change in variance before and after model aggregation.

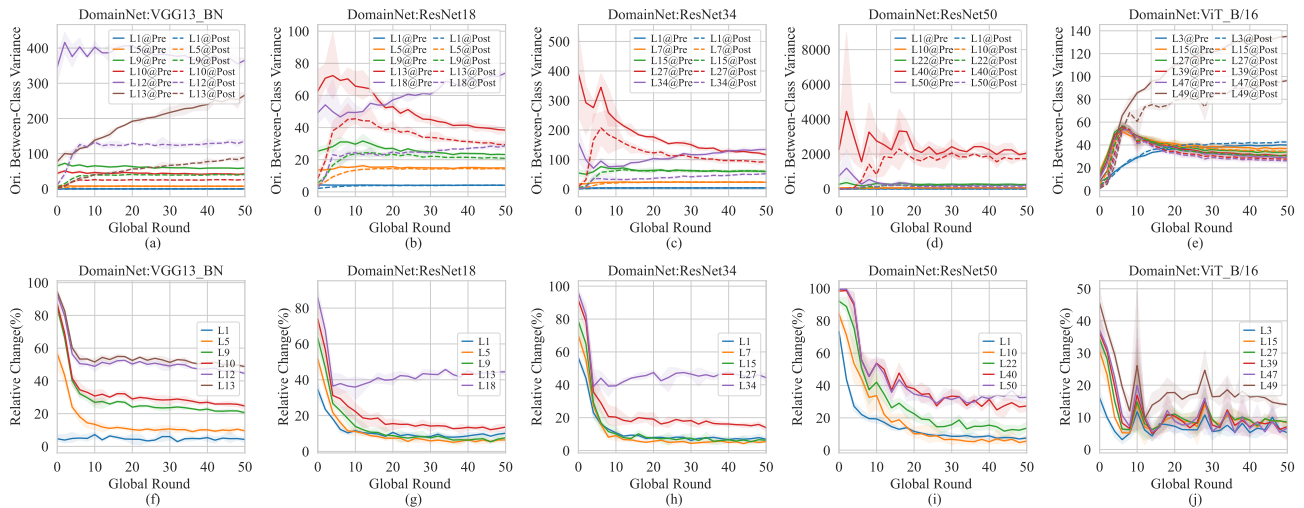


Figure 43. Changes in the original unnormalized between-class variance of features across FL training at specific model layers. The model is trained on DomainNet with multiple models that are randomly initialized. The top half of the figure shows the original unnormalized between-class variance, while the bottom half displays the relative change in variance before and after model aggregation.

H. Detailed Results of Alignment between Features and Parameters

In this section, we present the experimental results corresponding to the alignment of features and the parameters of the subsequent layers. From these results, we observe that the alignment between features and parameters improves as training progresses, with the alignment of penultimate layer features and the classifier increasing more rapidly.

After model aggregation, the alignment between features and parameters tends to decrease. However, the decrease is more pronounced in the classifier. This increased mismatch between penultimate layer features and the classifier, along with the degradation of the penultimate layer features, causes the aggregated model to perform significantly worse when sent back to

each client.

H.1. Changes of Alignment Across Layers

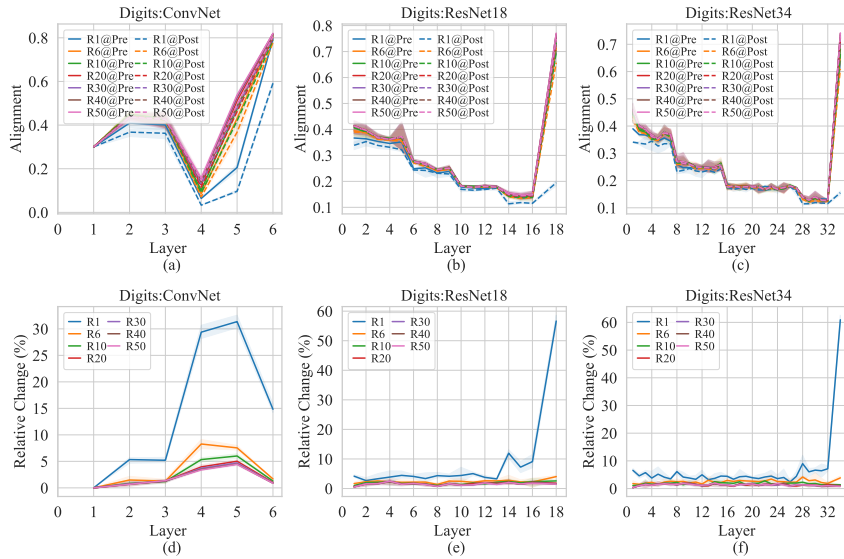


Figure 44. Changes in the alignment between features and parameters across model layers for specific global rounds, with larger X-axis values indicating deeper layers. The model is trained on Digit-Five with multiple models that are randomly initialized. The top half of the figure shows the original alignment values between features and parameters, while the bottom half displays the relative change in alignment before and after model aggregation.

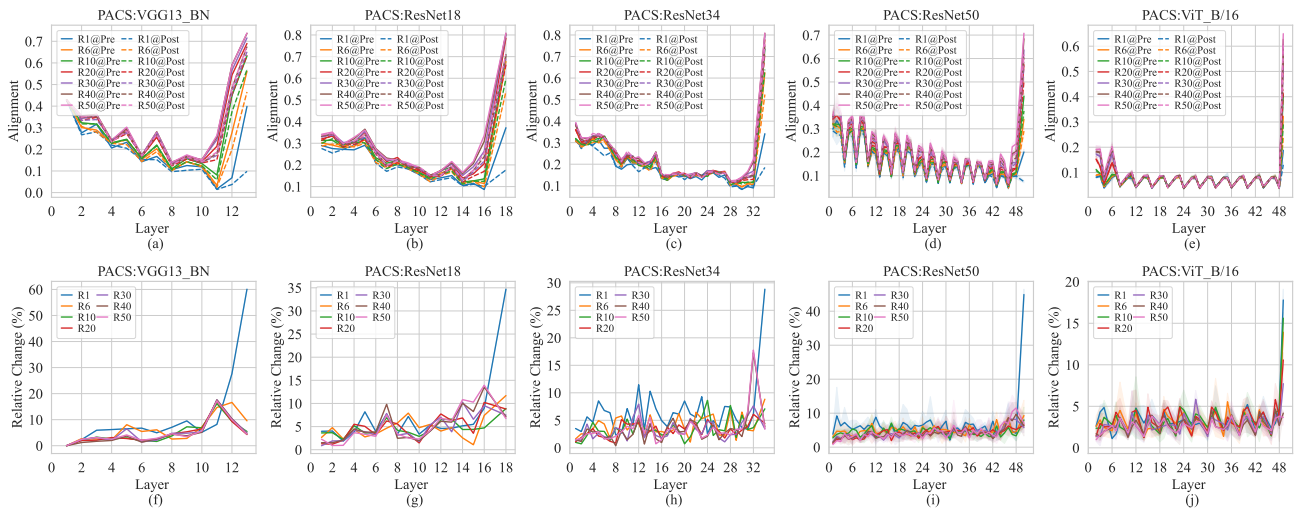


Figure 45. Changes in the alignment between features and parameters across model layers for specific global rounds, with larger X-axis values indicating deeper layers. The model is trained on PACS with multiple models that are randomly initialized. The top half of the figure shows the original alignment values between features and parameters, while the bottom half displays the relative change in alignment before and after model aggregation.

Unveiling the Downsides of Model Aggregation in Federated Learning from a Layer-peeled Perspective

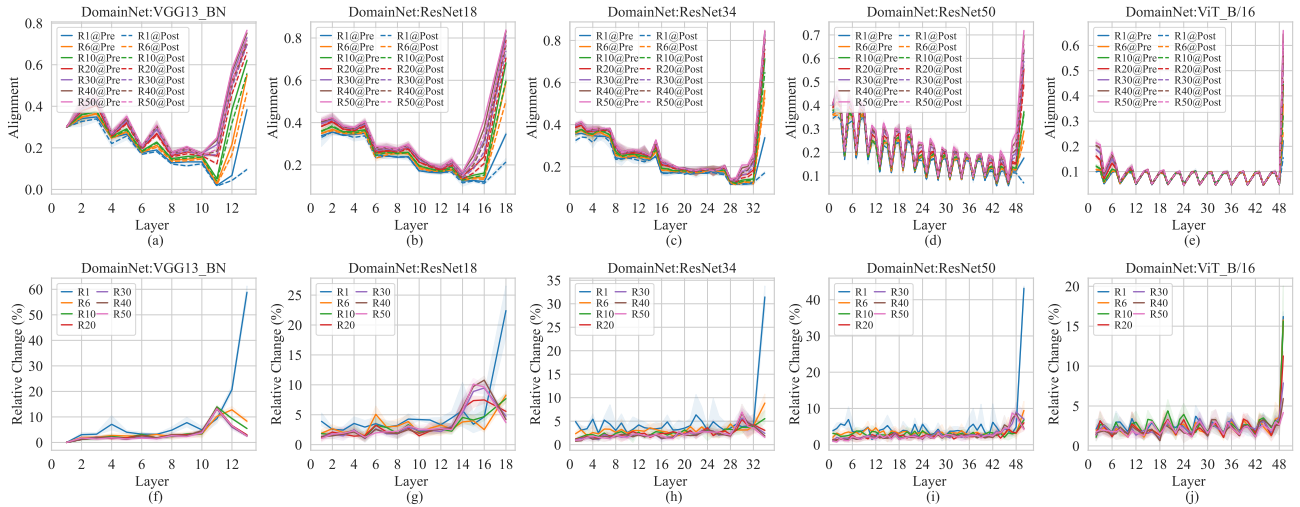


Figure 46. Changes in the alignment between features and parameters across model layers for specific global rounds, with larger X-axis values indicating deeper layers. The model is trained on DomainNet with multiple models that are randomly initialized. The top half of the figure shows the original alignment values between features and parameters, while the bottom half displays the relative change in alignment before and after model aggregation.

H.2. Changes of Alignment Across Training Rounds

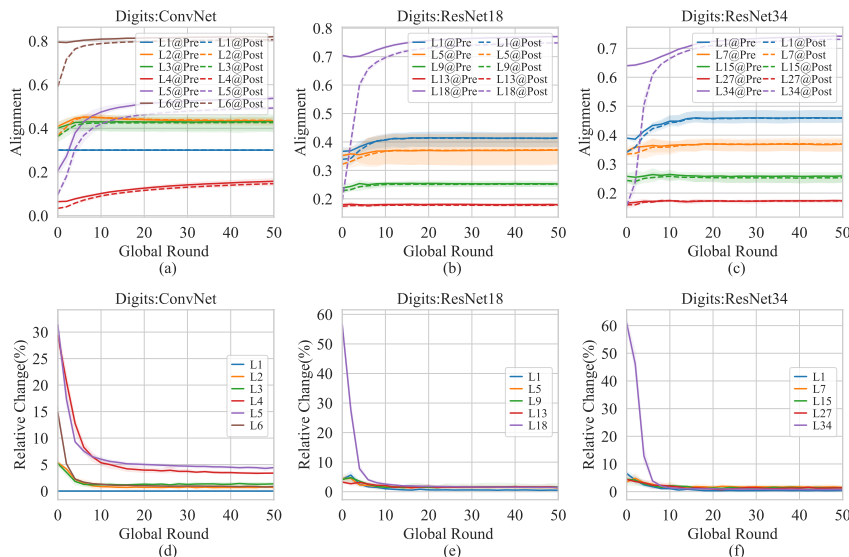


Figure 47. Changes in the alignment between features and parameters across FL training at specific model layers. The model is trained on Digit-Five with multiple models that are randomly initialized. The top half of the figure shows the original alignment values between features and parameters, while the bottom half displays the relative change in alignment before and after model aggregation.

Unveiling the Downsides of Model Aggregation in Federated Learning from a Layer-peeled Perspective

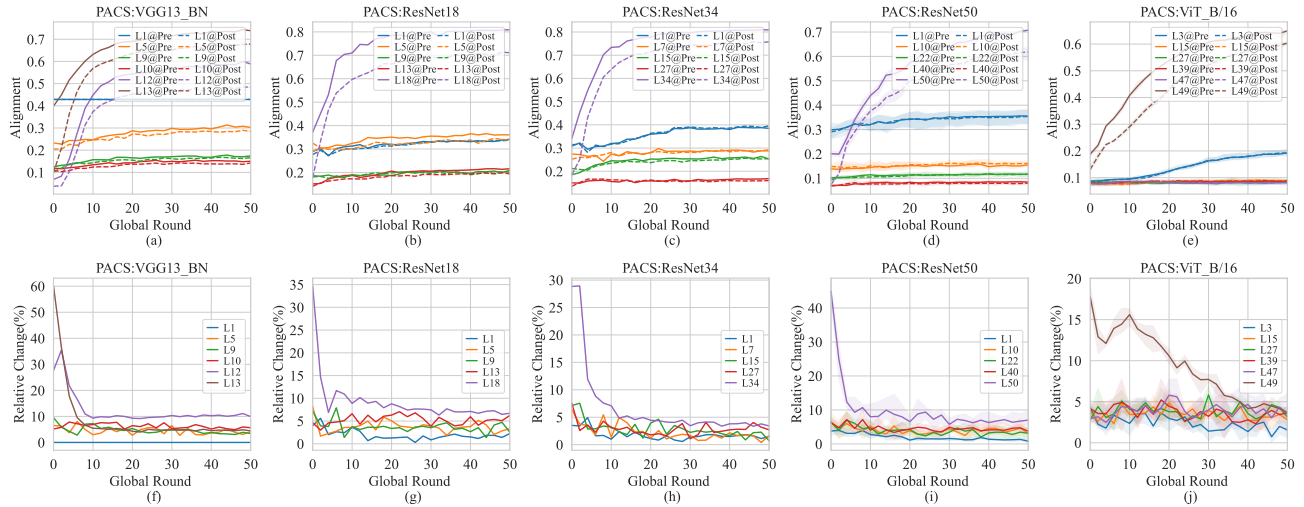


Figure 48. Changes in the alignment between features and parameters across FL training at specific model layers. The model is trained on PACS with multiple models that are randomly initialized. The top half of the figure shows the original alignment values between features and parameters, while the bottom half displays the relative change in alignment before and after model aggregation.

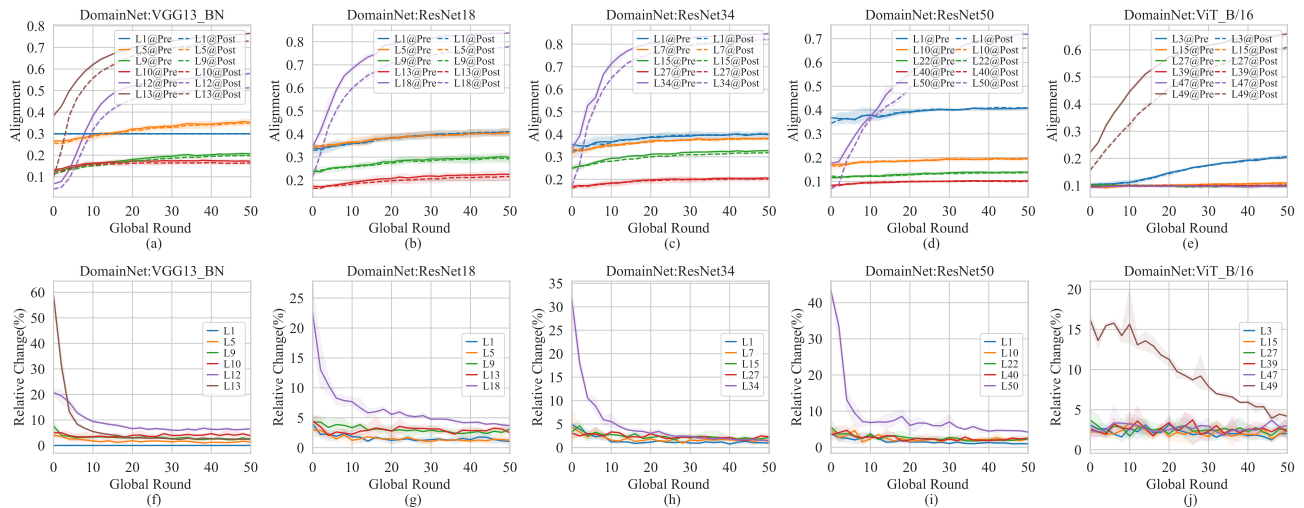


Figure 49. Changes in the alignment between features and parameters across FL training at specific model layers. The model is trained on DomainNet with multiple models that are randomly initialized. The top half of the figure shows the original alignment values between features and parameters, while the bottom half displays the relative change in alignment before and after model aggregation.

I. Detailed Results of Feature Stable Rank

In this section, we present the detailed experimental results corresponding to the stable rank of features. It can be observed that the stable rank increases as both the training process and layer depth progress. However, after model aggregation, the stable rank tends to decrease, which contradicts the training objective of FL.

I.1. Changes of Stable Rank Across Layers

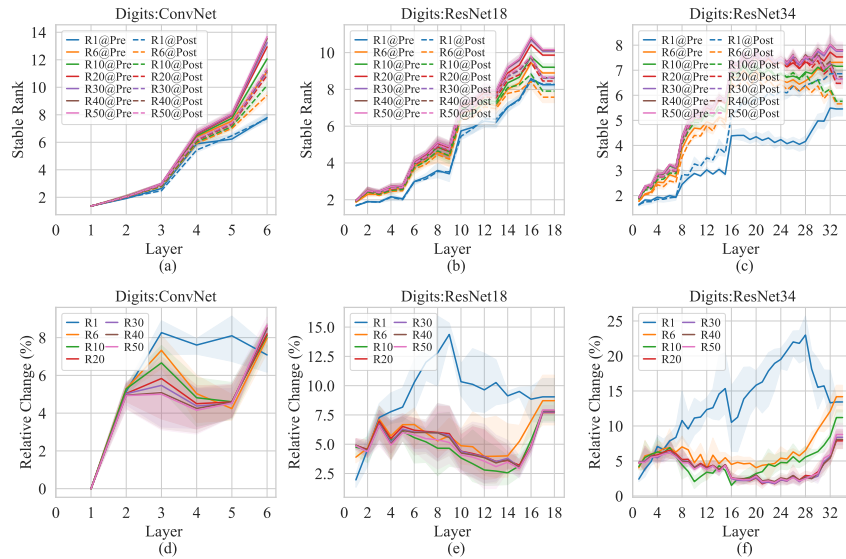


Figure 50. Changes in the stable rank of features across model layers for specific global rounds, with larger X-axis values indicating deeper layers. The model is trained on Digit-Five with multiple models that are randomly initialized. The top half of the figure shows the original stable rank of features, while the bottom half displays the relative change in stable rank before and after model aggregation.

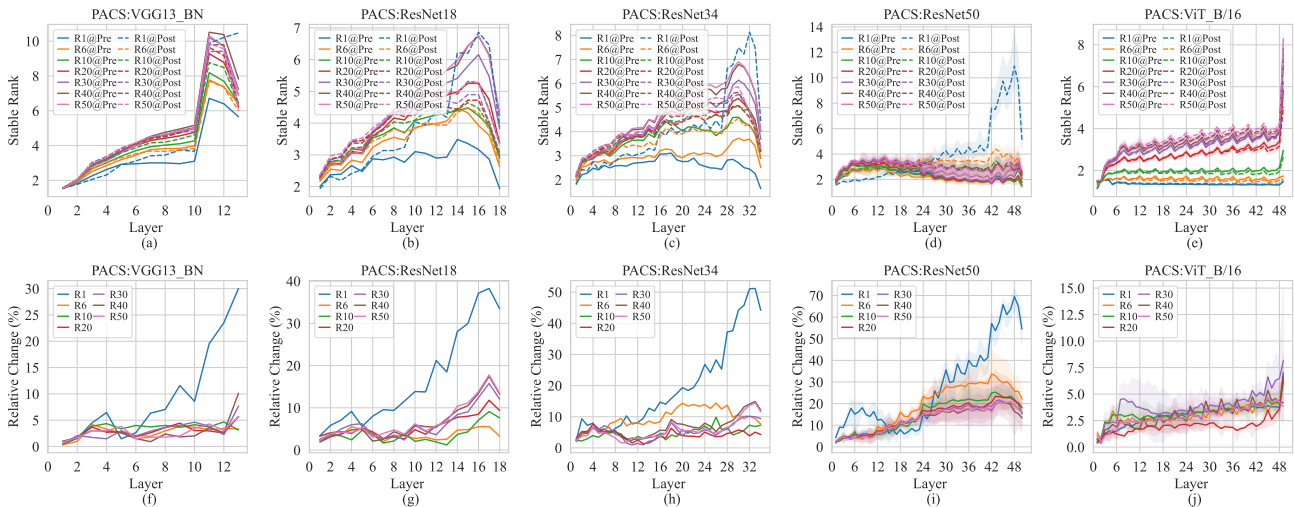


Figure 51. Changes in stable rank of features across model layers for specific global rounds, with larger X-axis values indicating deeper layers. The model is trained on PACS with multiple models that are randomly initialized. The top half of the figure shows the original stable rank of features, while the bottom half displays the relative change in stable rank before and after model aggregation.

Unveiling the Downsides of Model Aggregation in Federated Learning from a Layer-peeled Perspective

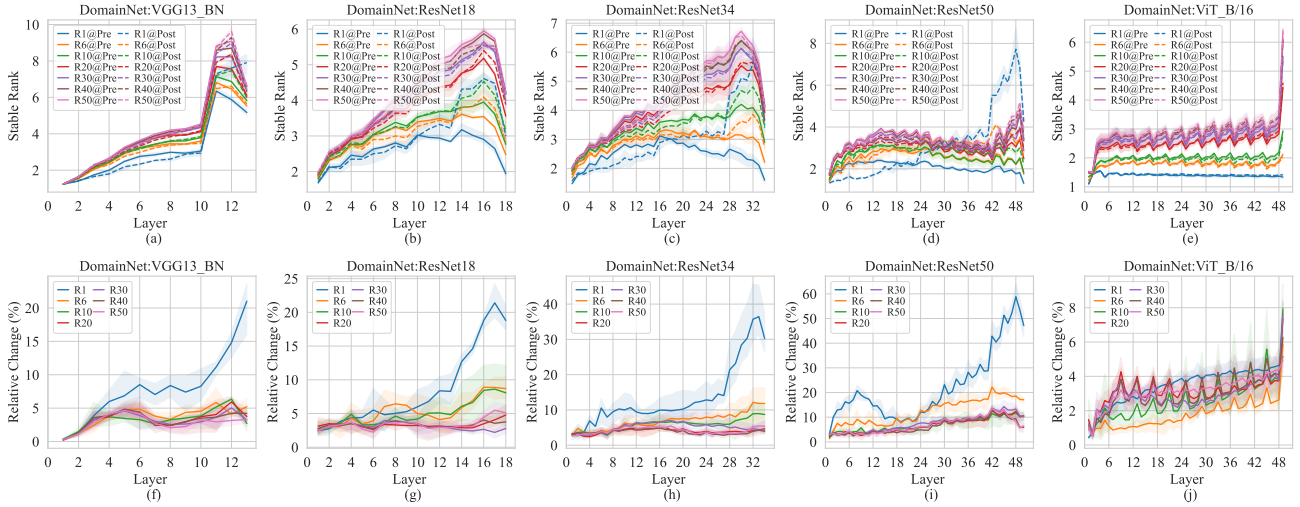


Figure 52. Changes in stable rank of features across model layers for specific global rounds, with larger X-axis values indicating deeper layers. The model is trained on DomainNet with multiple models that are randomly initialized. The top half of the figure shows the original stable rank of features, while the bottom half displays the relative change in stable rank before and after model aggregation.

I.2. Changes of Stable Rank Across Training Rounds

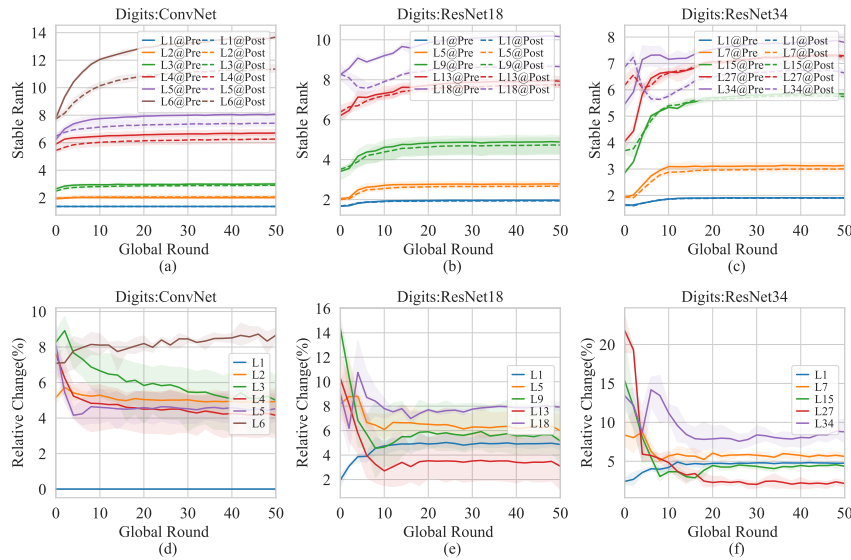


Figure 53. Changes in the stable rank of features across FL training at specific model layers. The model is trained on Digit-Five with multiple models that are randomly initialized. The top half of the figure shows the original stable rank of features, while the bottom half displays the relative change in stable rank before and after model aggregation.

Unveiling the Downsides of Model Aggregation in Federated Learning from a Layer-peeled Perspective

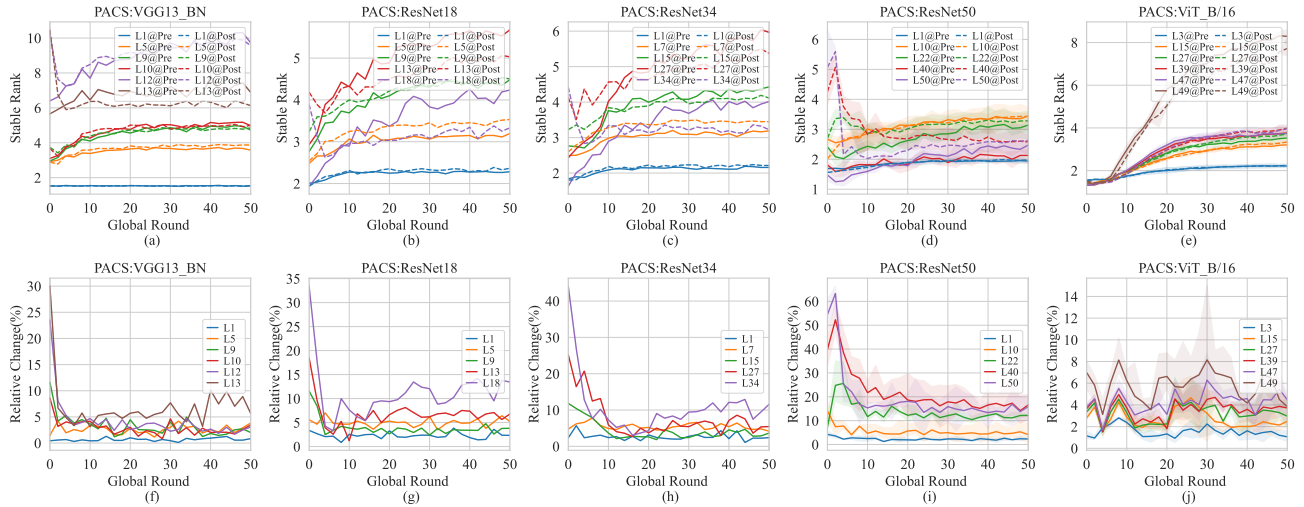


Figure 54. Changes in the stable rank of features across FL training at specific model layers. The model is trained on PACS with multiple models that are randomly initialized. The top half of the figure shows the original stable rank of features, while the bottom half displays the relative change in stable rank before and after model aggregation.

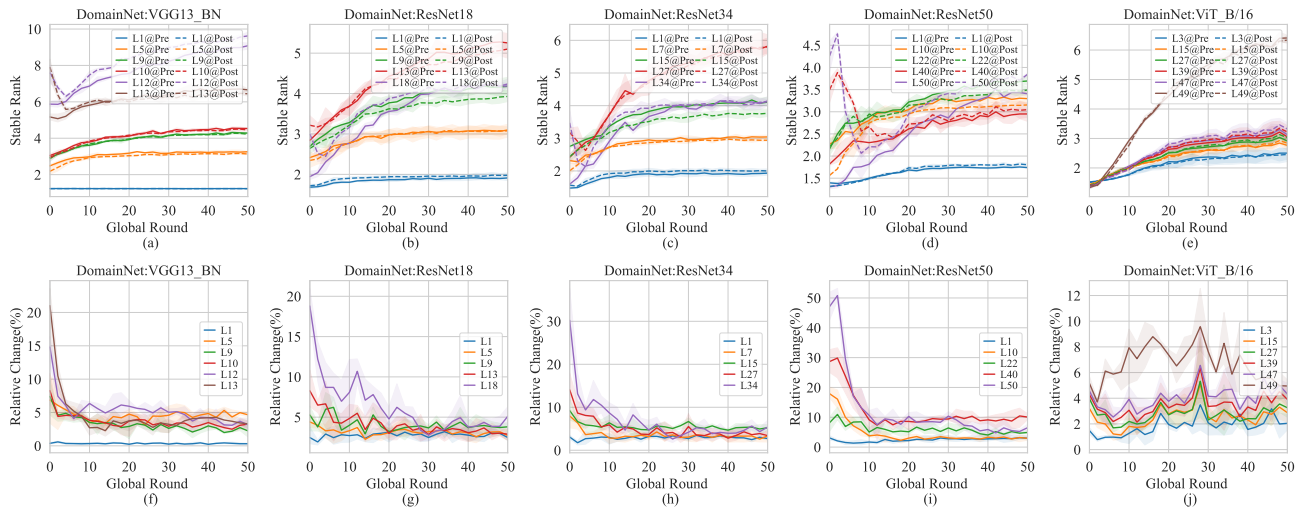


Figure 55. Changes in the stable rank of features across FL training at specific model layers. The model is trained on DomainNet with multiple models that are randomly initialized. The top half of the figure shows the original stable rank of features, while the bottom half displays the relative change in stable rank before and after model aggregation.

J. Visualization of Pre-aggregated and Post-aggregated Features

This section visualizes the comparison between pre-aggregated and post-aggregated features. It can be observed that, as layer depth increases, features become more compressed within the same class and more discriminative across different classes. However, after model aggregation, features become more scattered within the same class and less discriminative across classes. This phenomenon is particularly pronounced in the penultimate layer features (the leftmost subfigure). These observations are consistent with the findings from the quantitative metrics described earlier.

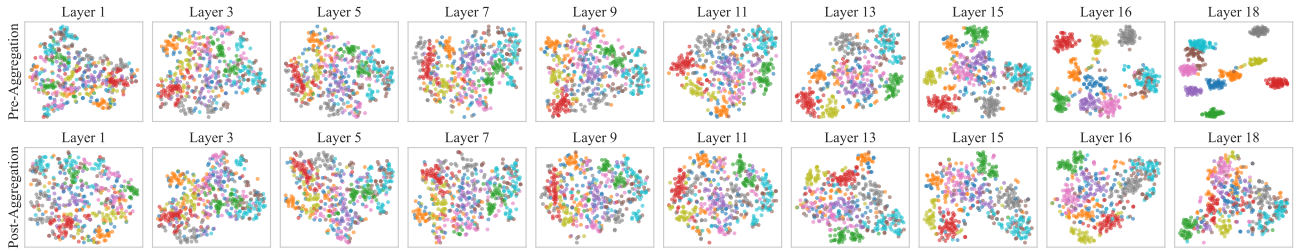


Figure 56. T-SNE visualization of features at different layers on the ‘Quickdraw’ domain of DomainNet before and after aggregation. The features are extracted from ResNet18 in the final global round of FL training, whose parameters are randomly initialized at the beginning.

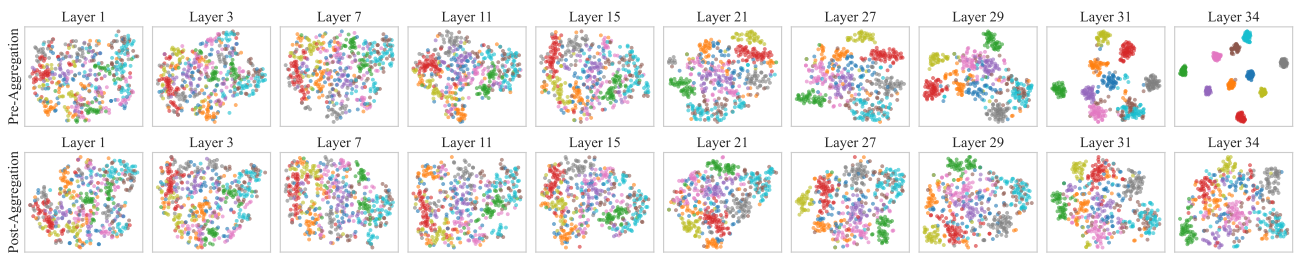


Figure 57. T-SNE visualization of features at different layers on the ‘Quickdraw’ domain of DomainNet before and after aggregation. The features are extracted from ResNet34 in the final global round of FL training, whose parameters are randomly initialized at the beginning.

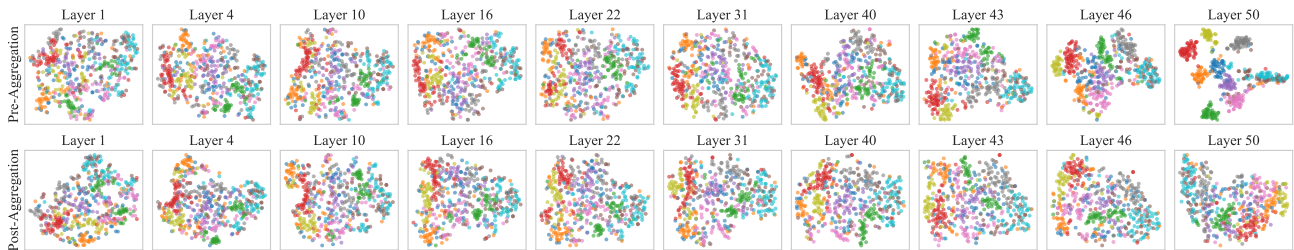


Figure 58. T-SNE visualization of features at different layers on the ‘Quickdraw’ domain of DomainNet before and after aggregation. The features are extracted from ResNet50 in the final global round of FL training, whose parameters are randomly initialized at the beginning.

K. Feature Distance and Parameter Distance

This section compares the distance between features and parameters in the pre-aggregated and post-aggregated models at each layer. It can be observed that, with the exception of the final classifier, the parameter distance between the pre-aggregated and post-aggregated models is significantly smaller than the feature distance. Furthermore, the distances between parameters and features show different trends across layers. While the parameter distance decreases, the feature distance increases as the layer depth increases. This demonstrates that even small variations in the parameter space can lead to significant feature variations, as the stacked structure of DNNs tends to magnify errors in feature extraction. This observation suggests that the ‘client drift’ proposed by previous studies may not be the root cause of performance drops during model aggregation.

Unveiling the Downsides of Model Aggregation in Federated Learning from a Layer-peeled Perspective

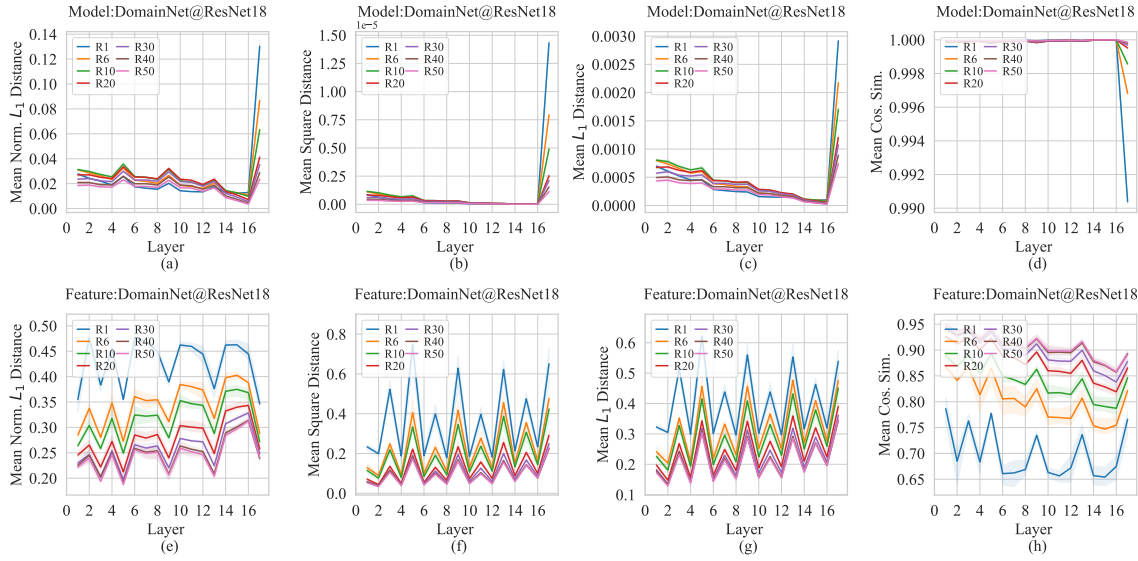


Figure 59. Changes in distance of the features and parameters obtained from models before and after aggregation across model layers for specific global rounds, with larger X-axis values indicating deeper layers. The model is trained on DomainNet using ResNet18. The distance is measured by 4 metric including mean normalized distance, mean squared distance, mean L_1 distance, and mean cosine similarity. The top half of the figure shows the distance between the parameters of pre-aggregated and post-aggregated models, while the bottom half displays the distance between the features of pre-aggregated and post-aggregated models.

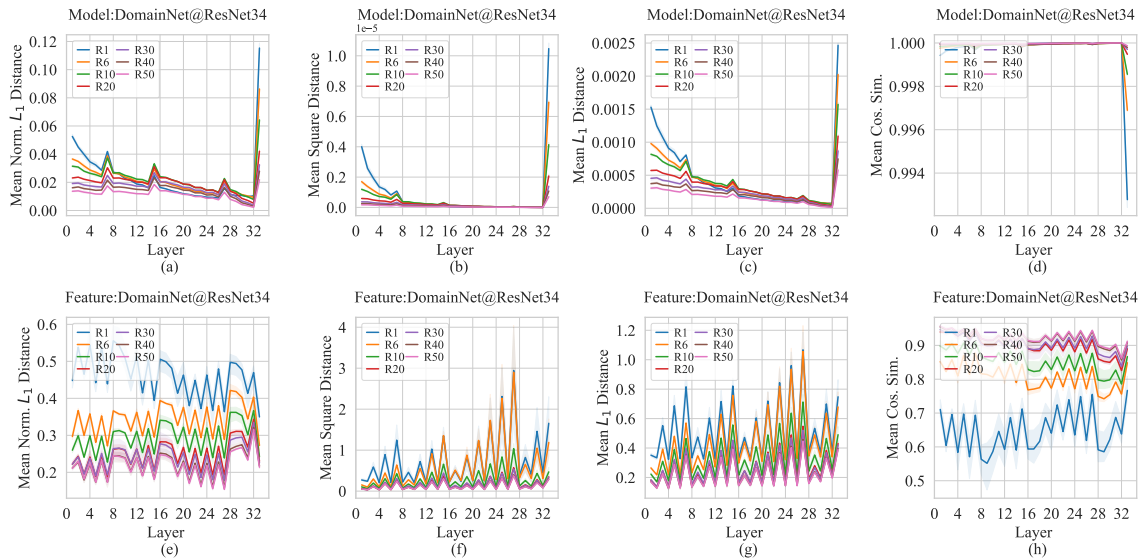


Figure 60. Changes in distance of the features and parameters obtained from models before and after aggregation across model layers for specific global rounds, with larger X-axis values indicating deeper layers. The model is trained on DomainNet using ResNet18. The distance is measured by 4 metric including mean normalized distance, mean squared distance, mean L_1 distance, and mean cosine similarity. The top half of the figure shows the distance between the parameters of pre-aggregated and post-aggregated models, while the bottom half displays the distance between the features of pre-aggregated and post-aggregated models.

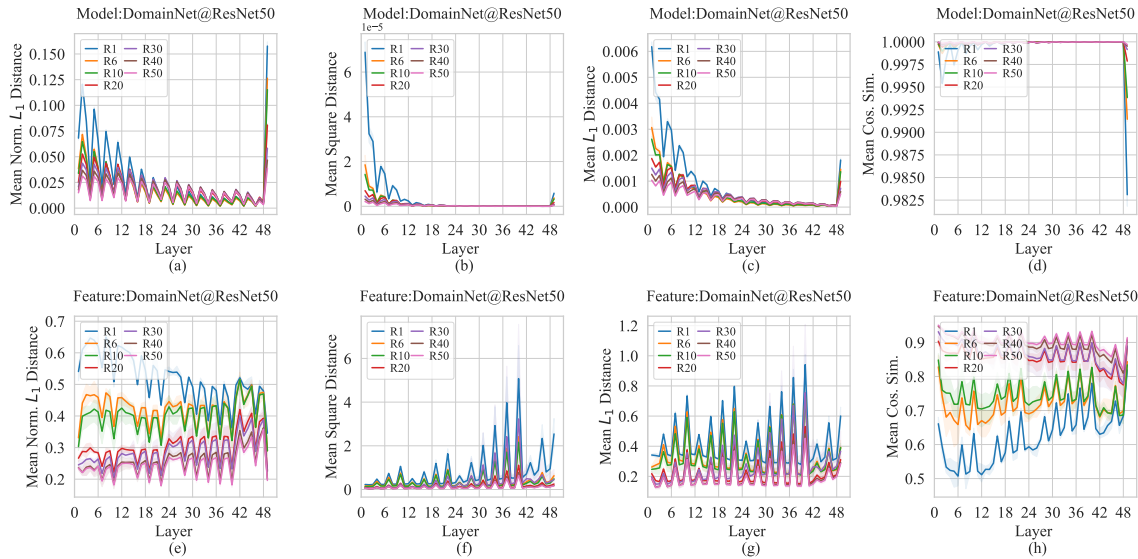


Figure 61. Changes in distance of the features and parameters obtained from models before and after aggregation across model layers for specific global rounds, with larger X-axis values indicating deeper layers. The model is trained on DomainNet using ResNet18. The distance is measured by 4 metric including mean normalized distance, mean squared distance, mean L_1 distance, and mean cosine similarity. The top half of the figure shows the distance between the parameters of pre-aggregated and post-aggregated models, while the bottom half displays the distance between the features of pre-aggregated and post-aggregated models.

L. Detailed Results of Linear Probing

This section evaluates the accuracy of linear probing across diverse data distributions. In our experiments, we use SGD with a learning rate of 0.01 to optimize the randomly initialized linear layer. The batch size is set to 64, and the total number of epochs is set to 100. We report the best test accuracy as the accuracy of linear probing.

From the experimental results, we observe that the features generated by the post-aggregated model perform well across diverse data distributions. In contrast, the pre-aggregated model only performs well on its local data distribution. This suggests that, while the model after aggregation may not extract task-specific features for local distributions, it is more capable of extracting generalized features that can be applied to different distributions. This is also how model aggregation improves performance compared to purely local training.

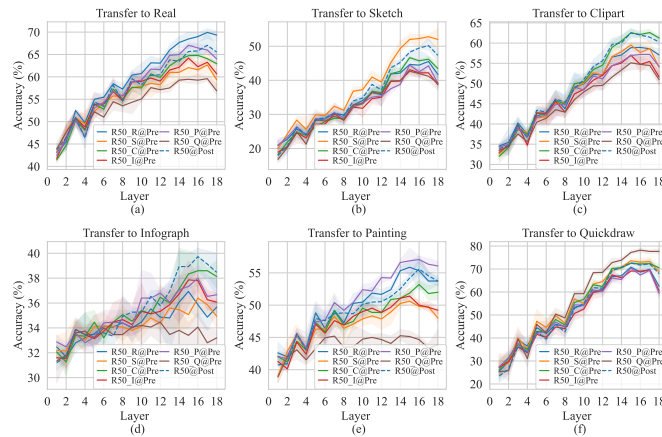


Figure 62. Accuracy of linear probing at different layers across different domains in DomainNet. The experiments are performed in global round 50 using ResNet18 as the backbone model. In the figures, E50@Post represents the results using the model after aggregation, while E50.*@Pre represents the results using the model before aggregation for domain*.

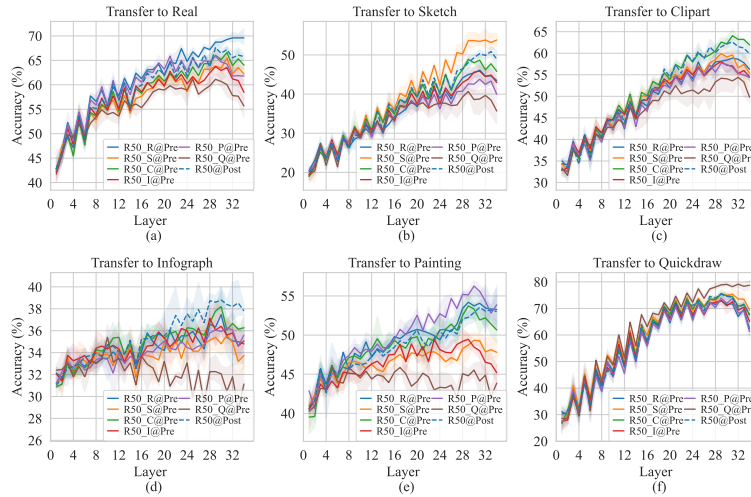


Figure 63. Accuracy of linear probing at different layers across different domains in DomainNet. The experiments are performed in global round 50 using ResNet34 as the backbone model. In the figures, E50@Post represents the results using the model after aggregation, while E50_*@Pre represents the results using the model before aggregation for domain *.

M. Effect of Residual Connection

This section analyzes the role of residual connections in DNNs when performing model aggregation. We use ResNet18 and ResNet34 as backbones and remove the residual connections from these models. We then employ these modified architectures for FL training. This section presents a comparison of accuracy and feature metrics between the models with and without residual connections. We observe that the relative change in feature metrics is more pronounced when the residual connections are removed, particularly during the early stages of model training and in the normalized within-class and between-class feature variance metrics. This may be because residual connections help mitigate feature degradation by allowing less disrupted features in lower layers to be propagated to deeper layers.

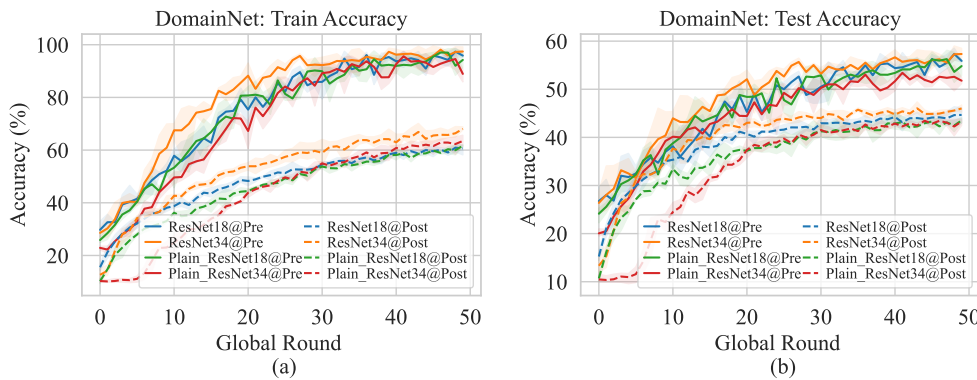


Figure 64. Averaged training and testing accuracy curves of the model before and after aggregation, evaluated on the local dataset during FL training. The experiments are conducted on the DomainNet dataset. The models trained include the original ResNet18 and ResNet, as well as their plain versions, with residual connections removed.

Unveiling the Downsides of Model Aggregation in Federated Learning from a Layer-peeled Perspective

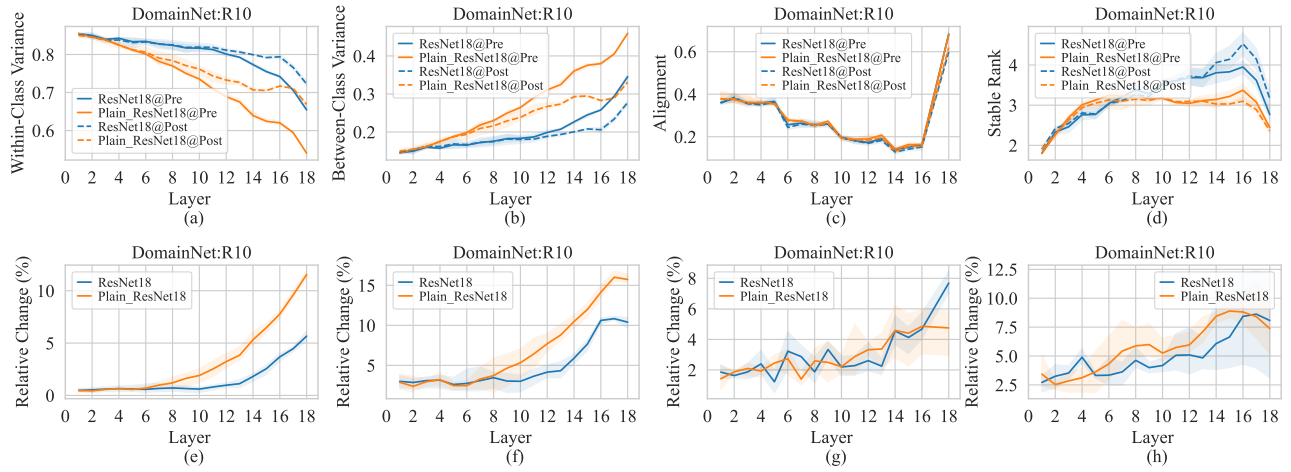


Figure 65. Comparison of feature metrics across layers with and without the use of residual connections (Plain_ResNet18) in ResNet18. This evaluation is performed on DomainNet using the model at global round 10.

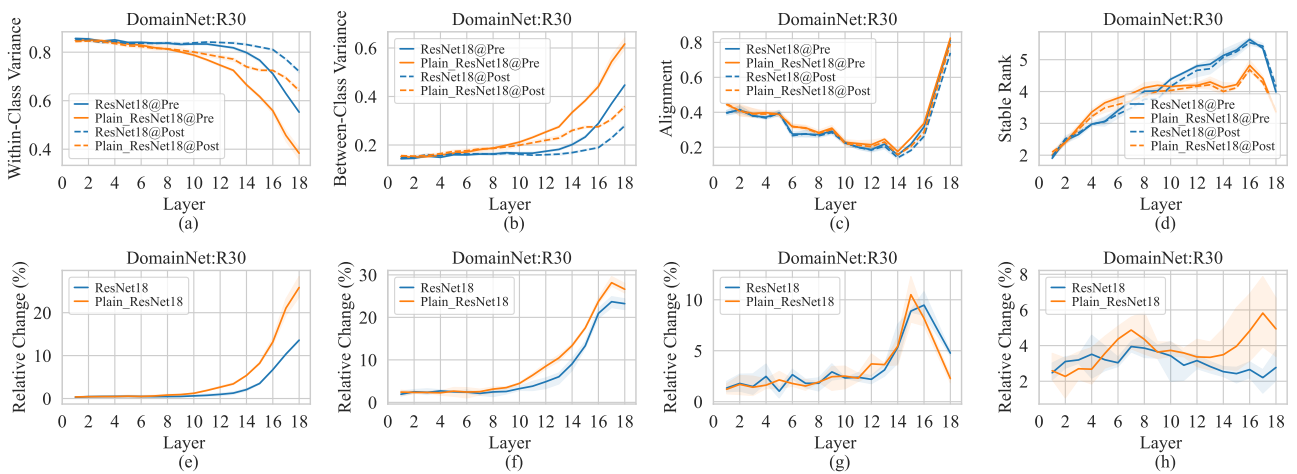


Figure 66. Comparison of feature metrics across layers with and without the use of residual connections (Plain_ResNet18) in ResNet18. This evaluation is performed on DomainNet using the model at global round 30.

Unveiling the Downsides of Model Aggregation in Federated Learning from a Layer-peeled Perspective

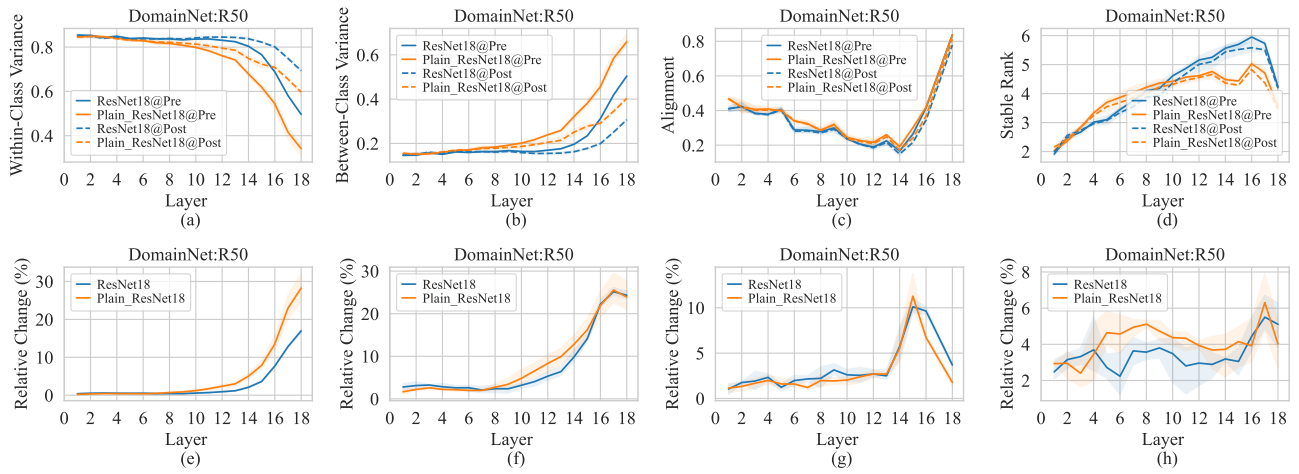


Figure 67. Comparison of feature metrics across layers with and without the use of residual connections (Plain_ResNet18) in ResNet18. This evaluation is performed on DomainNet using the model at global round 50.

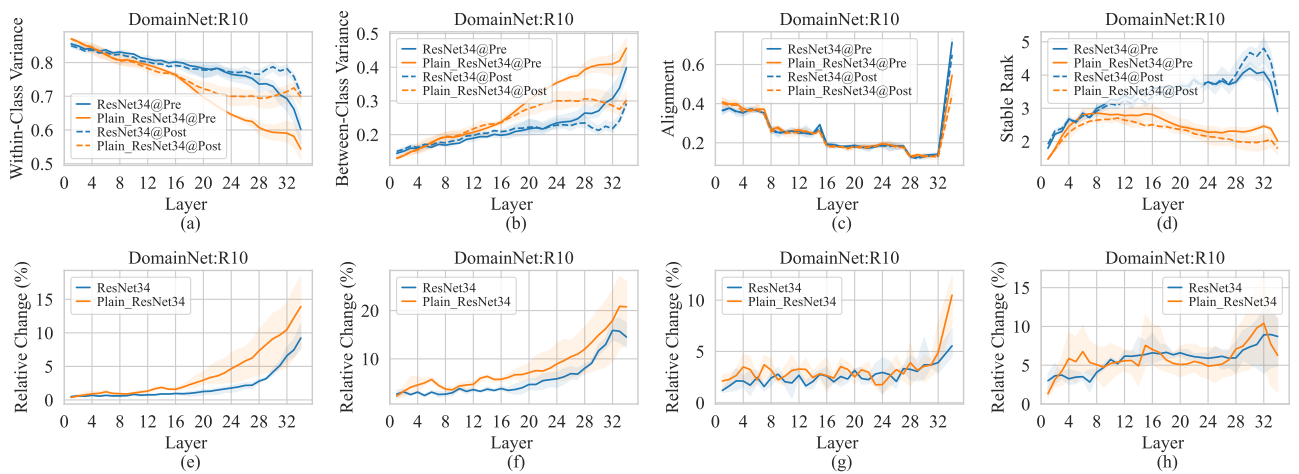


Figure 68. Comparison of feature metrics across layers with and without the use of residual connections (Plain_ResNet34) in ResNet34. This evaluation is performed on DomainNet using the model at global round 10.

Unveiling the Downsides of Model Aggregation in Federated Learning from a Layer-peeled Perspective

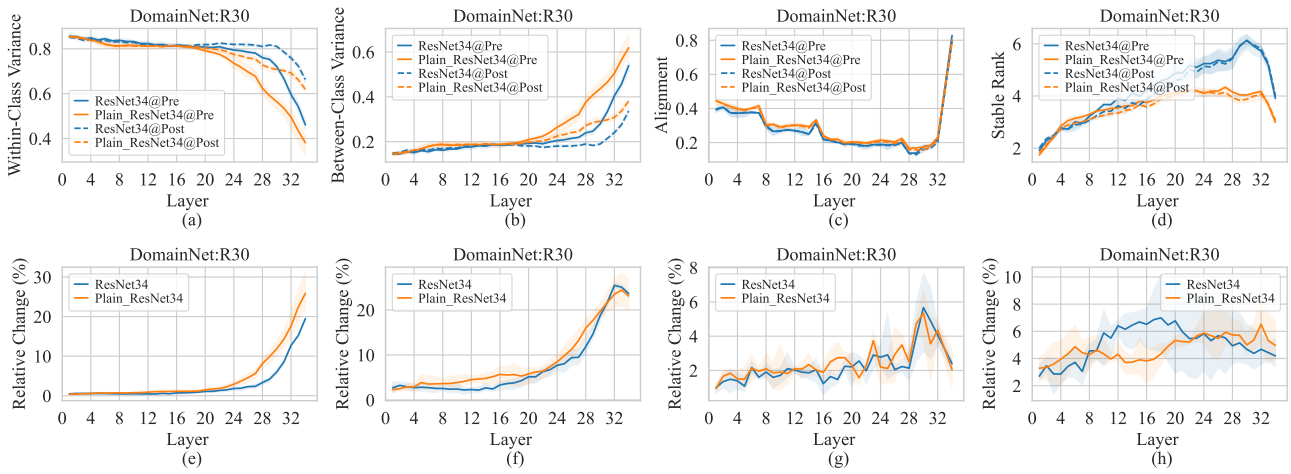


Figure 69. Comparison of feature metrics across layers with and without the use of residual connections (Plain_ResNet34) in ResNet34. This evaluation is performed on DomainNet using the model at global round 30.

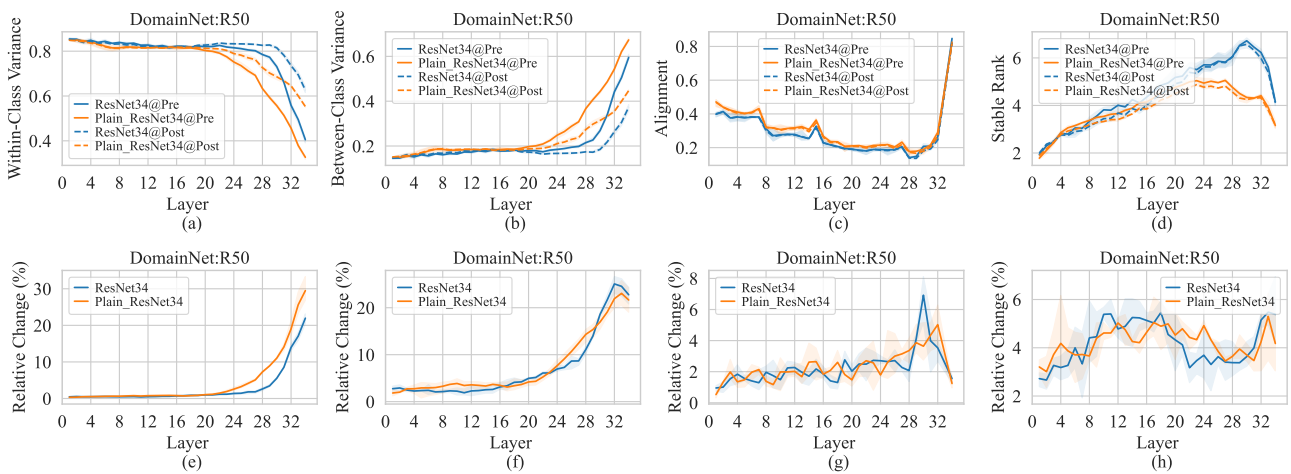


Figure 70. Comparison of feature metrics across layers with and without the use of residual connections (Plain_ResNet34) in ResNet34. This evaluation is performed on DomainNet using the model at global round 50.

Unveiling the Downsides of Model Aggregation in Federated Learning from a Layer-peeled Perspective

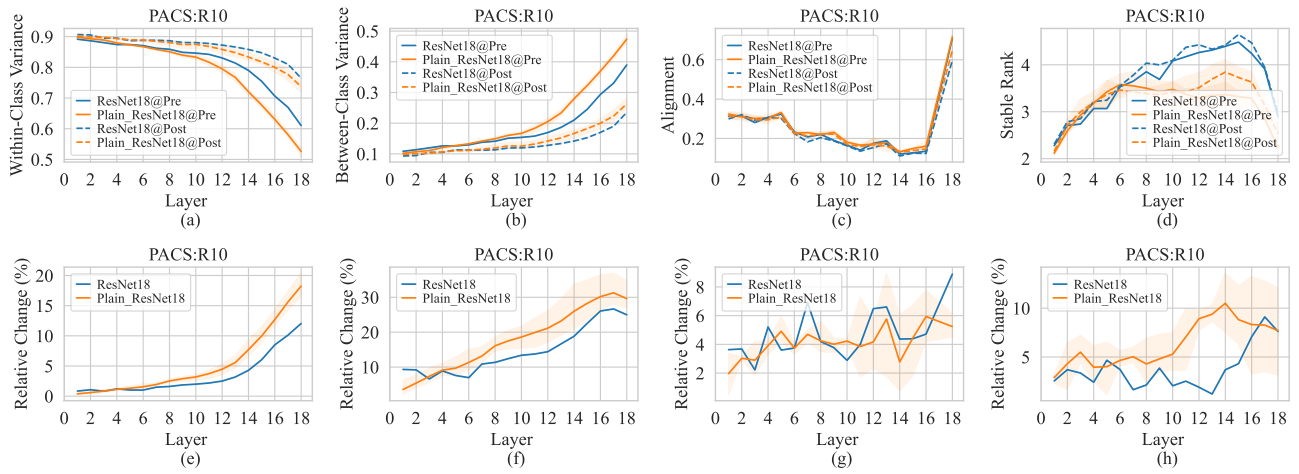


Figure 71. Comparison of feature metrics across layers with and without the use of residual connections (Plain_ResNet18) in ResNet18. This evaluation is performed on PACS using the model at global round 10.

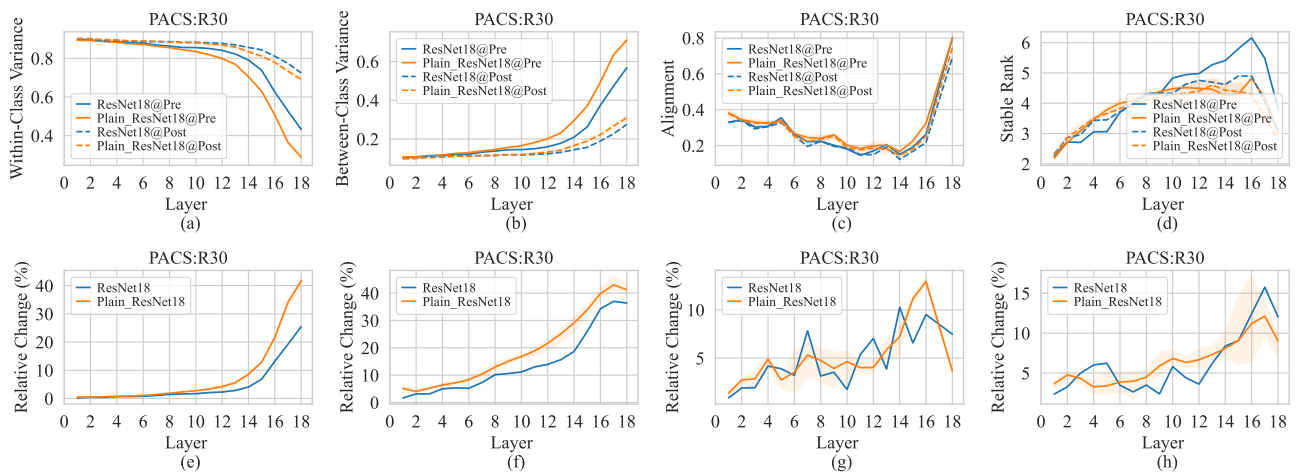


Figure 72. Comparison of feature metrics across layers with and without the use of residual connections (Plain_ResNet18) in ResNet18. This evaluation is performed on PACS using the model at global round 30.

Unveiling the Downsides of Model Aggregation in Federated Learning from a Layer-peeled Perspective

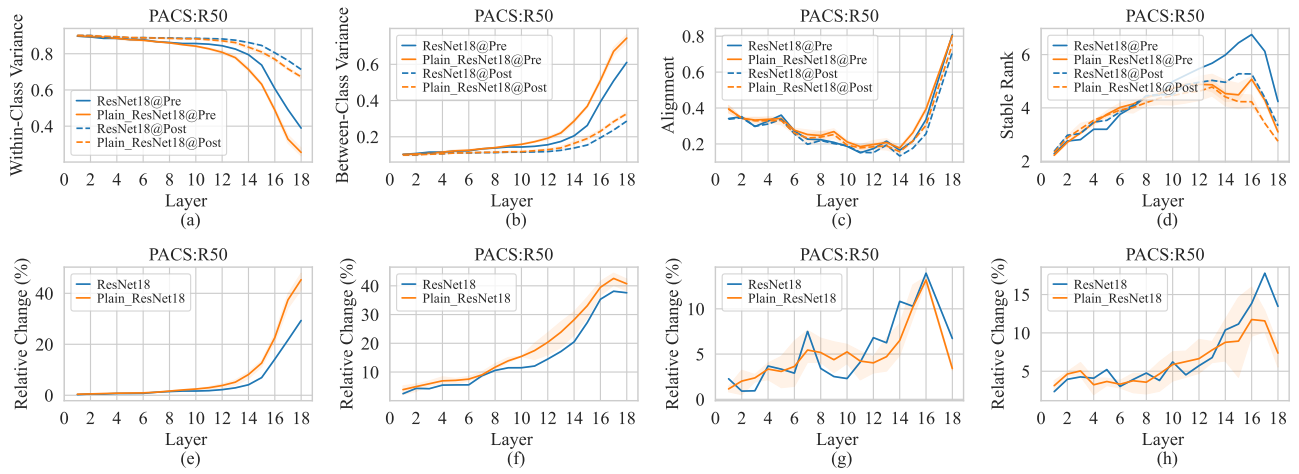


Figure 73. Comparison of feature metrics across layers with and without the use of residual connections (Plain_ResNet18) in ResNet18. This evaluation is performed on PACS using the model at global round 50.

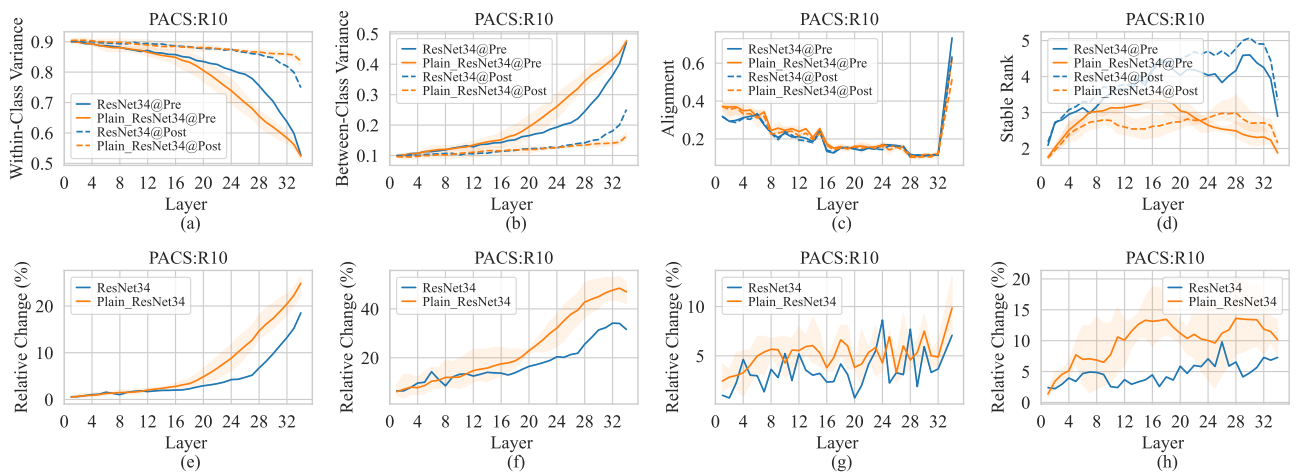


Figure 74. Comparison of feature metrics across layers with and without the use of residual connections (Plain_ResNet34) in ResNet34. This evaluation is performed on PACS using the model at global round 10.

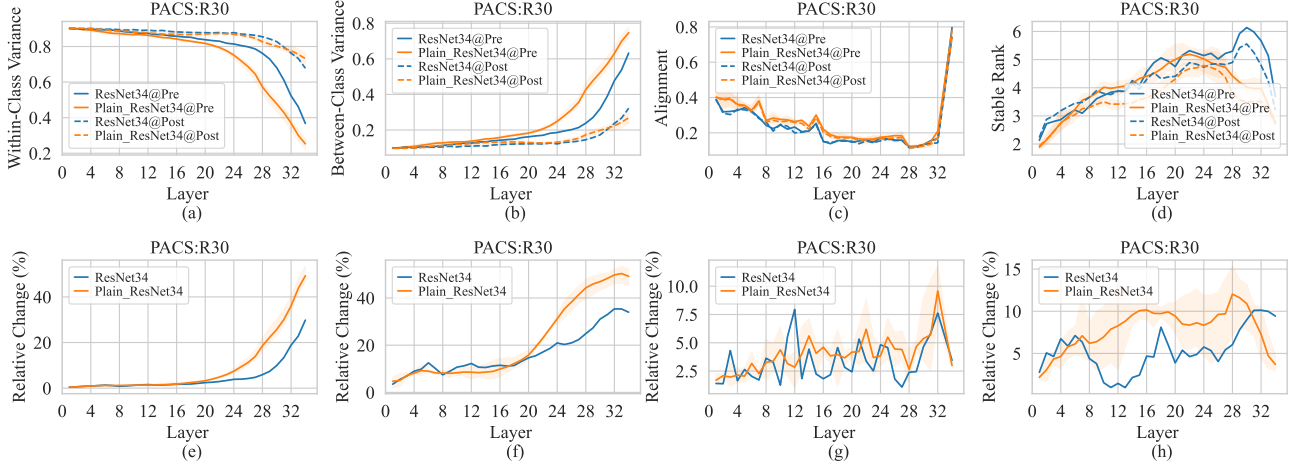


Figure 75. Comparison of feature metrics across layers with and without the use of residual connections (Plain_ResNet34) in ResNet34. This evaluation is performed on PACS using the model at global round 30.

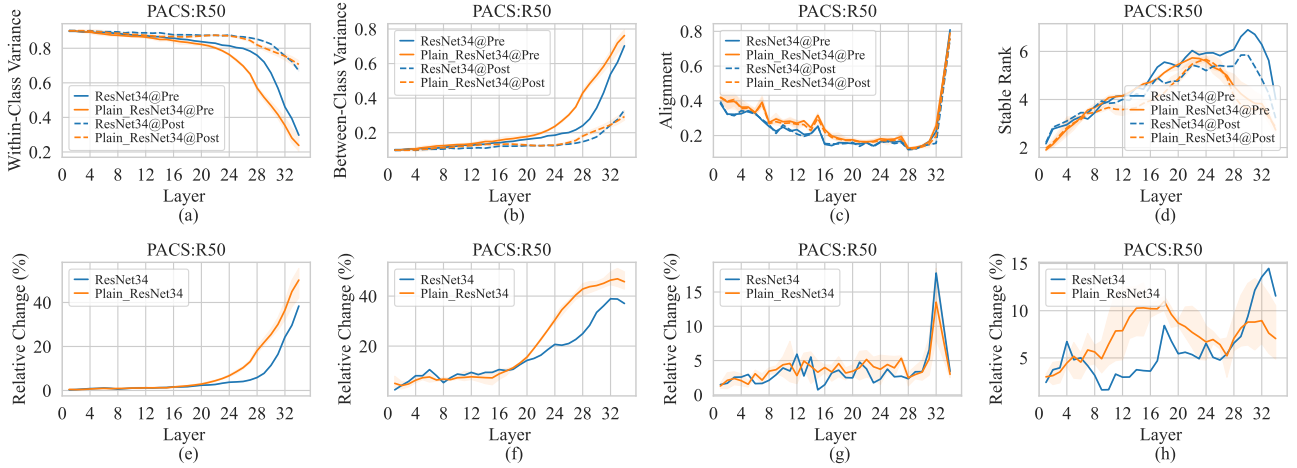


Figure 76. Comparison of feature metrics across layers with and without the use of residual connections (Plain_ResNet34) in ResNet34. This evaluation is performed on PACS using the model at global round 50.

N. Effect of Parameter Personalization

This section presents the detailed experimental results obtained by personalizing specific layers within the model during FL training, a method known as personalized federated learning (PFL). The experiments are conducted using the ResNet18 and ResNet34 models. As shown in Figure 77, both models can be divided into several blocks: the first convolutional layer, stages 1-4 (which consist of stacked convolutional layers), and the fully connected (FC) layer used for classification.

In the experiments, we explore PFL methods by personalizing specific layers within the model. Specifically, we first examine two commonly used PFL methods: FedPer (Arivazhagan et al., 2019), which personalizes the classifier, and FedBN (Li et al., 2021b), which personalizes the batch normalization (BN) layers. Additionally, motivated by (Sun et al., 2021), we consider two more strategies for parameter personalization: the successive parameter personalization strategy and the skip parameter personalization strategy. For the successive parameter personalization strategy, we personalize multiple consecutive layers starting from the first layer. In the skip parameter personalization strategy, we randomly select a layer or

block for personalization.

The experimental results show that these parameter personalization methods generally lead to better featured distributions on local data. Moreover, the relative changes introduced by model aggregation decrease as more parameters within the feature extractor are personalized. This improvement is due to the reduction in feature disruption accumulation, which is alleviated by personalizing these parameters, thereby maintaining their ability to extract locally task-specific features without being affected by model aggregation.

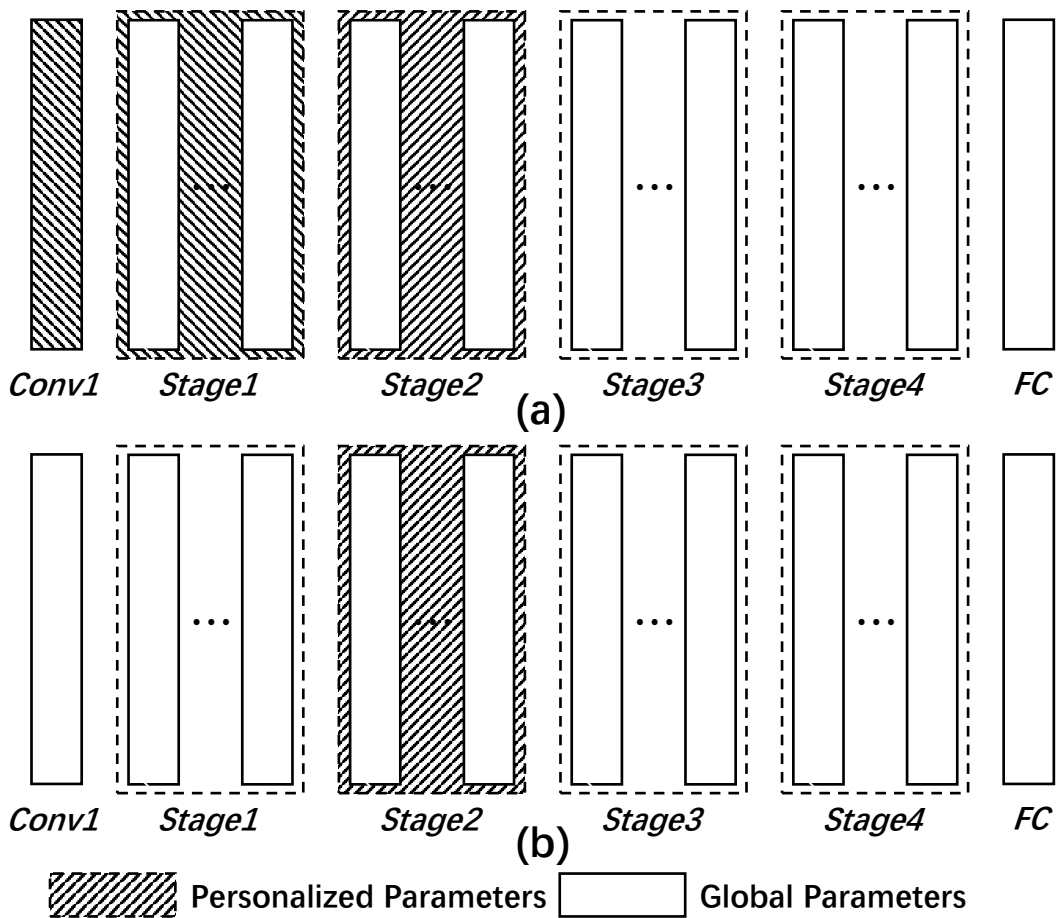


Figure 77. Illustration of the architectures of ResNet18 and ResNet34, along with the parameter personalization strategies: (a) Successive parameter personalization strategy, (b) Skip parameter personalization strategy.

N.1. Successive Parameter Personalization

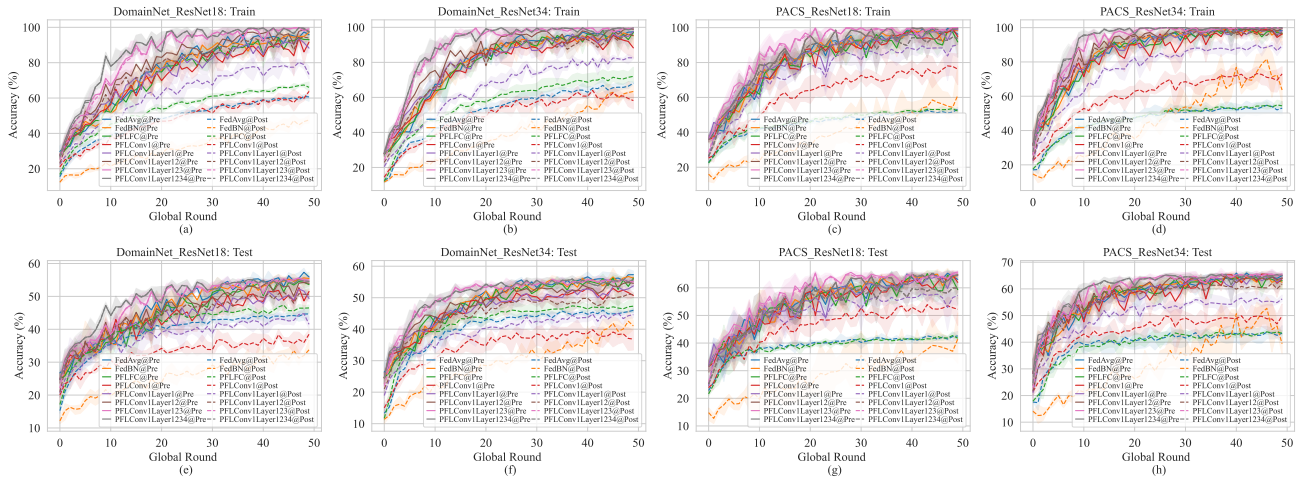


Figure 78. Accuracy curves when training FL models with different successive parameter personalization strategies, along with FedAvg, FedPer, and FedBN. In the legend, ‘C1’ is an abbreviation for the Conv1 layer, and ‘S*’ represents the abbreviation for Stage* block.

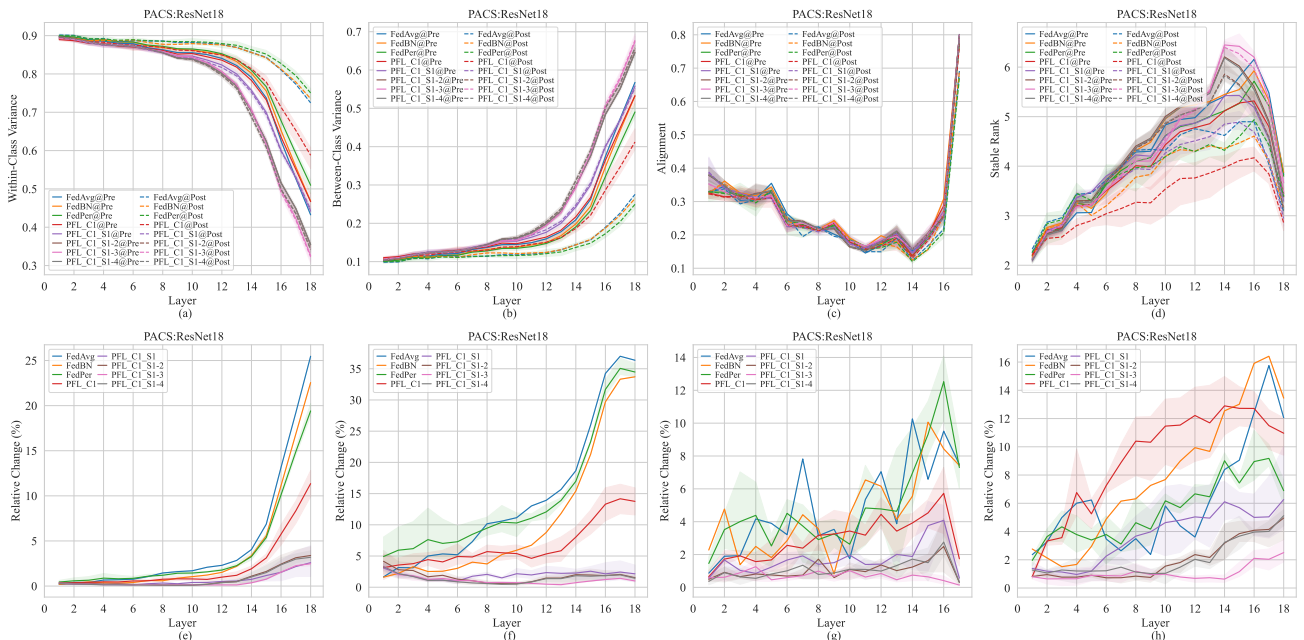


Figure 79. Feature metrics across layers at the global round 30 when training FL models with different successive parameter personalization strategies, along with FedAvg, FedPer, and FedBN. The experiments are conducted on the PACS dataset, using the ResNet18 model. In the legend, ‘C1’ is an abbreviation for the Conv1 layer, and ‘S*’ represents the abbreviation for Stage* block.

Unveiling the Downsides of Model Aggregation in Federated Learning from a Layer-peeled Perspective

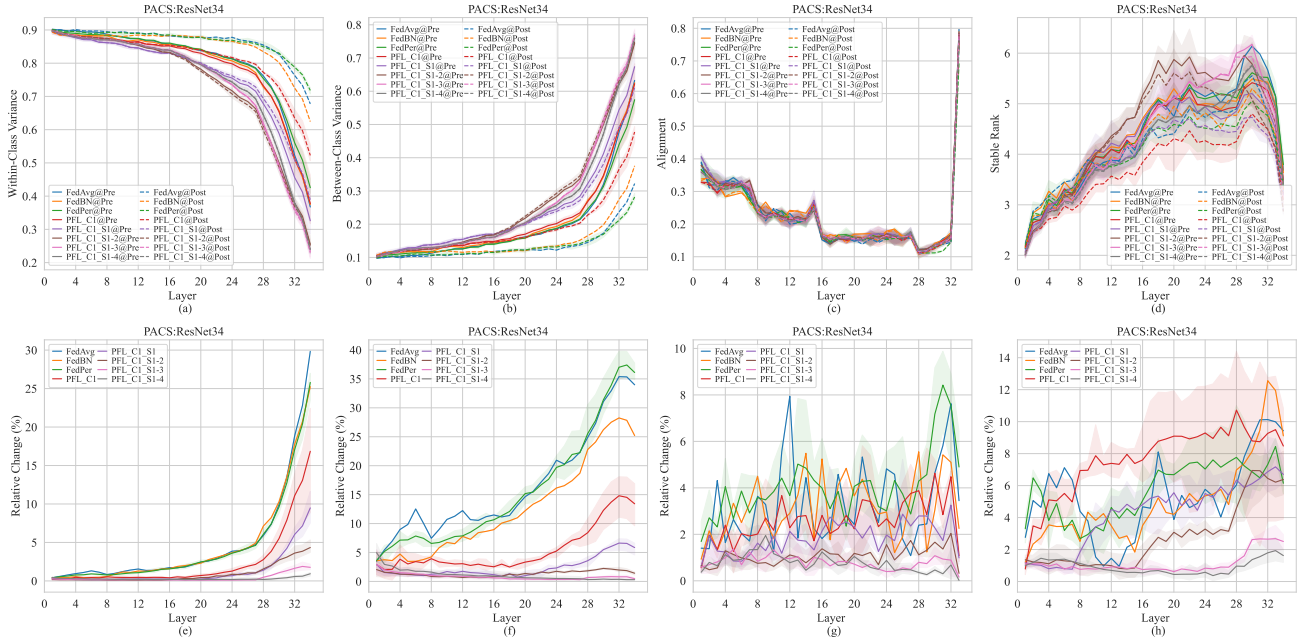


Figure 80. Feature metrics across layers at the global round 30 when training FL models with different successive parameter personalization strategies, along with FedAvg, FedPer, and FedBN. The experiments are conducted on the PACS dataset, using the ResNet34 model. In the legend, ‘C1’ is an abbreviation for the Conv1 layer, and ‘S*’ represents the abbreviation for Stage* block.

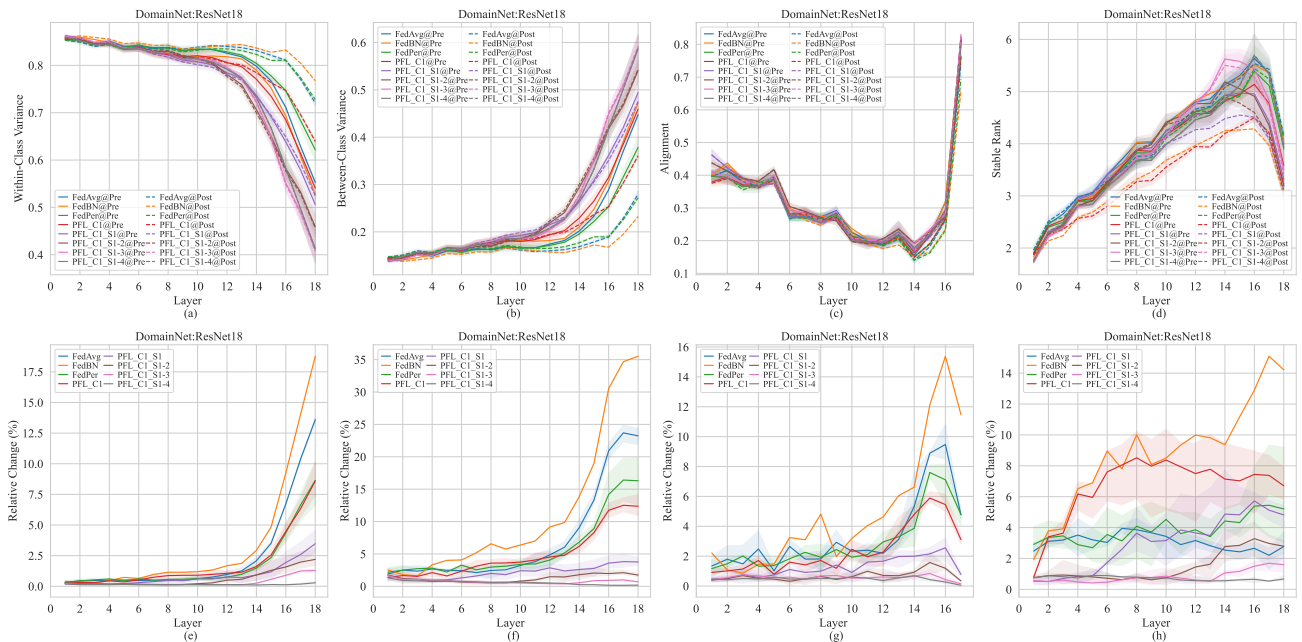


Figure 81. Feature metrics across layers at the global round 30 when training FL models with different successive parameter personalization strategies, along with FedAvg, FedPer, and FedBN. The experiments are conducted on the DomainNet dataset, using the ResNet18 model. In the legend, ‘C1’ is an abbreviation for the Conv1 layer, and ‘S*’ represents the abbreviation for Stage* block.

Unveiling the Downsides of Model Aggregation in Federated Learning from a Layer-peeled Perspective

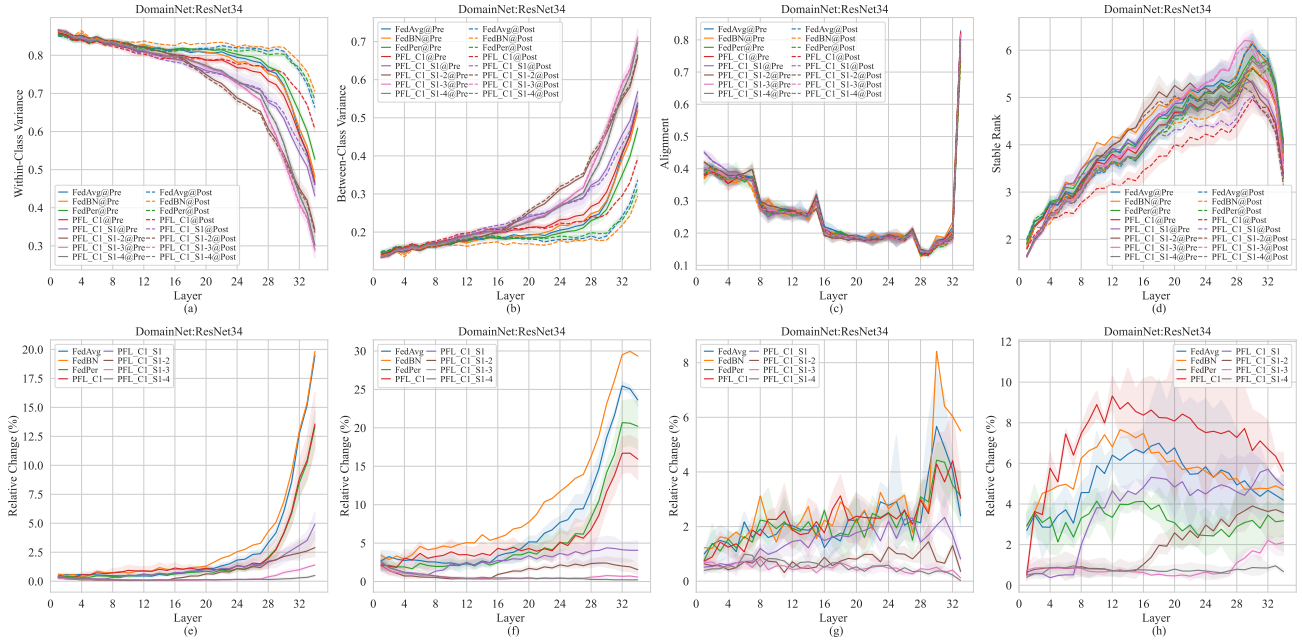


Figure 82. Feature metrics across layers at the global round 30 when training FL models with different successive parameter personalization strategies, along with FedAvg, FedPer, and FedBN. The experiments are conducted on the DomainNet dataset, using the ResNet34 model. In the legend, ‘C1’ is an abbreviation for the Conv1 layer, and ‘S*’ represents the abbreviation for Stage* block.

N.2. Skip Parameter Personalization

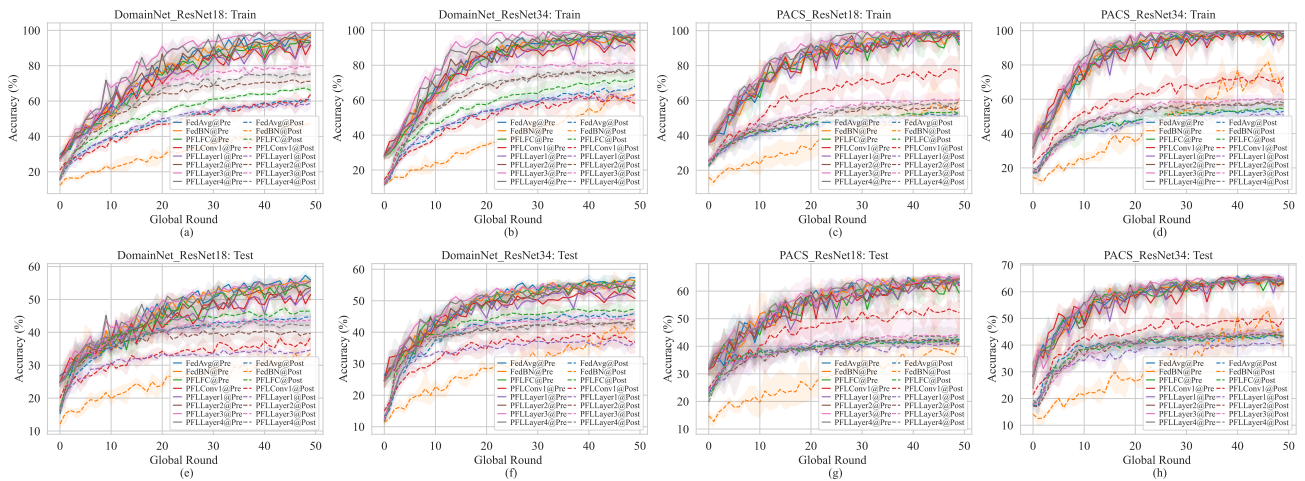


Figure 83. Accuracy curves when training FL models with different skip parameter personalization strategies, along with FedAvg, FedPer, and FedBN. In the legend, ‘C1’ is an abbreviation for the Conv1 layer, and ‘S*’ represents the abbreviation for Stage* block.

Unveiling the Downsides of Model Aggregation in Federated Learning from a Layer-peeled Perspective

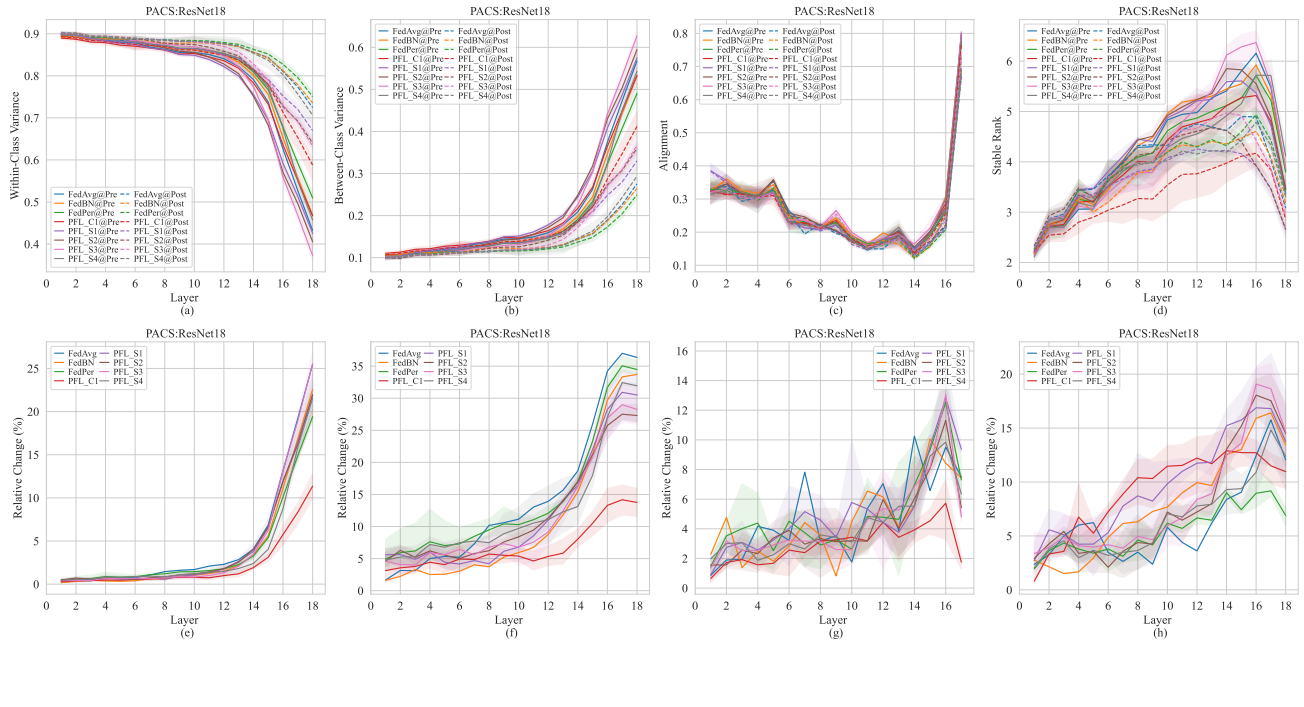


Figure 84. Feature metrics across layers at the global round 30 when training FL models with different skip parameter personalization strategies, along with FedAvg, FedPer, and FedBN. The experiments are conducted on the PACS dataset, using the ResNet18 model. In the legend, ‘C1’ is an abbreviation for the Conv1 layer, and ‘S*’ represents the abbreviation for Stage* block.

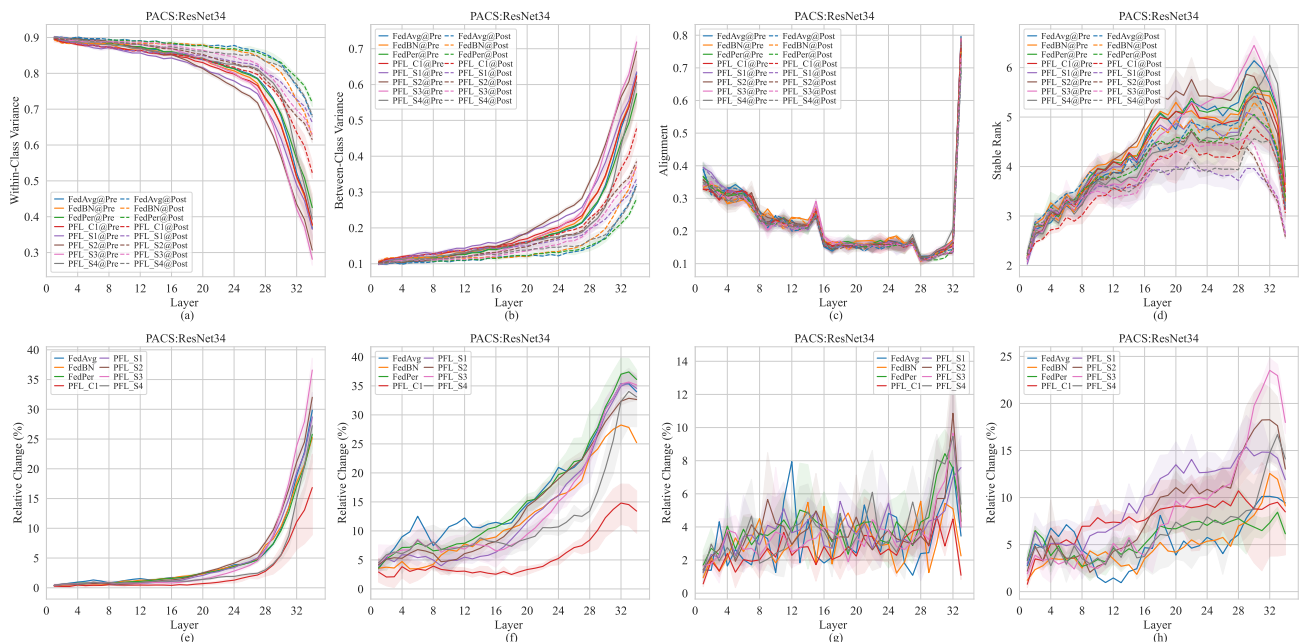


Figure 85. Feature metrics across layers at the global round 30 when training FL models with different skip parameter personalization strategies, along with FedAvg, FedPer, and FedBN. The experiments are conducted on the PACS dataset, using the ResNet34 model. In the legend, ‘C1’ is an abbreviation for the Conv1 layer, and ‘S*’ represents the abbreviation for Stage* block.

Unveiling the Downsides of Model Aggregation in Federated Learning from a Layer-peeled Perspective

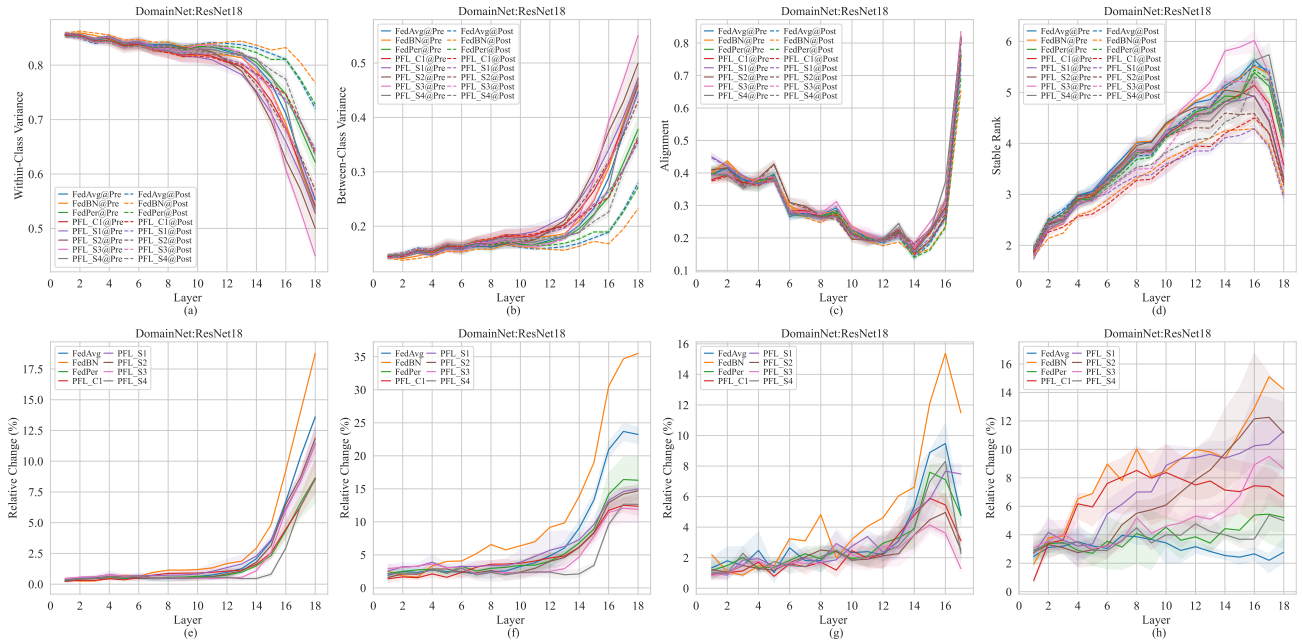


Figure 86. Feature metrics across layers at the global round 30 when training FL models with different skip parameter personalization strategies, along with FedAvg, FedPer, and FedBN. The experiments are conducted on the DomainNet dataset, using the ResNet18 model. In the legend, ‘C1’ is an abbreviation for the Conv1 layer, and ‘S*’ represents the abbreviation for Stage* block.

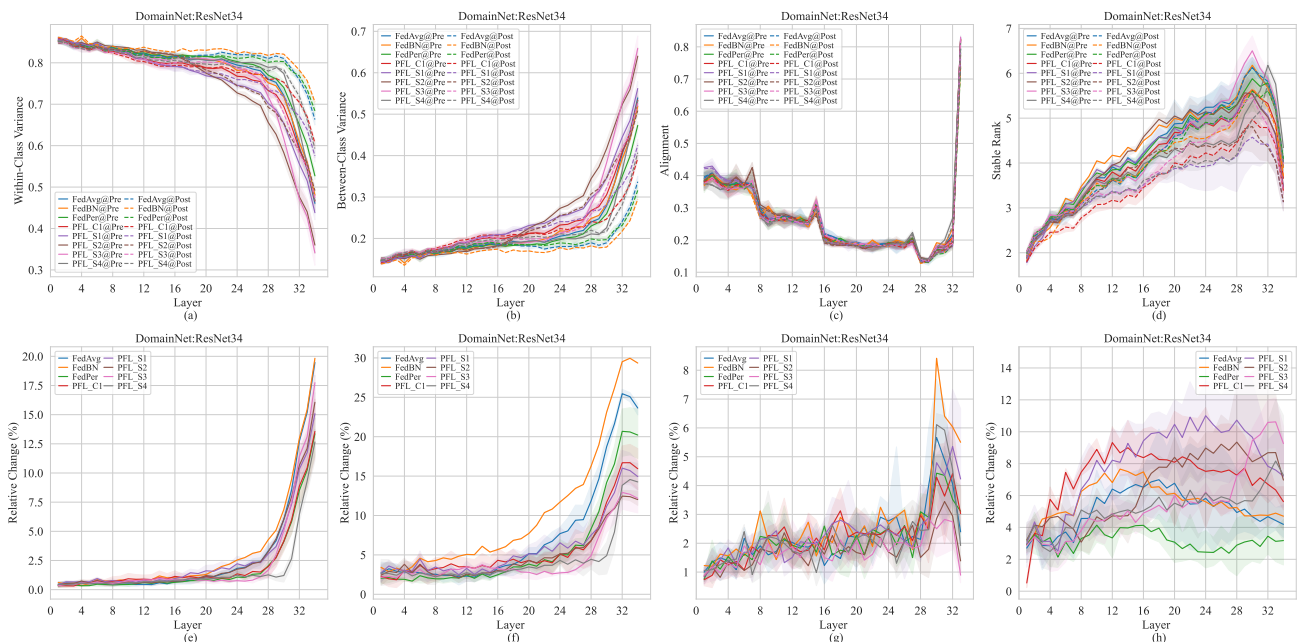


Figure 87. Feature metrics across layers at the global round 30 when training FL models with different parameter personalization strategies, along with FedAvg, FedPer, and FedBN. The experiments are conducted on the DomainNet dataset, using the ResNet34 model. In the legend, ‘C1’ is an abbreviation for the Conv1 layer, and ‘S*’ represents the abbreviation for Stage* block.

O. Detailed Results when Fine-tuning Classifier

This section provides detailed experimental results on fine-tuning the classifier to reduce the mismatch between the features extracted by the global feature extractor and the classifier. The experiments are conducted on DomainNet using ResNet18 and ResNet34 as backbones. During fine-tuning, we use SGD with momentum as the optimizer, with a learning rate of 0.01 and momentum set to 0.1. We perform only 10 epochs of fine-tuning.

It can be observed that, after fine-tuning the classifier, the alignment between the features and the classifier consistently improves using models at different global rounds during the FL training. As a result, the testing accuracy also improves.

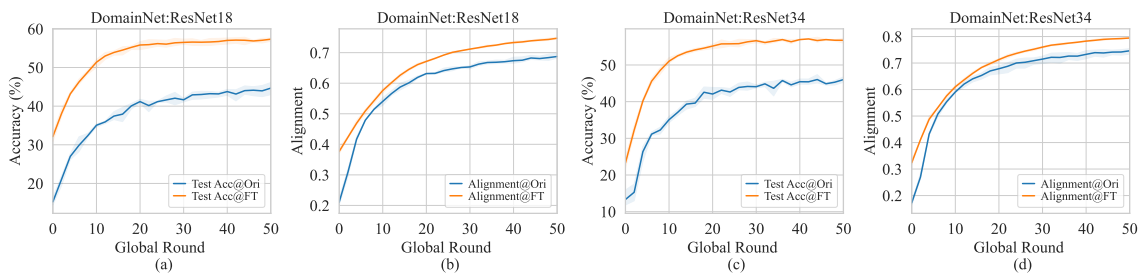


Figure 88. Accuracy and alignment between features and parameters during classifier fine-tuning across global rounds. The experiments are conducted on DomainNet dataset, using ResNet18 and ResNet34 as backbone model.

P. Effect of Pre-trained Parameter

In this section, we present detailed experimental results from using pre-trained parameters as initialization for FL training. These experiments follow the same setup as the ones described above, with the only difference being that the model is initialized with parameters pre-trained on large-scale datasets. The experimental results include the changes in feature variance across layers and training rounds, the alignment between features and parameters across layers and rounds, the stable rank of features, and the visualization of pre-aggregated and post-aggregated features. From these experiments, we find that initializing with pre-trained parameters effectively mitigates the accumulation of feature degradation. This conclusion is based on observations from experiments with randomly initialized parameters, where deeper layers only begin to converge once shallow features have reached a specific state. This is primarily because the degradation of unconverged features in the shallow layers propagates to the deeper layers, preventing them from converging until the shallow layers are well-trained. This significantly hinders the convergence rate of FL training. However, when initialized with pre-trained parameters, we find that the features of most shallow layers converge early in training, as the model already possesses strong feature extraction capabilities from being trained on a large-scale dataset. This significantly reduces the feature degradation accumulation introduced by model aggregation, thereby stabilizing and accelerating the convergence of FL training.

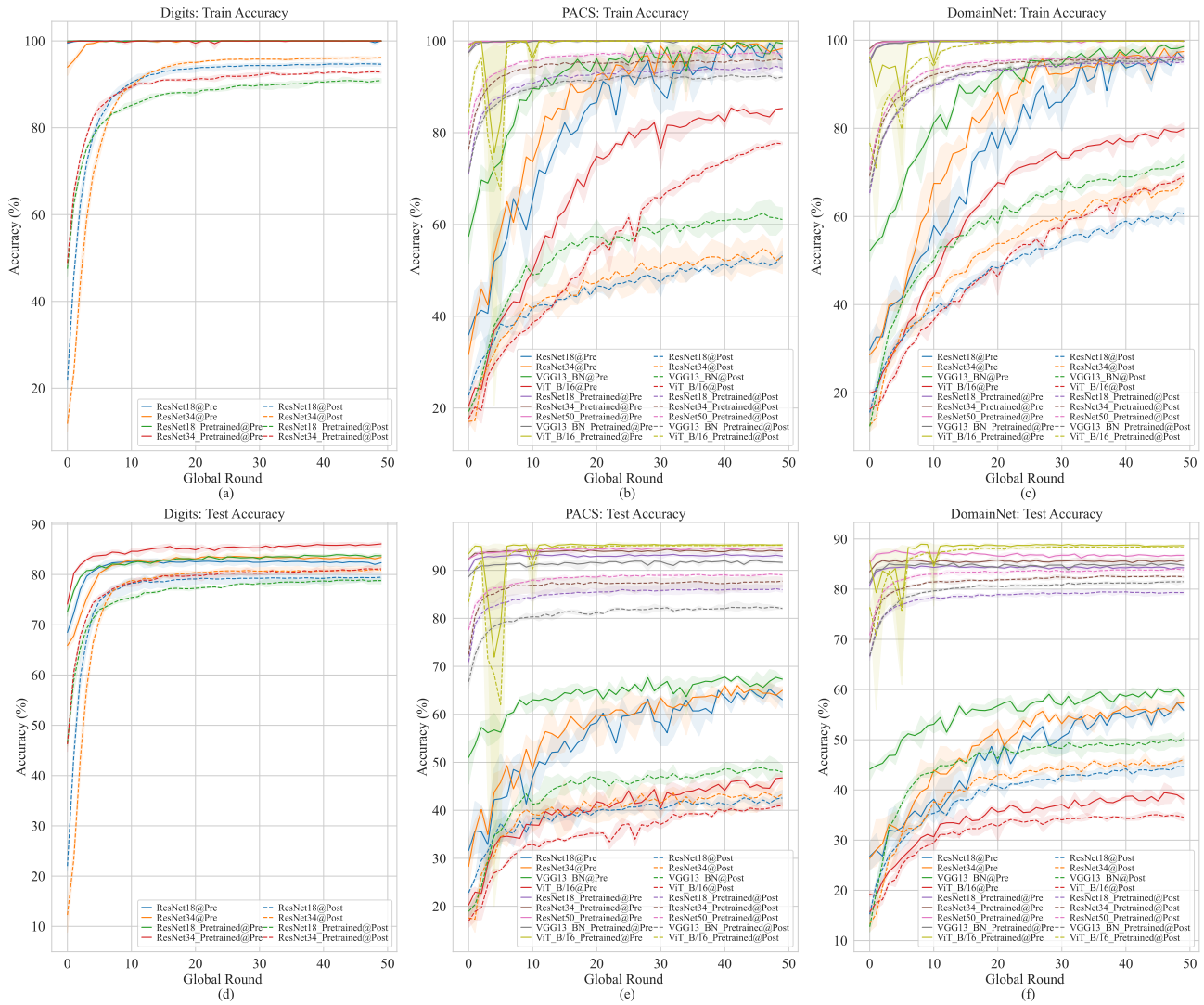


Figure 89. Comparison of accuracy with and without pre-trained parameters as initialization. The performance drop can be significantly mitigated by using pre-trained parameters.

P.1. Comparison of Training and Testing Accuracy

P.2. Changes of Feature Variance Across Layers

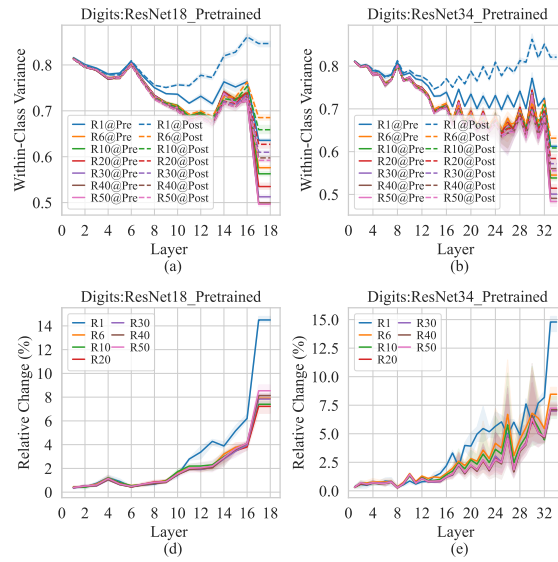


Figure 90. Changes in the normalized within-class variance of features across model layers for specific global rounds, with larger X-axis values indicating deeper layers. The model is trained on Digit-Five with multiple models that are initialized by parameters pre-trained on large-scaled datasets. The top half of the figure shows the normalized within-class variance, while the bottom half displays the relative change in variance before and after model aggregation.

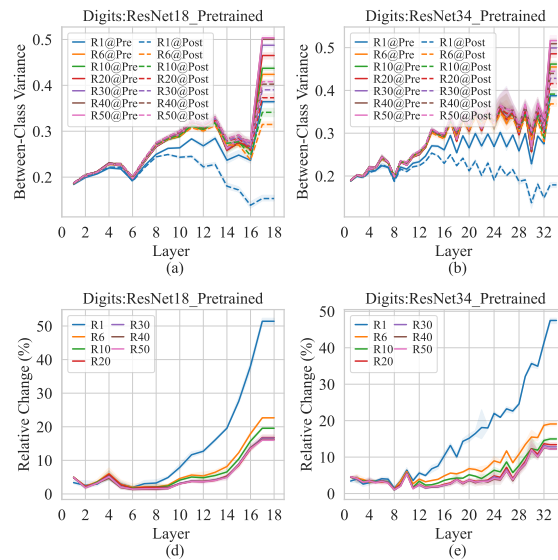


Figure 91. Changes in the normalized between-class variance of features across model layers for specific global rounds, with larger X-axis values indicating deeper layers. The model is trained on Digit-Five with multiple models that are initialized by parameters pre-trained on large-scaled datasets. The top half of the figure shows the normalized between-class variance, while the bottom half displays the relative change in variance before and after model aggregation.

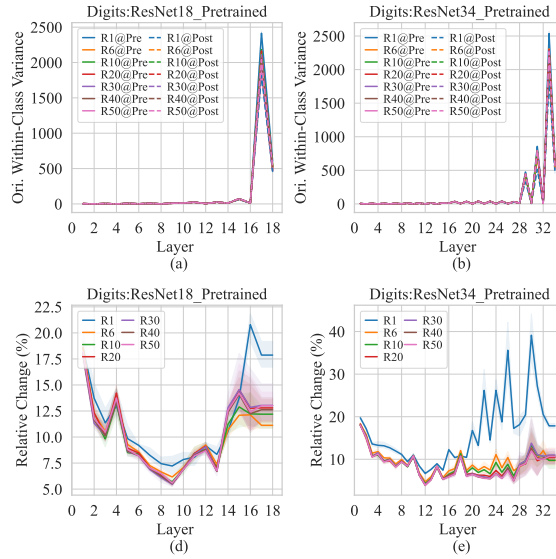


Figure 92. Changes in the original unnormalized within-class variance of features across model layers for specific global rounds, with larger X-axis values indicating deeper layers. The model is trained on Digit-Five with multiple models that are initialized by parameters pre-trained on large-scaled datasets. The top half of the figure shows the original unnormalized within-class variance, while the bottom half displays the relative change in variance before and after model aggregation.

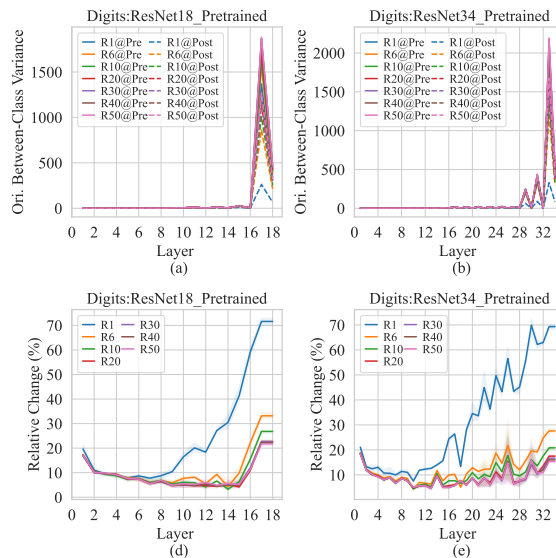


Figure 93. Changes in the original unnormalized between-class variance of features across model layers for specific global rounds, with larger X-axis values indicating deeper layers. The model is trained on Digit-Five with multiple models that are initialized by parameters pre-trained on large-scaled datasets. The top half of the figure shows the original unnormalized between-class variance, while the bottom half displays the relative change in variance before and after model aggregation.

Unveiling the Downsides of Model Aggregation in Federated Learning from a Layer-peeled Perspective

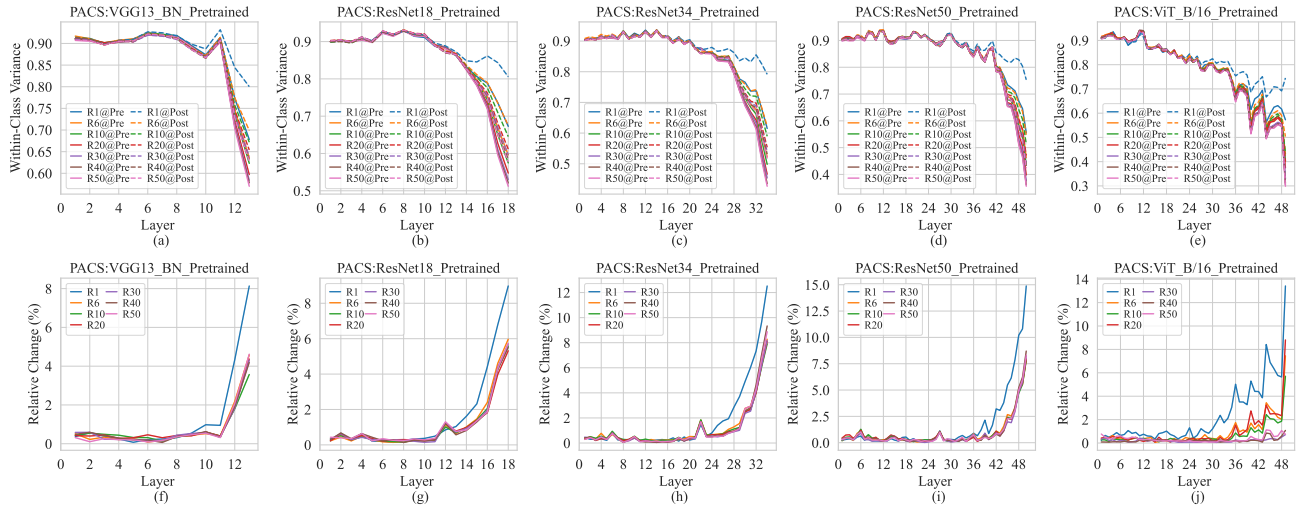


Figure 94. Changes in the normalized within-class variance of features across model layers for specific global rounds, with larger X-axis values indicating deeper layers. The model is trained on PACS with multiple models that are initialized by parameters pre-trained on large-scaled datasets. The top half of the figure shows the normalized within-class variance, while the bottom half displays the relative change in variance before and after model aggregation.

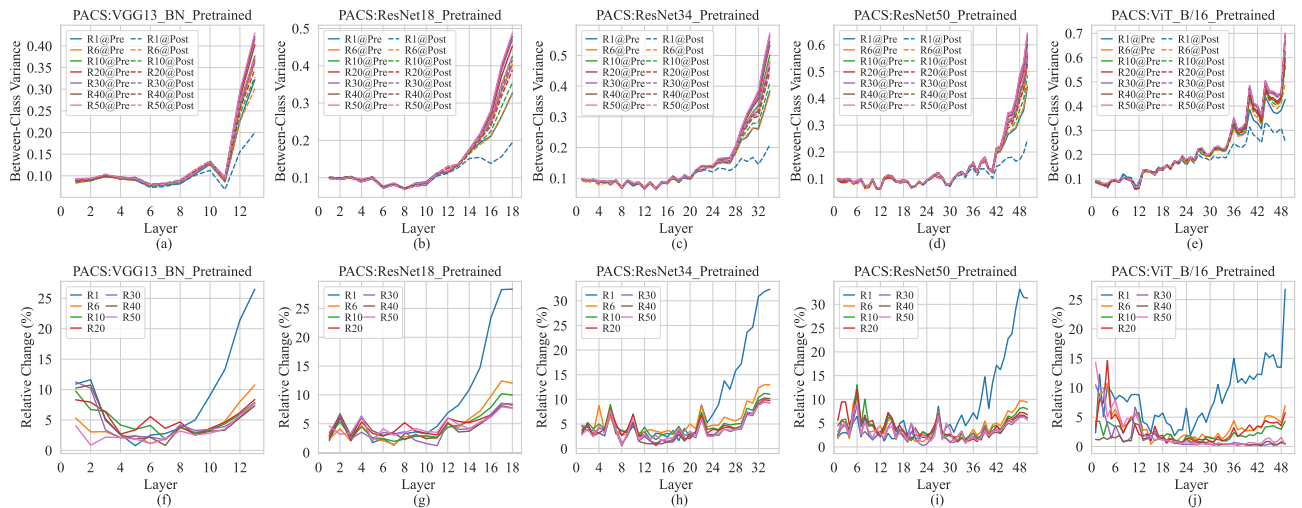


Figure 95. Changes in the normalized between-class variance of features across model layers for specific global rounds, with larger X-axis values indicating deeper layers. The model is trained on PACS with multiple models that are initialized by parameters pre-trained on large-scaled datasets. The top half of the figure shows the normalized between-class variance, while the bottom half displays the relative change in variance before and after model aggregation.

Unveiling the Downsides of Model Aggregation in Federated Learning from a Layer-peeled Perspective

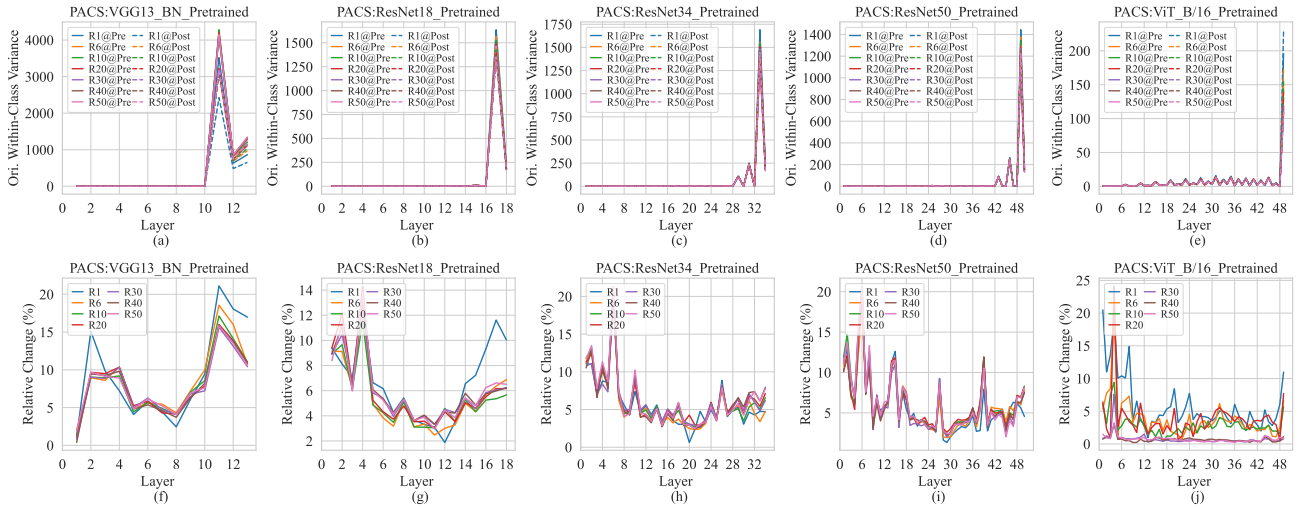


Figure 96. Changes in the original unnormalized within-class variance of features across model layers for specific global rounds, with larger X-axis values indicating deeper layers. The model is trained on PACS with multiple models that are initialized by parameters pre-trained on large-scaled datasets. The top half of the figure shows the original unnormalized within-class variance, while the bottom half displays the relative change in variance before and after model aggregation.

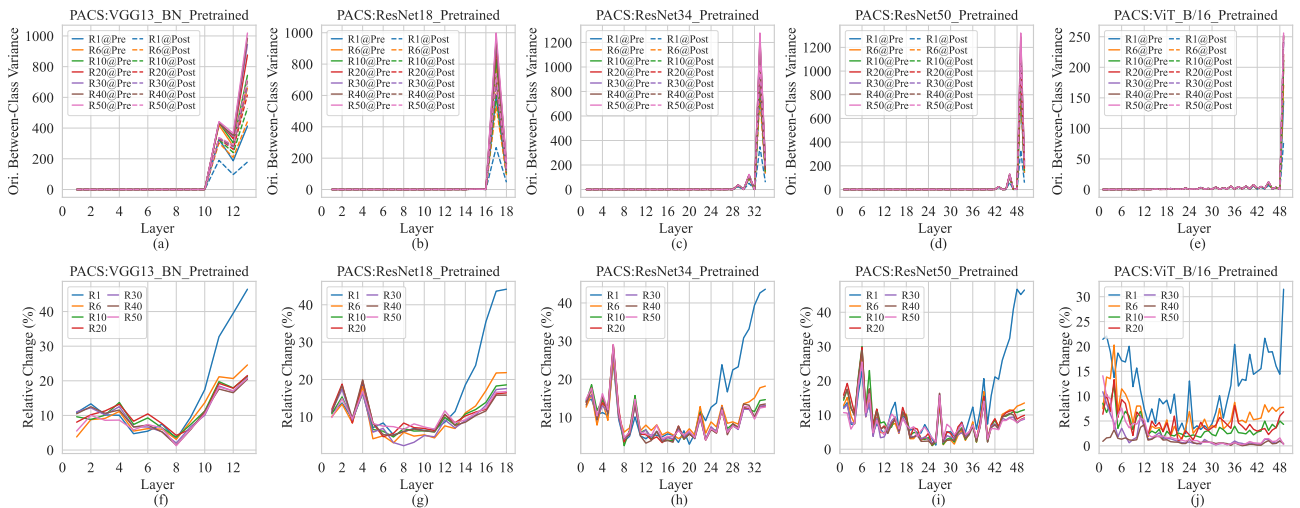


Figure 97. Changes in the original unnormalized between-class variance of features across model layers for specific global rounds, with larger X-axis values indicating deeper layers. The model is trained on PACS with multiple models that are initialized by parameters pre-trained on large-scaled datasets. The top half of the figure shows the original unnormalized between-class variance, while the bottom half displays the relative change in variance before and after model aggregation.

Unveiling the Downsides of Model Aggregation in Federated Learning from a Layer-peeled Perspective

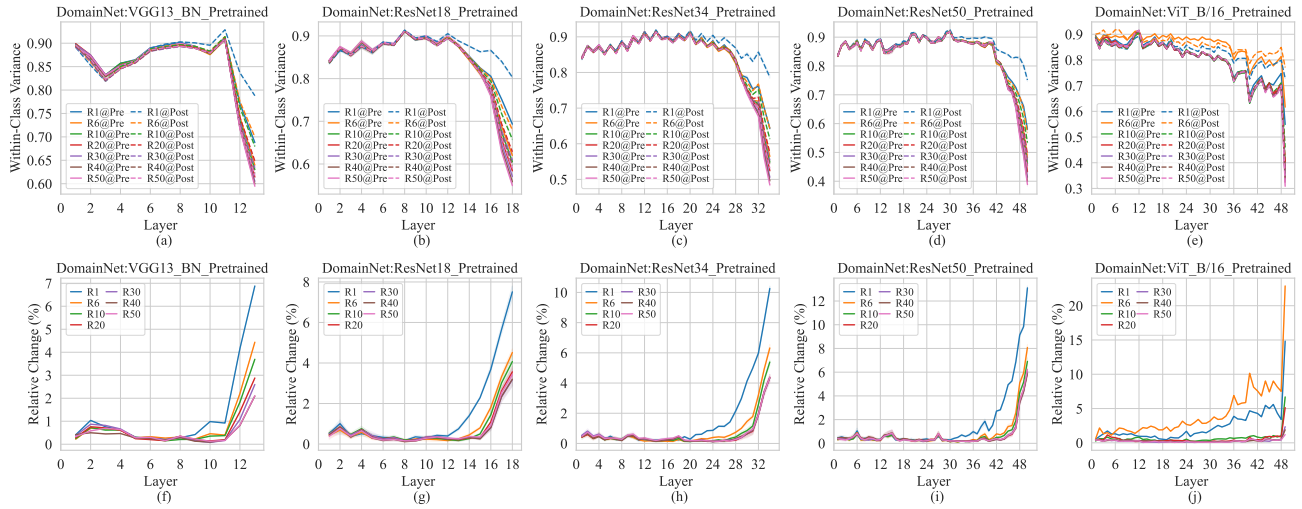


Figure 98. Changes in the normalized within-class variance of features across model layers for specific global rounds, with larger X-axis values indicating deeper layers. The model is trained on DomainNet with multiple models that are initialized by parameters pre-trained on large-scaled datasets. The top half of the figure shows the normalized within-class variance, while the bottom half displays the relative change in variance before and after model aggregation.

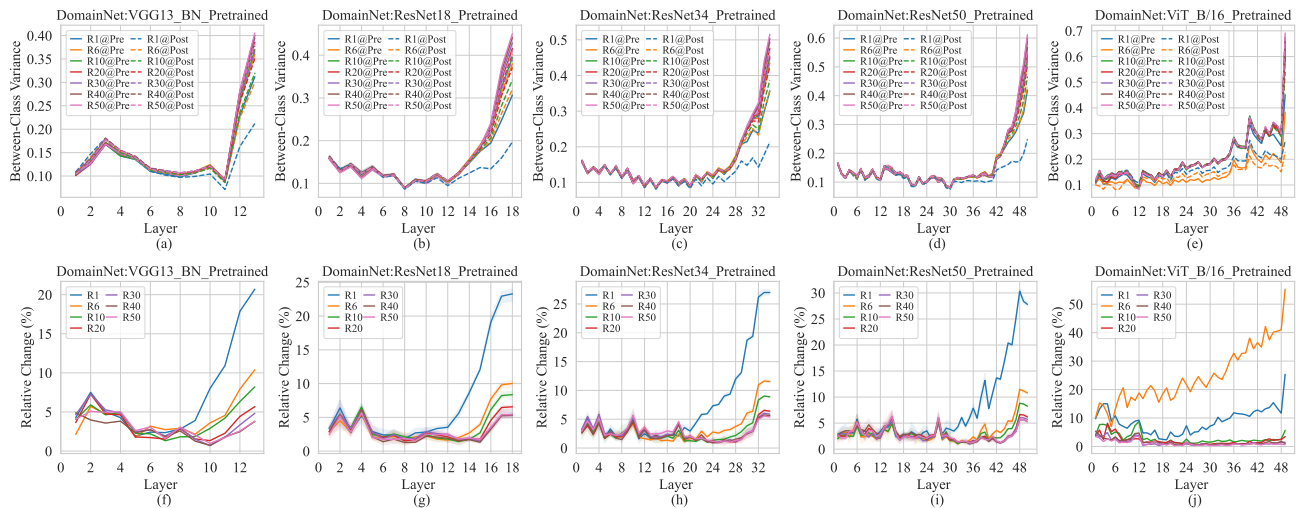


Figure 99. Changes in the normalized between-class variance of features across model layers for specific global rounds, with larger X-axis values indicating deeper layers. The model is trained on DomainNet with multiple models that are initialized by parameters pre-trained on large-scaled datasets. The top half of the figure shows the normalized between-class variance, while the bottom half displays the relative change in variance before and after model aggregation.

Unveiling the Downsides of Model Aggregation in Federated Learning from a Layer-peeled Perspective

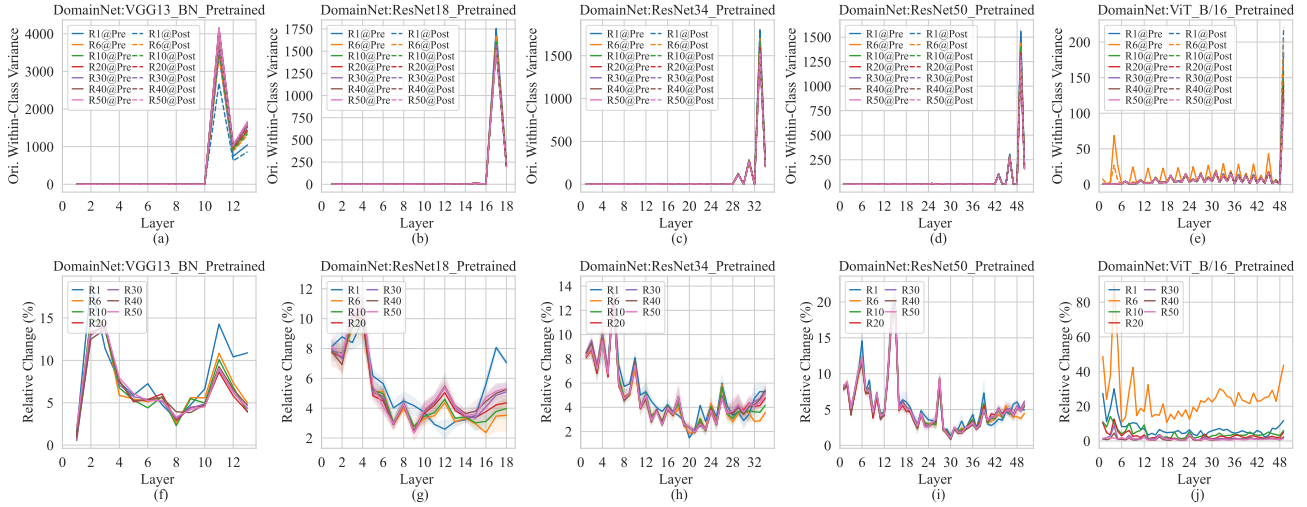


Figure 100. Changes in the unnormalized within-class variance of features across model layers for specific global rounds, with larger X-axis values indicating deeper layers. The model is trained on DomainNet with multiple models that are initialized by parameters pre-trained on large-scaled datasets. The top half of the figure shows the original unnormalized within-class variance, while the bottom half displays the relative change in variance before and after model aggregation.

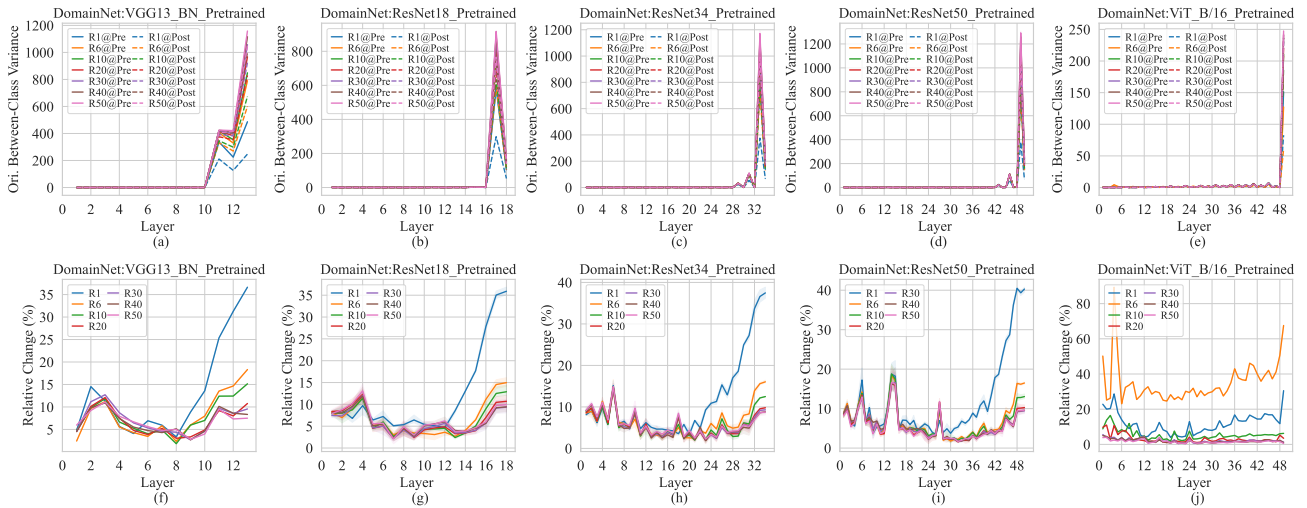


Figure 101. Changes in the unnormalized between-class variance of features across model layers for specific global rounds, with larger X-axis values indicating deeper layers. The model is trained on DomainNet with multiple models that are initialized by parameters pre-trained on large-scaled datasets. The top half of the figure shows the original unnormalized between-class variance, while the bottom half displays the relative change in variance before and after model aggregation.

P.3. Changes of Feature Variance Across Training Rounds

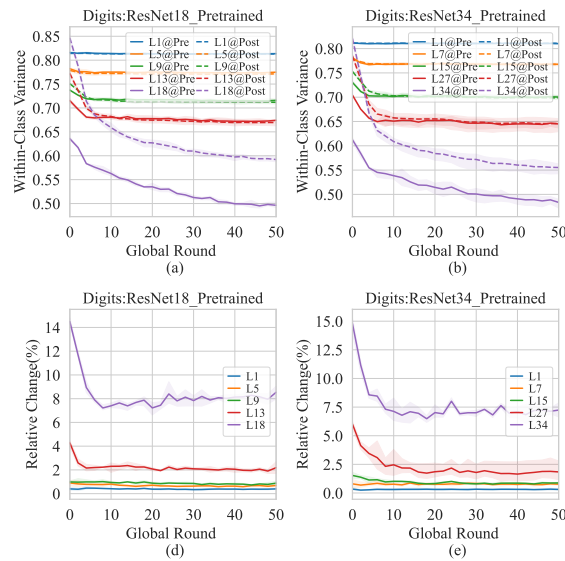


Figure 102. Changes in the normalized within-class variance of features across FL training at specific model layers. The model is trained on Digit-Five with multiple models that are initialized by parameters pre-trained on large-scaled datasets. The top half of the figure shows the original normalized within-class variance, while the bottom half displays the relative change in variance before and after model aggregation.

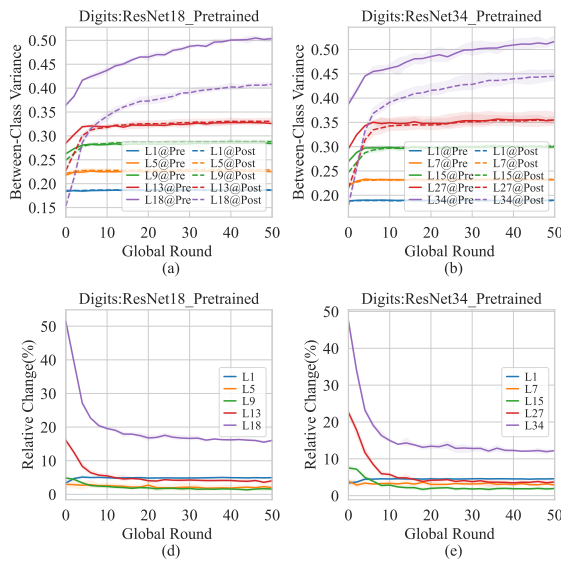


Figure 103. Changes in the normalized between-class variance of features across FL training at specific model layers. The model is trained on Digit-Five with multiple models that are initialized by parameters pre-trained on large-scaled datasets. The top half of the figure shows the normalized within-class variance, while the bottom half displays the relative change in variance before and after model aggregation.

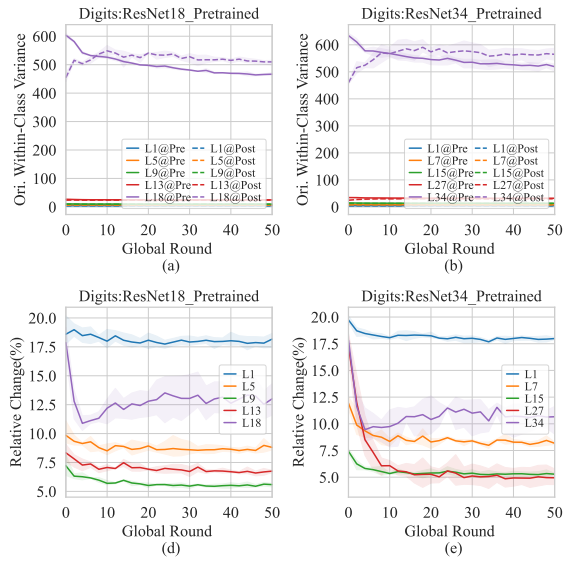


Figure 104. Changes in the original unnormalized within-class variance of features across FL training at specific model layers. The model is trained on Digit-Five with multiple models that are initialized by parameters pre-trained on large-scaled datasets. The top half of the figure shows the original unnormalized within-class variance, while the bottom half displays the relative change in variance before and after model aggregation.

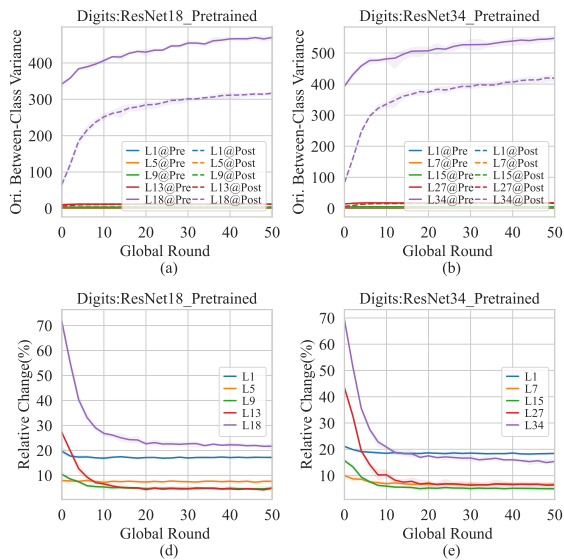


Figure 105. Changes in the original unnormalized between-class variance of features across FL training at specific model layers. The model is trained on Digit-Five with multiple models that are initialized by parameters pre-trained on large-scaled datasets. The top half of the figure shows the original unnormalized between-class variance, while the bottom half displays the relative change in variance before and after model aggregation.

Unveiling the Downsides of Model Aggregation in Federated Learning from a Layer-peeled Perspective

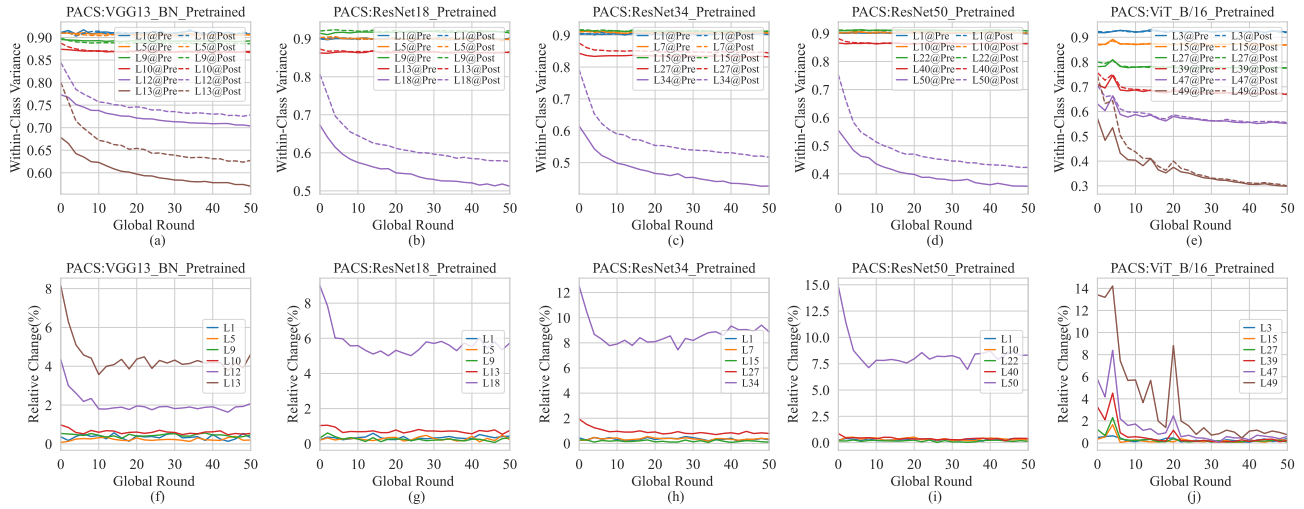


Figure 106. Changes in the normalized within-class variance of features across FL training at specific model layers. The model is trained on PACS with multiple models that are initialized by parameters pre-trained on large-scaled datasets. The top half of the figure shows the normalized within-class variance, while the bottom half displays the relative change in variance before and after model aggregation.

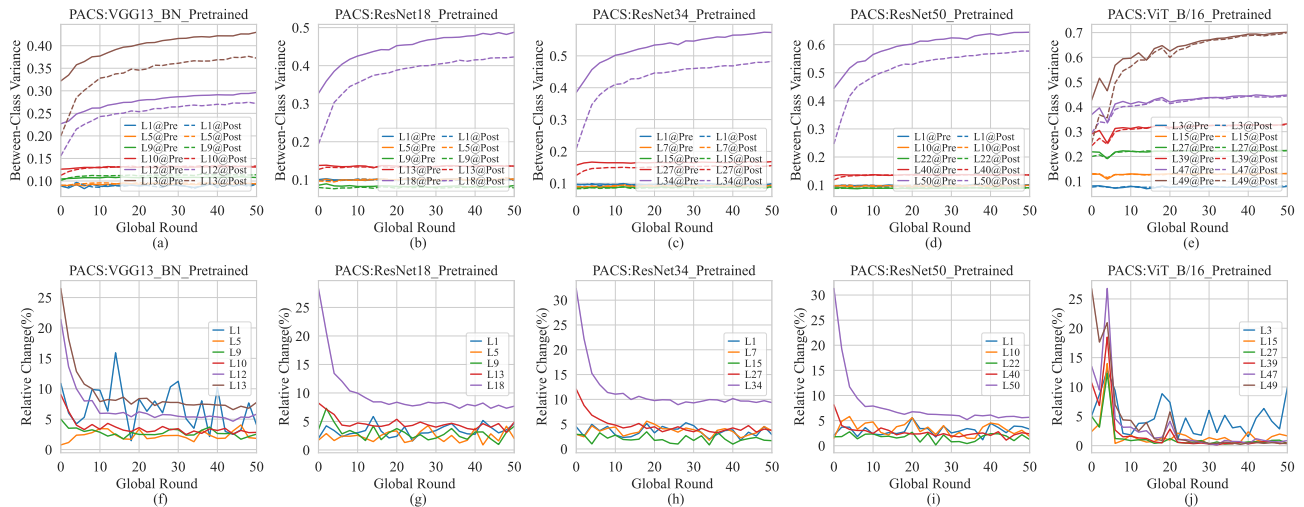


Figure 107. Changes in the normalized between-class variance of features across FL training at specific model layers. The model is trained on PACS with multiple models that are initialized by parameters pre-trained on large-scaled datasets. The top half of the figure shows the normalized between-class variance, while the bottom half displays the relative change in variance before and after model aggregation.

Unveiling the Downsides of Model Aggregation in Federated Learning from a Layer-peeled Perspective

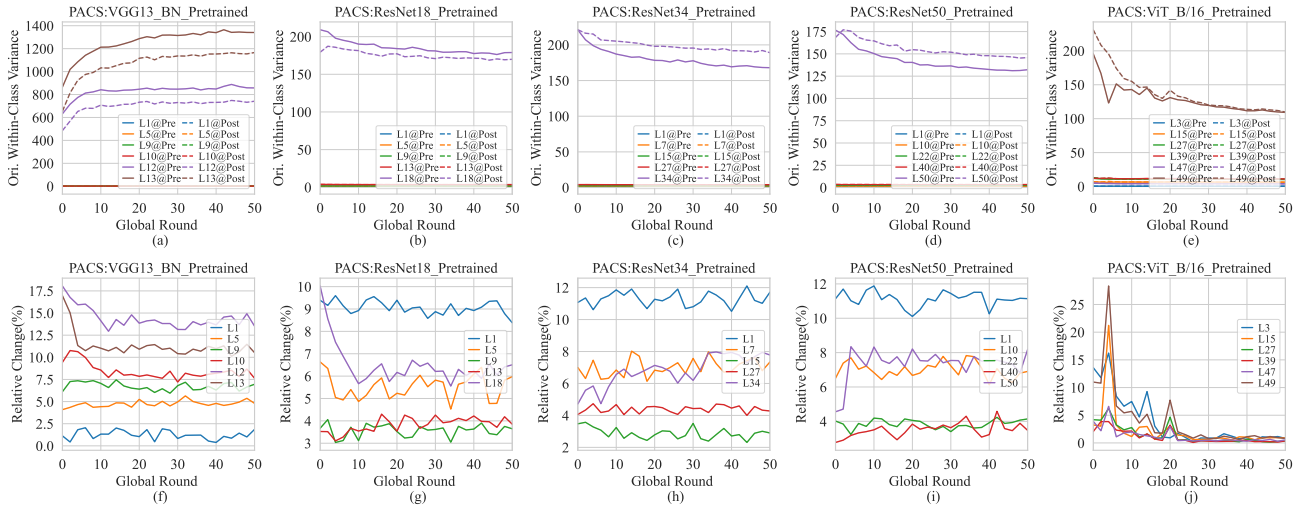


Figure 108. Changes in the original unnormalized within-class variance of features across FL training at specific model layers. The model is trained on PACS with multiple models that are initialized by parameters pre-trained on large-scaled datasets. The top half of the figure shows the original unnormalized within-class variance, while the bottom half displays the relative change in variance before and after model aggregation.

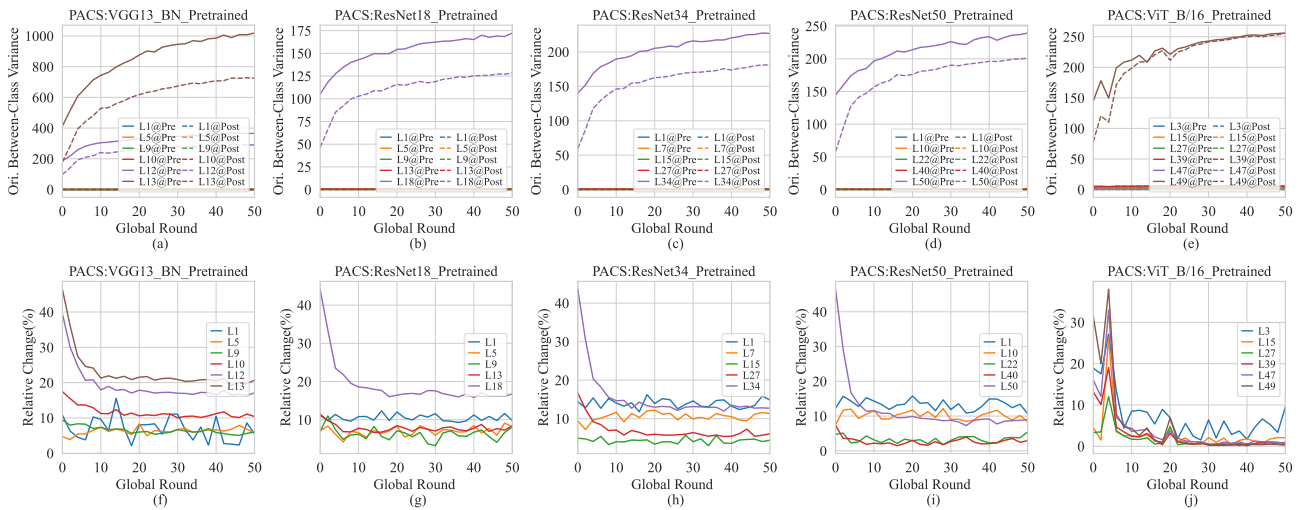


Figure 109. Changes in the original unnormalized between-class variance of features across FL training at specific model layers. The model is trained on PACS with multiple models that are initialized by parameters pre-trained on large-scaled datasets. The top half of the figure shows the original unnormalized between-class variance, while the bottom half displays the relative change in variance before and after model aggregation.

Unveiling the Downsides of Model Aggregation in Federated Learning from a Layer-peeled Perspective

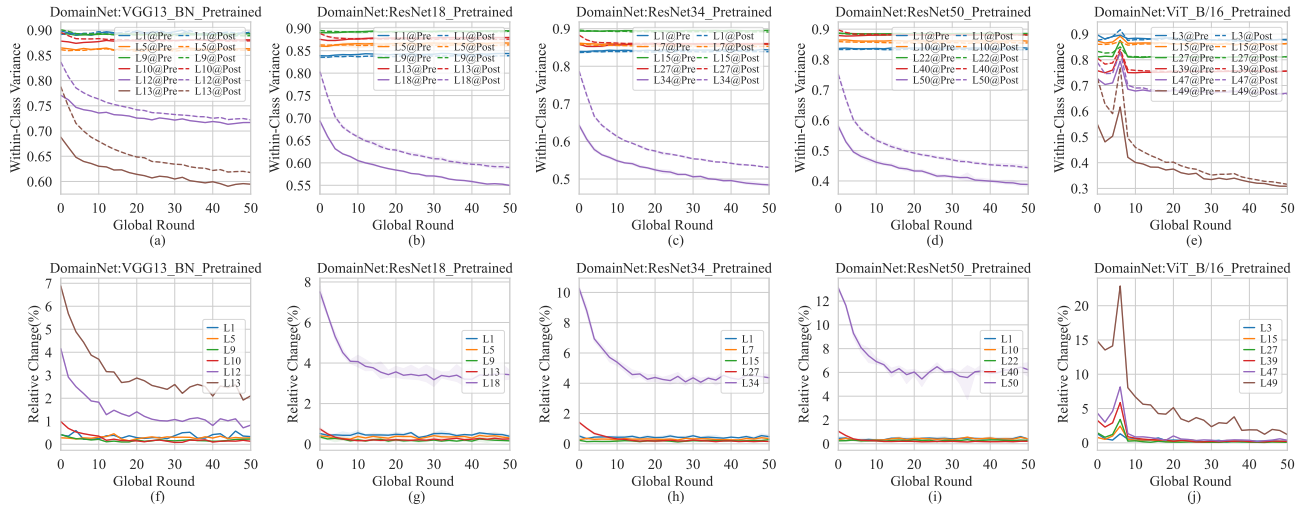


Figure 110. Changes in the normalized within-class variance of features across FL training at specific model layers. The model is trained on DomainNet with multiple models that are initialized by parameters pre-trained on large-scaled datasets. The top half of the figure shows the normalized within-class variance, while the bottom half displays the relative change in variance before and after model aggregation.

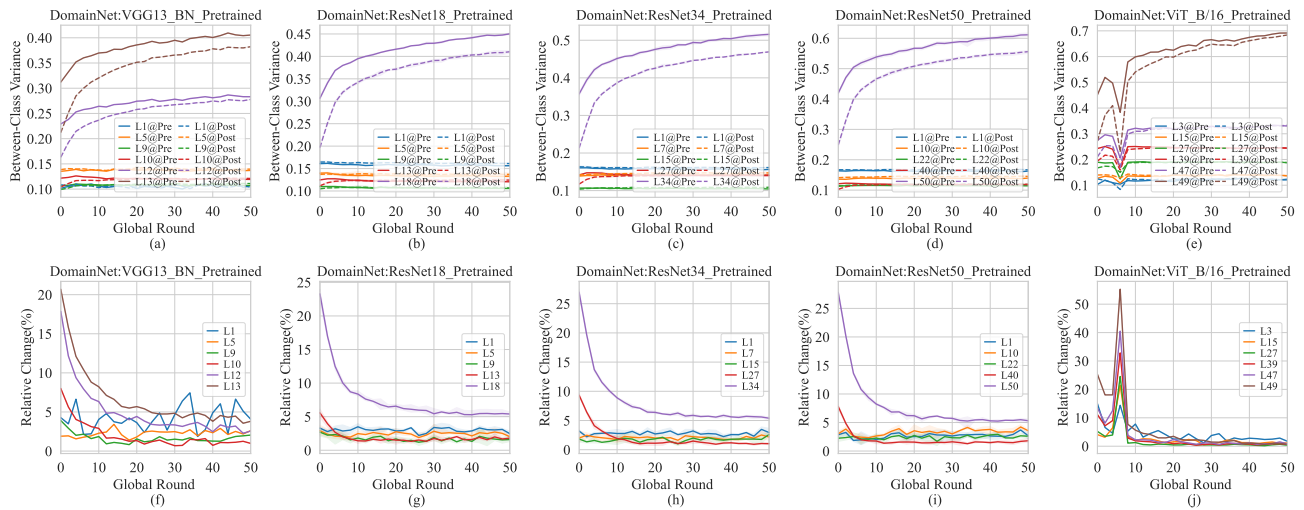


Figure 111. Changes in the normalized between-class variance of features across FL training at specific model layers. The model is trained on DomainNet with multiple models that are initialized by parameters pre-trained on large-scaled datasets. The top half of the figure shows the normalized between-class variance, while the bottom half displays the relative change in variance before and after model aggregation.

Unveiling the Downsides of Model Aggregation in Federated Learning from a Layer-peeled Perspective

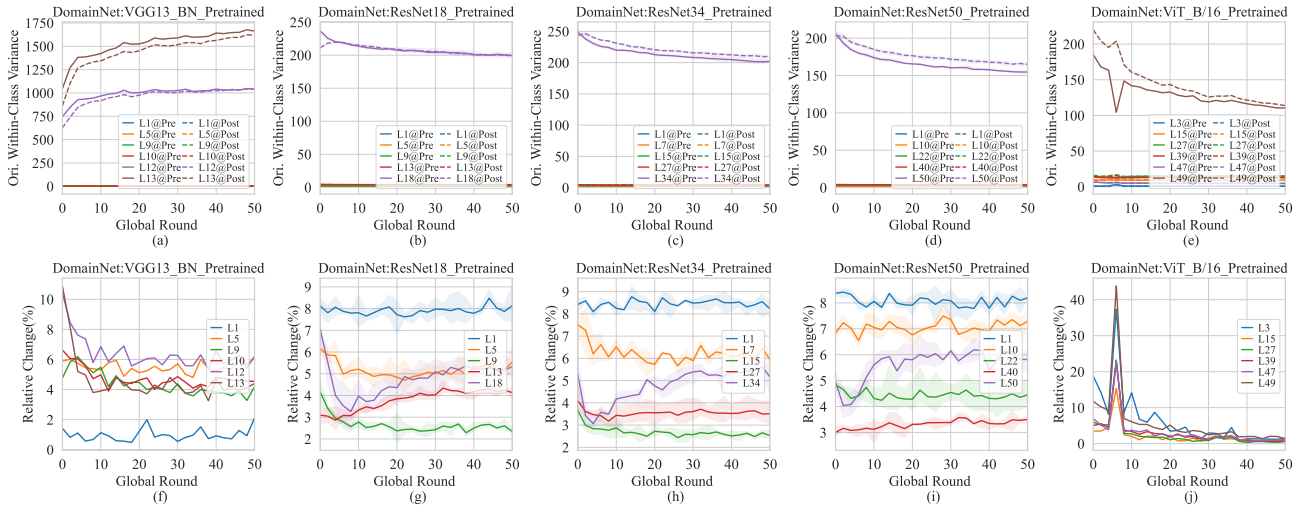


Figure 112. Changes in the original unnormalized within-class variance of features across FL training at specific model layers. The model is trained on DomainNet with multiple models that are initialized by parameters pre-trained on large-scaled datasets. The top half of the figure shows the original unnormalized within-class variance, while the bottom half displays the relative change in variance before and after model aggregation.

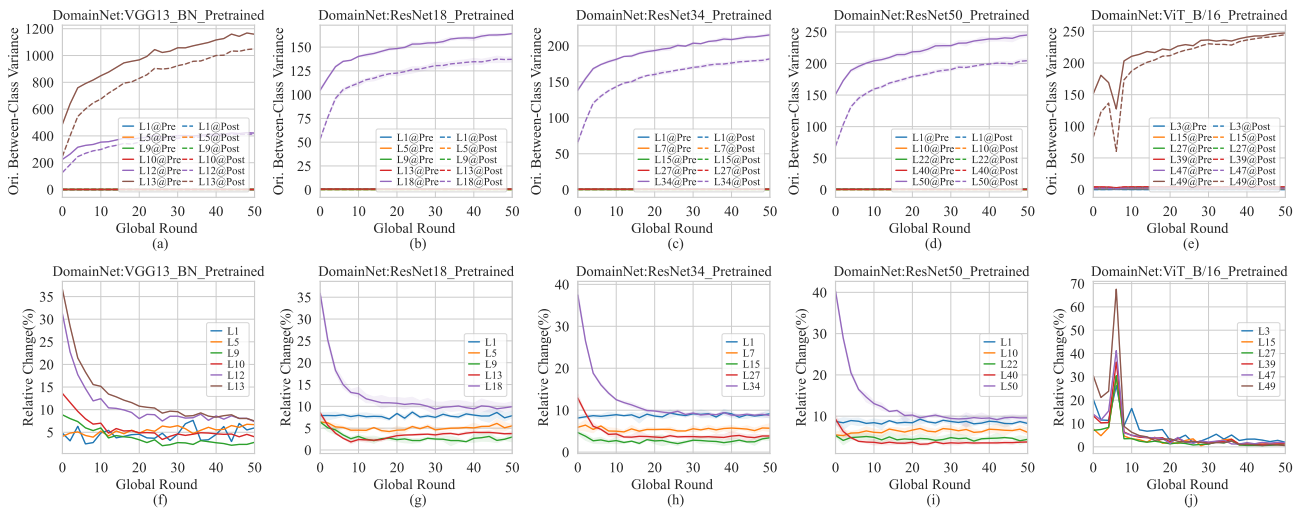


Figure 113. Changes in the original unnormalized between-class variance of features across FL training at specific model layers. The model is trained on DomainNet with multiple models that are initialized by parameters pre-trained on large-scaled datasets. The top half of the figure shows the original unnormalized between-class variance, while the bottom half displays the relative change in variance before and after model aggregation.

P.4. Changes of Alignment Across Layers

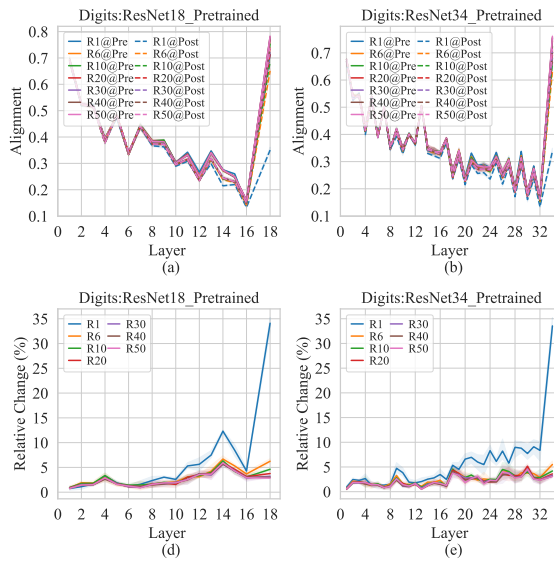


Figure 114. Changes in the alignment between features and parameters across model layers for specific global rounds, with larger X-axis values indicating deeper layers. The model is trained on Digit-Five with multiple models that are initialized by parameters pre-trained on large-scaled datasets. The top half of the figure shows the original alignment values between features and parameters, while the bottom half displays the relative change in alignment values before and after model aggregation.

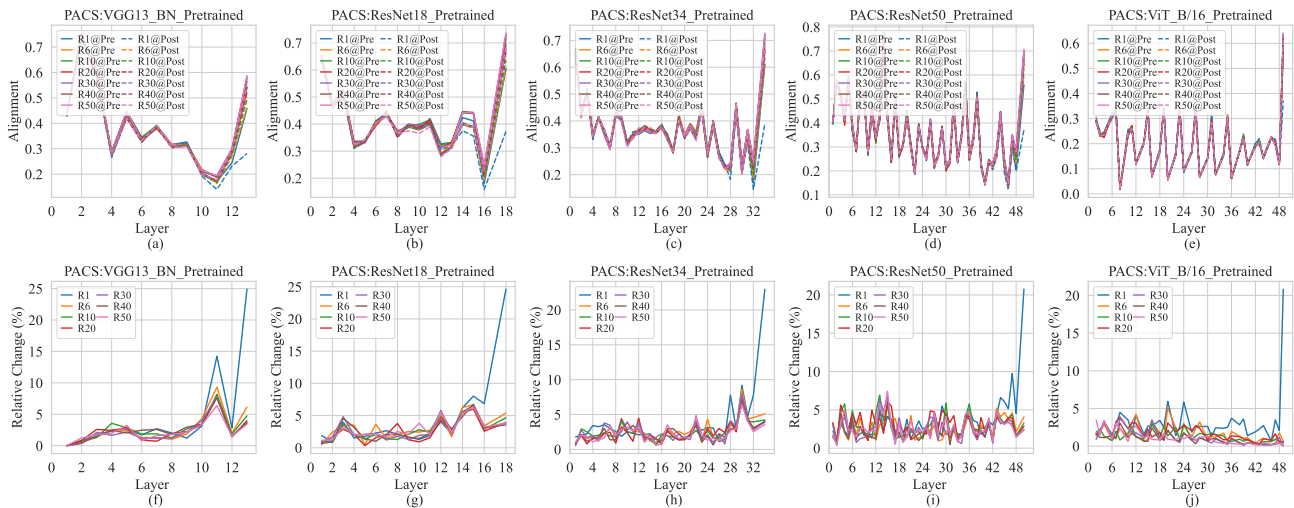


Figure 115. Changes in the alignment between features and parameters across model layers for specific global rounds, with larger X-axis values indicating deeper layers. The model is trained on PACS with multiple models that are initialized by parameters pre-trained on large-scaled datasets. The top half of the figure shows the original alignment values between features and parameters, while the bottom half displays the relative change in alignment before and after model aggregation.

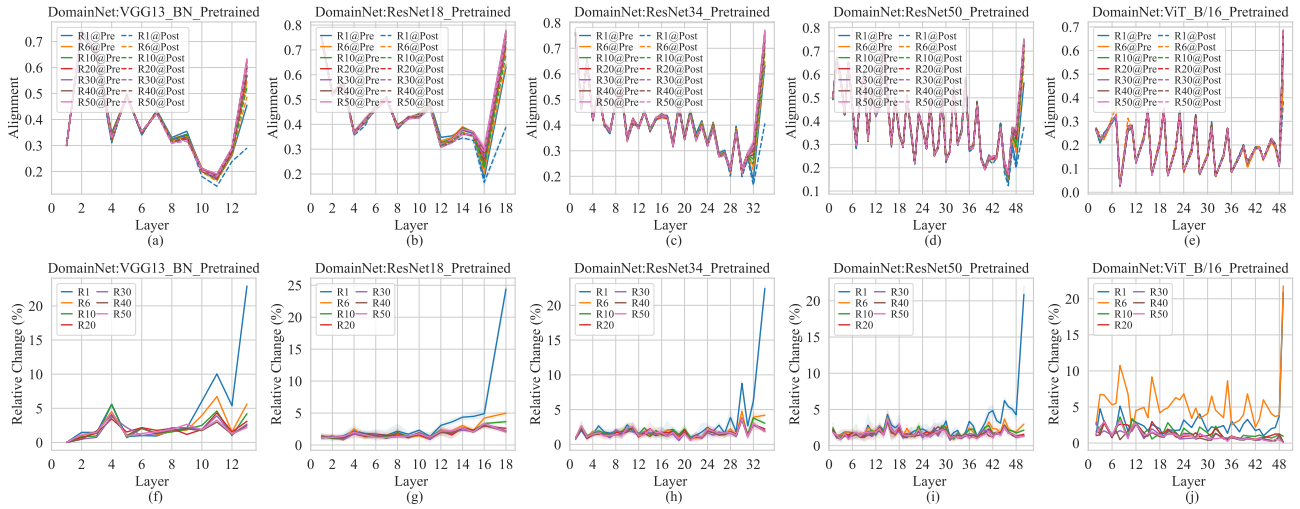


Figure 116. Changes in the alignment between features and parameters across model layers for specific global rounds, with larger X-axis values indicating deeper layers. The model is trained on DomainNet with multiple models that are initialized by parameters pre-trained on large-scaled datasets. The top half of the figure shows the original alignment values between features and parameters, while the bottom half displays the relative change in alignment before and after model aggregation.

P.5. Changes of Alignment Across Training Rounds

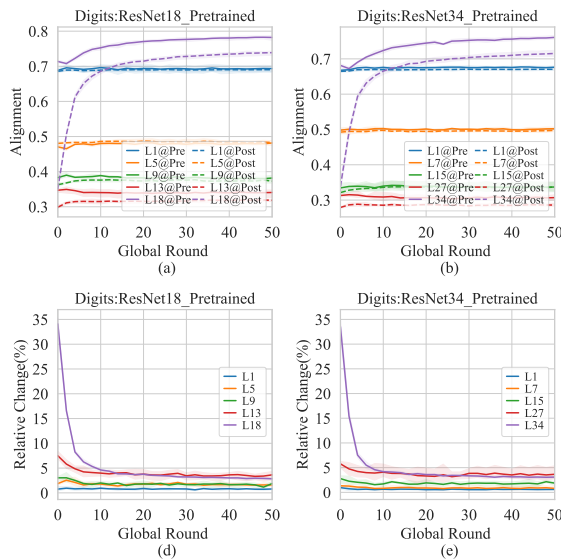


Figure 117. Changes in the alignment between features and parameters across FL training at specific model layers. The model is trained on Digit-Five with multiple models that are initialized by parameters pre-trained on large-scaled datasets. The top half of the figure shows the original alignment values between features and parameters, while the bottom half displays the relative change in alignment before and after model aggregation.

Unveiling the Downsides of Model Aggregation in Federated Learning from a Layer-peeled Perspective

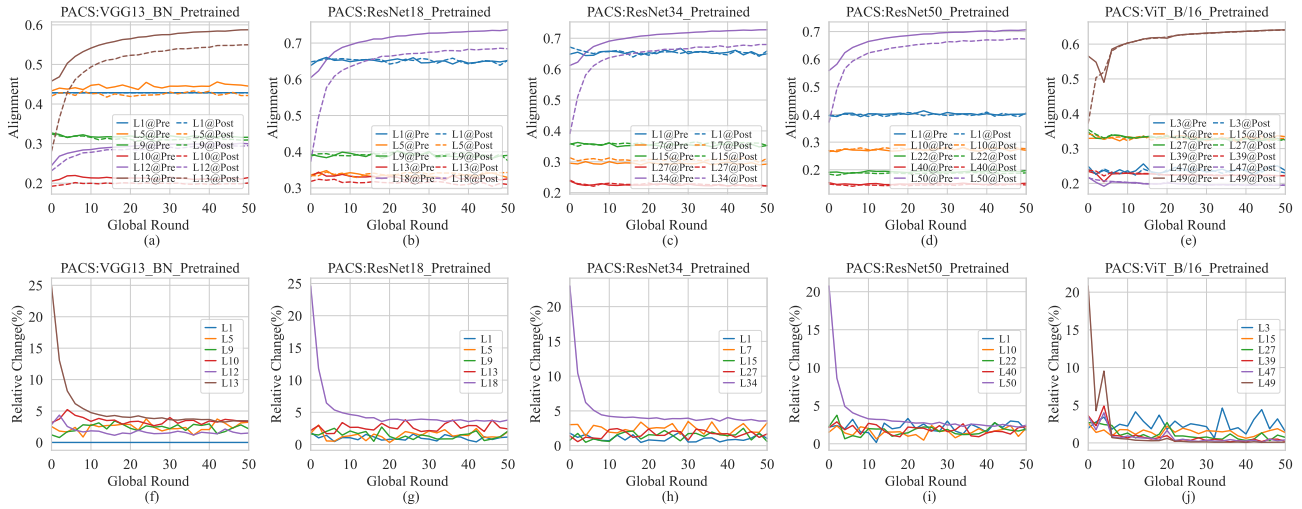


Figure 118. Changes in the alignment between features and parameters across FL training at specific model layers. The model is trained on PACS with multiple models that are initialized by parameters pre-trained on large-scaled datasets. The top half of the figure shows the original alignment values between features and parameters, while the bottom half displays the relative change in alignment before and after model aggregation.

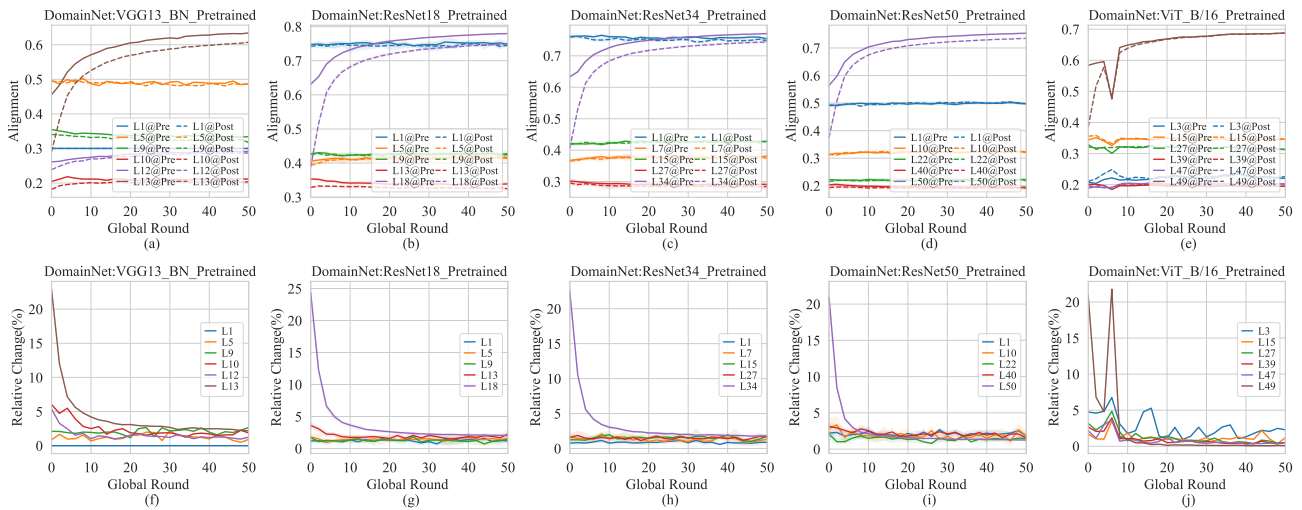


Figure 119. Changes in the alignment between features and parameters across FL training at specific model layers. The model is trained on DomainNet with multiple models that are initialized by parameters pre-trained on large-scaled datasets. The top half of the figure shows the original alignment values between features and parameters, while the bottom half displays the relative change in alignment before and after model aggregation.

P.6. Changes of Stable Rank Across Layers

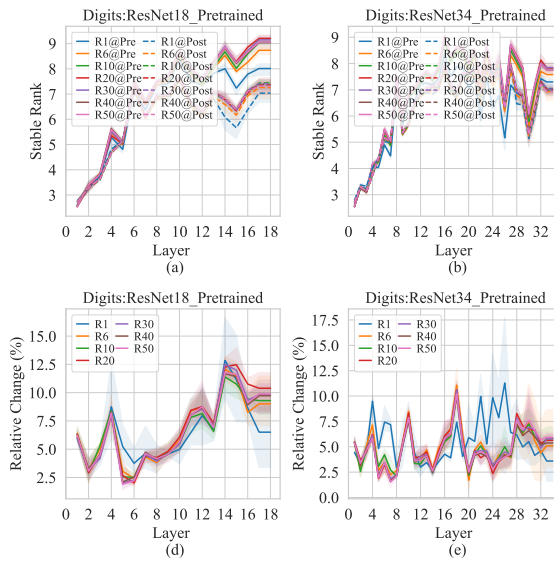


Figure 120. Changes in the stable rank of features across model layers for specific global rounds, with larger X-axis values indicating deeper layers. The model is trained on Digit-Five with multiple models that are initialized by parameters pre-trained on large-scaled datasets. The top half of the figure shows the original stable rank of features, while the bottom half displays the relative change in stable rank before and after model aggregation.

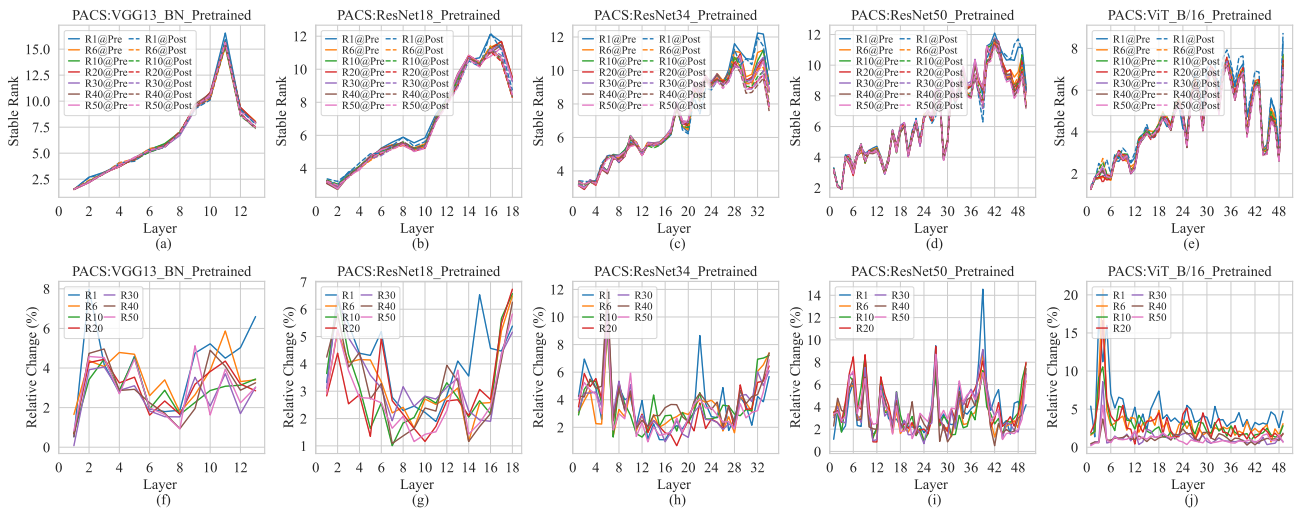


Figure 121. Changes in the stable rank of features across model layers for specific global rounds, with larger X-axis values indicating deeper layers. The model is trained on PACS with multiple models that are initialized by parameters pre-trained on large-scaled datasets. The top half of the figure shows the original stable rank of features and parameters, while the bottom half displays the relative change in stable rank before and after model aggregation.

Unveiling the Downsides of Model Aggregation in Federated Learning from a Layer-peeled Perspective

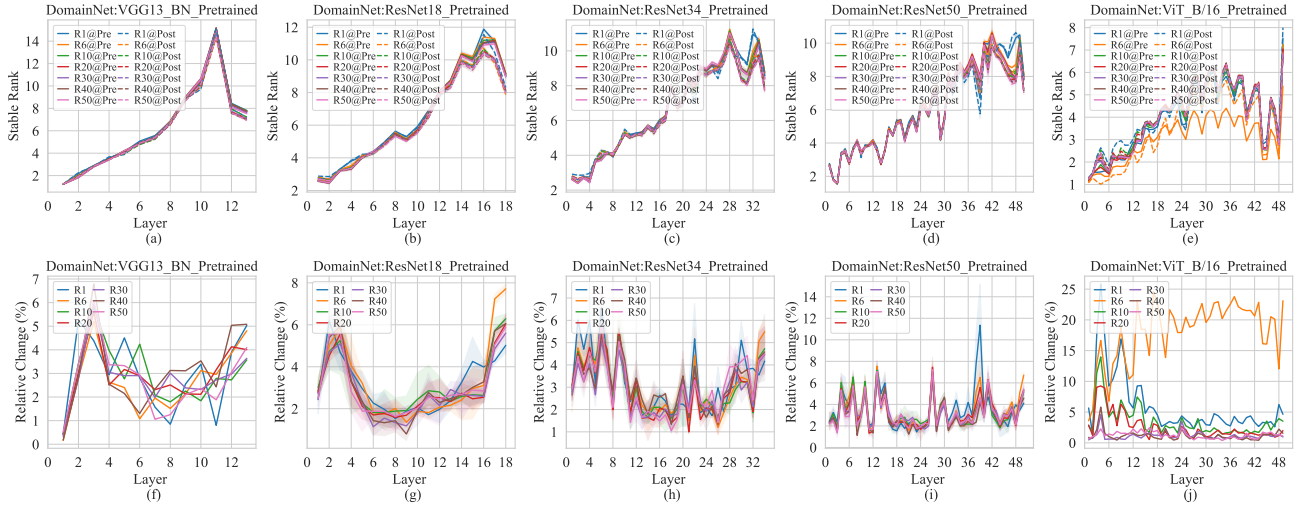


Figure 122. Changes in the stable rank of features across model layers for specific global rounds, with larger X-axis values indicating deeper layers. The model is trained on PACS with multiple models that are initialized by parameters pre-trained on large-scaled datasets. The top half of the figure shows the stable rank of features, while the bottom half displays the relative change in stable rank before and after model aggregation.

P.7. Changes of Stable Rank Across Training Rounds

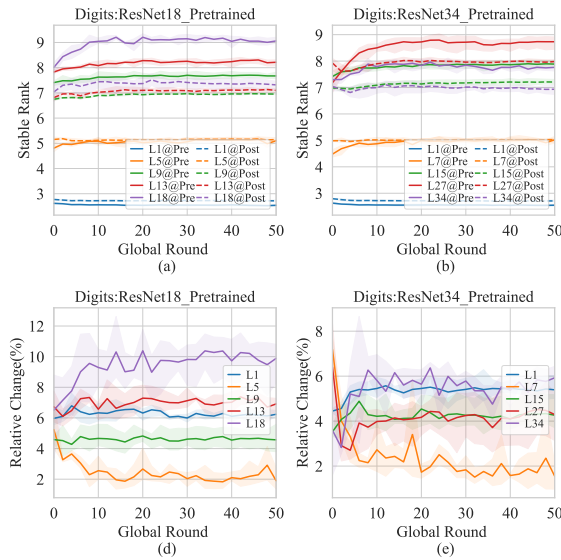


Figure 123. Changes in the stable rank of features across FL training at specific model layers. The model is trained on Digit-Five with multiple models that are initialized by parameters pre-trained on large-scaled datasets. The top half of the figure shows the original stable rank of features, while the bottom half displays the relative change in stable rank before and after model aggregation.

Unveiling the Downsides of Model Aggregation in Federated Learning from a Layer-peeled Perspective

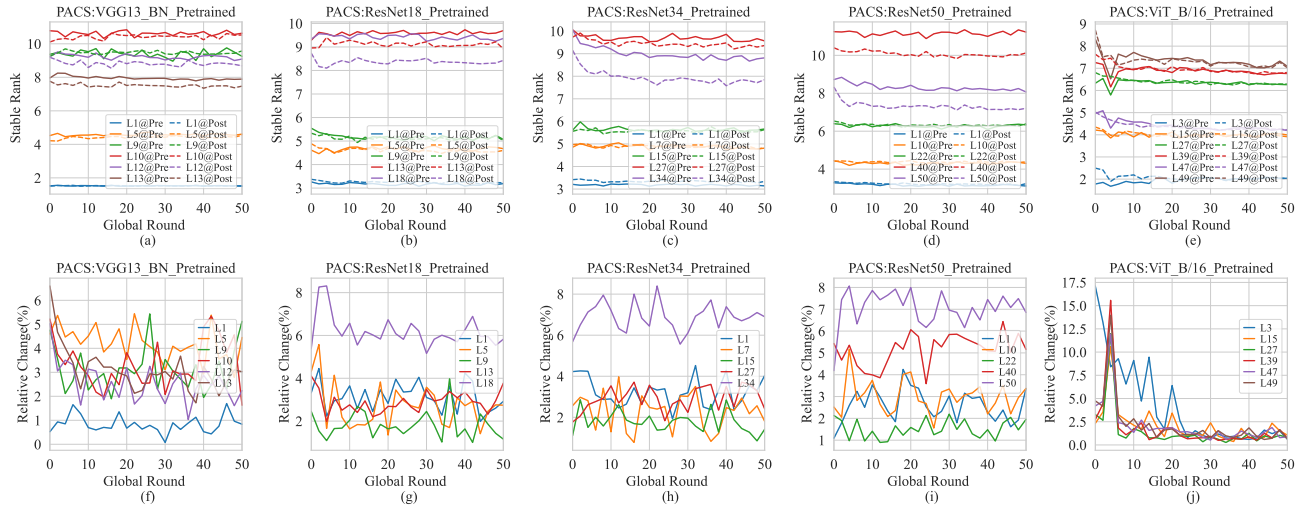


Figure 124. Changes in the stable rank of features across FL training at specific model layers. The model is trained on PACS with multiple models that are initialized by parameters pre-trained on large-scaled datasets. The top half of the figure shows the original stable rank of features, while the bottom half displays the relative change in stable rank before and after model aggregation.

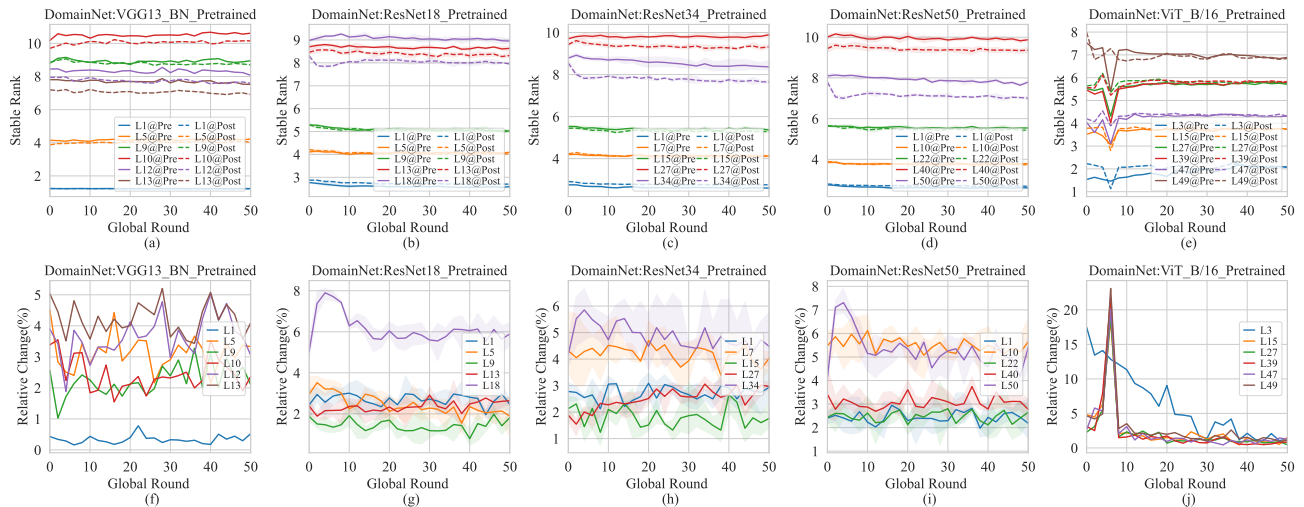


Figure 125. Changes in the stable rank of features across FL training at specific model layers. The model is trained on DomainNet with multiple models that are initialized by parameters pre-trained on large-scaled datasets. The top half of the figure shows the original stable rank of features, while the bottom half displays the relative change in stable rank before and after model aggregation.

P.8. Visualization of Pre-aggregated and Post-aggregated Features

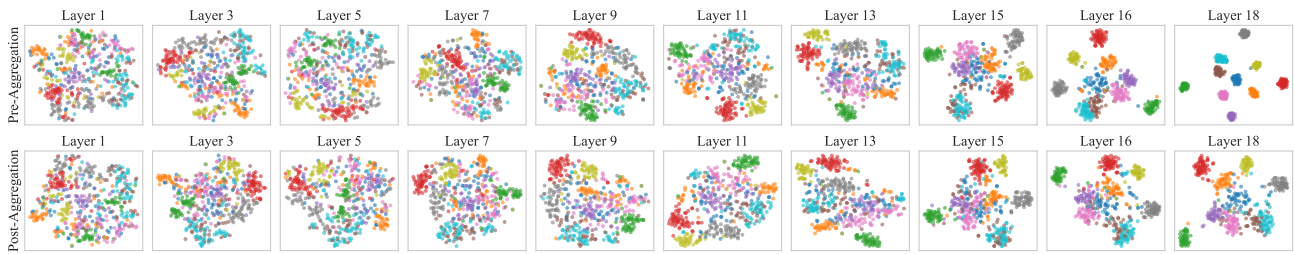


Figure 126. T-SNE visualization of features at different layers on the ‘Quickdraw’ domain of DomainNet before and after aggregation. The features are extracted from ResNet18 in the final global round of FL training, whose parameters are initialized by the parameters pre-trained on large-scaled datasets at the beginning.

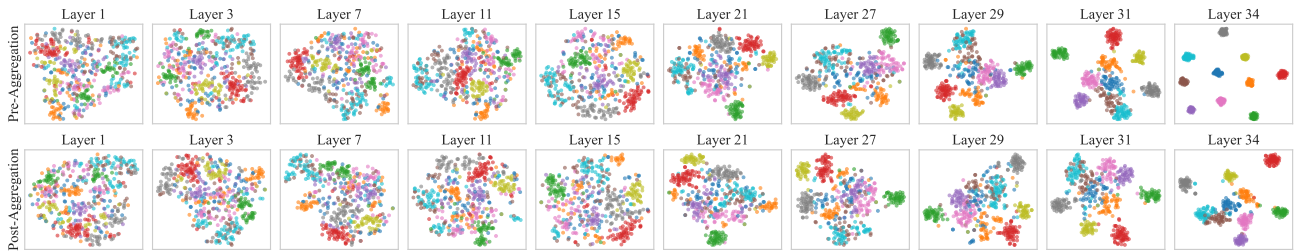


Figure 127. T-SNE visualization of features at different layers on the ‘Quickdraw’ domain of DomainNet before and after aggregation. The features are extracted from ResNet34 in the final global round of FL training, whose parameters are initialized by the parameters pre-trained on large-scaled datasets at the beginning.